REACTIVITY OF TITANOCENE METHYLIDENE WITH METAL HALIDES, ALKENE SULFIDES, AND ALKENE OXIDES.

Thesis by

Joon Won Park

In Partial Fulfillment of the Requirements

for the Degree of

Doctor of Philosophy

California Institute of Technology

Pasadena, California

1989

(submitted October 13, 1988)

To my loving wife, Hye Ryung,

and devoted parents, parents-in-law

ACKNOWLEDGMENTS

I would like to acknowledge a number of people who have made my stay at Caltech enjoyable. First and foremost is my graduate advisor, Bob Grubbs who made working here a pleasure. In addition to exceptional science, his encouragement and good example have been an invaluable part of my graduate education.

I owe a great deal to members of the Grubbs' research group, both past and present. Many thanks to those who took the time to discuss research, lend advice, and teach English. Special thanks to Peter Mackenzie and Bob Waymouth, who helped me to start research. Many thanks to the other NMR GLA's (Doug Meinhart, Eric Ansyln, and Dave Wheeler) and several close friends and supporters: Tim Swager, Ernest Wysong, Floyd Klavetter, and Bruce Novak. Also, I owe special thanks to Jong Sung for his friendship and many pleasurable weekends.

The X-ray crystallographic work in this thesis was done in collaboration with Dr. William Schaefer and Lawrence Henling; many thanks for their expertise and patience. I also acknowledge Caltech for its support through graduate fellowships.

My parents and parents-in-law have always supported and helped my each and every goal and I am deeply grateful.

Finally, I would like to thank my wife, Hye Ryung, for her patience and endeavor to raise two babies with little assistance. Without her help, our fruitful four years in this country would not have been possible.

ABSTRACT

Titanocene metallacyclobutanes show a wide variety of reactivites with organic and inorganic reagents. Their reactions include methylene transfer to organic carbonyls, formation of enolates, electron transfer from activated alkyl chlorides, olefin metathesis, ring opening polymerization. Recently, preparations of heterobinuclear μ-methylene complexes were reported. In this thesis, mechanistic, synthetic, and structural studies of the heterobinuclear μ-methylene complexes will be described. Also, the reaction of titanocene methylidene trimethylphosphine complex with alkene sulfide and styrene sulfide will be presented.

Heterobinuclear μ-methylene–μ-methyl complexes $Cp_2Ti(\mu\text{-}CH_2)$-$(\mu\text{-}CH_3)M(1,5\text{-}COD)$ have been prepared (M = Rh, Ir). X-ray crystallography showed that the methyl group of the complex was bonded to the rhodium and bridges to the titanium through an agostic bond. The ^1H, ^{13}C NMR, IR spectra along with partial deuteration studies supported the structure in both solution and solid state. Activation of the agostic bond is demonstrated by the equilibration of the $\mu\text{-}CH_3$ and $\mu\text{-}CH_2$ groups. A nonlinear Arrhenius plot, an unusually large kinetic isotope effect (24(5)), and a large negative activation entropy (–64(3) eu) can be explained by the quantum-mechanical tunneling. Calculated rate constants with Bell-type barrier fitted well with the observed one. This equilibration was best explained by a 4e-4c mechanism (or σ bond metathesis) with the character of quantum-mechanical tunneling.

Heterobinuclear μ-methylene–μ-phenyl complexes were synthesized. Structural study of $Cp_2Ti(\mu\text{-}CH_2)(\mu\text{-}p\text{-}Me_2NC_6H_4)Rh(1,5\text{-}COD)$ showed that the two metal atoms are bridged by the methylene carbon and the *ipso* carbon of

the *p-N,N*-dimethylaminophenyl group. The analogous structure of Cp_2Ti-(μ-CH_2)(μ-*o*-$MeOC_6H_4$)Rh(1,5-COD) has been verified by the differential NOE. The aromaticity of the phenyl group observed by ^1H NMR, was confirmed by the comparison of the C-C bond lengths in the crystallographic structure. The unusual downfield shifts of the *ipso* carbon in the ^{13}C NMR are assumed to be an indication of the interaction between the *ipso* carbon and electron-deficient titanium.

Titanium–platinum heterobinuclear μ-methylene complexes Cp_2Ti-(μ-CH_2)(μ-X)Pt(Me)(PMe_2Ph) have been prepared (X = Cl, Me). Structural studies indicate the following: (1) the Ti–CH_2 bond possesses residual double bond character, (2) there is a dative Pt → Ti interaction which may be regarded as a π back donation from the platinum atom to the "Ti=CH_2" group, and (3) the μ-CH_3 group is bound to the titanium atom through a three-center, two-electron agostic bond.

Titanocene (η^2-thioformaldehyde)·PMe_3 was prepared from $Cp_2Ti{=}CH_2{\cdot}PMe_3$ and sulfur-containing organic compounds (e.g. alkene sulfide, triphenylphosphine sulfide) including elemental sulfur. Mechanistic studies utilizing *trans*-styrene sulfide-d_1 suggested the stepwise reaction to explain equimolar mixture of *trans*- and *cis*-styrene-d_1 as by-products. The product reacted with methyl iodide to produce cationic titanocene (η^2-thio-methoxymethyl) complex. Complexes having less coordinating anion like BF_4 or BPh_4 could be obtained through metathesis. Together with structural analyses, the further reactivities of the complexes have been explored.

The complex $Cp_2\overline{TiOCH_2CH(Ph)CH_2}$ was prepared from the compound $Cp_2Ti{=}CH_2{\cdot}PMe_3$ and styrene oxide. The product was characterized with ^1H-^1H correlated 2-dimensional NMR, selective decoupling of ^1H NMR, and

differential NOE. Stereospecificity of deuterium in the product was lost when *trans*-styrene oxide-d_1 was allowed to react. Relative rates of the reaction were measured with varying substituents on the phenyl ring. Better linearity ($r = -0.98$, $\rho^+ = -0.79$) was observed with σ_p^+ than σ ($r = -0.87$, $\rho = -1.26$). The small magnitude of ρ^+ value and stereospecificity loss during the formation of product were best explained by the generation of biradicals, but partial generation of charge cannot be excluded. Carbonylation of the product followed by exposure to iodine yields the corresponding β-phenyl γ-lactone.

TABLE OF CONTENTS

LIST OF TABLES

CHAPTER 5.

APPENDIX I.

APPENDIX II.

APPENDIX III.

APPENDIX IV.

APPENDIX V.

LIST OF FIGURES AND SCHEMES

CHPATER 1.

CHPATER 2.

CHPATER 3.

CHAPTER 1

Carbon–Hydrogen Bond Activation through a Binuclear C–H Bond Complex

ABSTRACT

Heterobinuclear μ-methylene–μ-methyl complexes $Cp_2Ti(\mu\text{-}CH_2)$-$(\mu\text{-}CH_3)M(COD)$ have been prepared: M = Rh (**4a**), M = Ir (**4b**). The complex **4a** crystallized in the orthorhombic space group *Pbcm* (#57) with a = 8.219(1) Å, b = 16.330(2) Å, c = 12.613(2) Å, and Z = 4. Final goodness of fit was 1.98 for 1560 data and 134 parameters. The methyl group of the complex **4a** was bonded to the rhodium and bridged to the titanium through an agostic bond. The ^1H, ^{13}C NMR, IR spectra along with partial deuteration studies supported the structure in both solution and solid state. The complete line-shape analysis in the ^1H NMR spectra revealed that the activation enthalpy ($\Delta H^{\neq}$) and entropy ($\Delta S^{\neq}$) for the rotation of methyl group about the rhodium-carbon bond was 9.2(2) Kcal/mol and –1.9(6) eu, respectively.

Activation of the agostic bond is demonstrated by the equilibration of the $\mu\text{-}CH_3$ and $\mu\text{-}CH_2$ groups in **4a, 4b**. A nonlinear Arrhenius plot, an unusually large kinetic isotope effect (24(5)), and a large negative activation entropy (–64(3) eu) can be explained by the quantum-mechanical tunneling. Calculated rate constants with Bell-type barrier fitted well with the observed one. This equilibration was best explained by a 4e-4c mechanism (or σ bond metathesis) with the character of quantum-mechanical tunneling.

INTRODUCTION

Recently much attention has been focused upon early transition-metal–late transition-metal heterobinuclear complexes[1] because of their potential applications in catalytic reactions,[2] where the different electronic nature of two counterparts is utilized. Also, these complexes have been studied in order to gain an understanding of the phenomenon of so-called "strong metal-support interactions (SMSI)" in heterogeneous catalysis.[3] It is well documented that late transition-metals, which are finely dispersed on early transition-metal oxide supports such as TiO_2 and ZrO_2, serve as highly active catalysts in the catalytic hydrogenation of carbon monoxide. SMSI have been observed in such systems. While the exact nature of the interaction is still unclear, the SMSI-induced alterations in the heats of chemisorption of CO and H_2 result in improved cataytic property in many cases.

Bridging methylene species[4] were suggested as key intermediates in Fischer-Tropsch chemistry. Recently a convenient synthetic route to titanium–late transition-metal μ-methylene complexes was developed. These complexes serve as possible models[6] for surface methylene species on catalysts that exhibit the SMSI phenomenon and/or Fischer-Tropsch reaction. Reaction of the "$Cp_2Ti{=}CH_2$" species generated from bis(cyclopentadienyl)titana-cyclobutanes[7] or Tebbe's reagent[8] with late transition-metal chlorides (L_nMCl) give a new class of μ-methylene complexes $Cp_2\overline{TiCH_2M(Cl)}L_n$ (**2**).[9] The μ-chloride functionality of this family of the compounds allows the introduction of wide variety of the other bridging groups via metathesis.[10]

There is increasing interest in agostic interactions between a metal and a

carbon–hydrogen bond.[11] This interaction is thought to be important in the carbon–hydrogen bond activation process (eq 1).[12] The C–H bond activation, an essential part of organometallic chemistry, continues to draw both experimental and theoretical interest.[13] (Observation of analogous interaction between a metal and a hydrogen-hydrogen bond[14] showed the generality of such interactions.) Systems that show such interactions are useful as models to provide characteristic reaction types and spectroscopic features. Heteronuclear systems with such interactions, which can be thought of as the simplest models for mixed-metal heterogenous catalysts,[15] were realized through the utilization of the above new class of μ-methylene complexes.

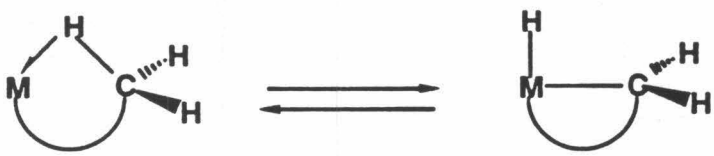

(1)

RESULTS AND DISCUSSION

Synthesis. Recently an efficient route to binuclear μ-methylene complexes $Cp_2TiML_n(\mu\text{-}CH_2)(\mu\text{-}Cl)$ (M = Rh, Ir, Pt, Pd, Au, Ti and Zr) was developed. Subsequently the reactivitites of the complexes have been explored. Also, structures of the complex were studied with single crystal X-ray crystallography and spectroscopic data.[9,10] Among the complexes, $Cp_2TiM(COD)(\mu\text{-}CH_2)(\mu\text{-}Cl)$ (M = Rh, Ir),[16] produced an intriguing thermally stable complex by metathesis of a bridging chloride with a methyl group.[17]

β,β-dimethyltitanacyclobutane **1**[7] reacted at room temperature with $[M(COD)Cl]_2$ (M = Rh, Ir) in toluene to give red bridging methylene complexes **3a, 3b**. Treatment of crude **3a, 3b** with two equiv of methyl lithium, methyl magnesium chloride, respectively, yielded yellow-orange $\mu\text{-}CH_3$ complexes **4a, 4b**. The bridging methyl complexes were formed in reasonable yields (31, 49% as determined by ^1H NMR), but could only be isolated in poor yields (~ 10%) due to difficulties encountered in purifying those complexes (eq 2–4). One of the C–H bonds in the bridging methyl group formed an agostic interaction with titanium as identified through various methods (*vide infra*). This type of methyl group is one of three basic types of bridging conformation in polynuclear complexes:[4d,19] (1) a symmetric pyramidal bridge, (2) an asymmetric bridge, and (3) a symmetric planar bridge.[20]

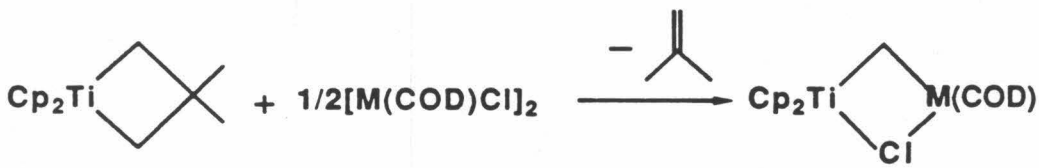

(2)

1 **2a** M = Rh **2b** M = Ir **3a** M = Rh **3b** M = Ir

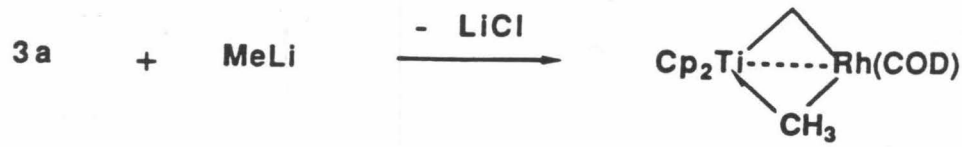

(3)

4a

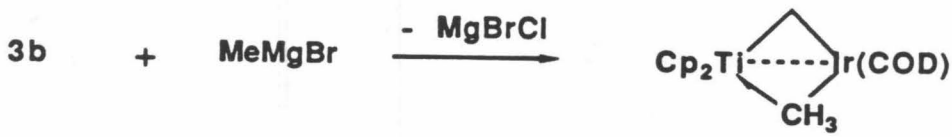

(4)

4b

NMR. The ^{1}H and ^{13}C NMR resonances for the μ-CH_2 group of **4a**, **4b** appeared in the typical regions reported for binuclear μ-methylene complexes.[4d] The $^1J_{CH}$ values are 129, 132 Hz; the values are slightly larger than those for pure sp^2 and sp^3 carbons.[21] At room temperature, the μ-CH_3 group of **4a** (**4b**) showed broad resonance at –3.13 (–2.93) ppm in the ^{1}H NMR spectra. When cooled to –92 °C, this resonance was replaced by a doublet at 1.28 (1.14) ppm and a triplet at –12.15 (–11.5) ppm (J_{HH} = 12.8 Hz). This high-field resonance along with small ^{13}C–^{1}H coupling constant (*vide infra*) for the bridging proton was indicative of the interaction of C–H bond with titanium.

The resonance in the ^{13}C NMR spectrum at room temperature for the μ-CH_3 group of **4a** (**4b**) occurred at 49.7 (48.8) ppm (doublet of quartet, J_{CH} = 114 Hz, J_{CRh} = 29 Hz for **4a**; quartet, J_{CH} = 115 Hz for **4b**). The carbon-rhodium coupling constant for the μ-CH_3 group is markedly different from values for $[Rh(COD)(\mu\text{-}CH_3)]_2$ (9.5 Hz),[22] which implies that the bonding character of the methyl group is considerably different. At –92 °C, the μ-CH_3 of **4a-$^{13}CH_3$** (**4b-$^{13}CH_3$**) showed a resonance at 51.1 (49.6) ppm. The coupling constant for the bridging proton ($^bJ_{CH}$) was 87.7 (91,0) Hz; for the terminal proton, this value ($^tJ_{CH}$) was 126.7 (127.3) Hz. As expected, small ^{13}C–^{1}H coupling constants for the agostic hydrogen were found at low temperature.

The fluxionality of μ-CH_3 group, which is rotating about the carbon-rhodium bond, was studied by VT NMR. The coalescence temperatures for **3a**, **3b** at 90 MHz ^1H NMR were –40 °C, which correspond to rotational activation-energy ($\Delta G^{\neq}$) of +9.8, 9.9 Kcal/mol,[23] respectively. This activation-energy can be thought as the approximate agostic bond-energy.[24] Rotational activation-enthalpy of 9.2(2) Kcal/mol and activation-entropy of –1.9(6) eu from complete line-shape analysis (Table I) showed negligible entropy effect, as expected.

X-ray Structure. As shown in ORTEP diagram (Figure 1), the four central atoms – Ti, Rh, the μ-methylene carbon (CB1), and the other bridging atom (CB2) – form a four membered ring lying in a plane with a Cp ring above and below the plane. (Selected bond lengths and angles are listed in Table II, crystal and intensity collection data are shown in Table III.) The coordination geometry about titanium is pseudotetrahedral, whereas the rhodium is basically in a square-planar environment. The plane composed of the methylene carbon and the two methylene hydrogens is tilted toward the rhodium. (Ti–CB1–CB1H angle is 123(2)°; Rh–CB1–CB1H angle is 105(2)°.) The μ-methyl group forms a three-center, two-electron agostic bond with the titanium atom. The Ti–H (CB2B) distance of 2.02(5) Å is shorter than Ti–C (CB2) distance (2.294(6) Å). These distances can be compared to those in $Cp_2Ti(\mu\text{-}CH_2)(\mu\text{-}CH_3)Pt(CH_3)(PMe_2Ph)$ (1.935(5), 2.395(8) Å)[10b] and $Ti(dmpe)(Et)Cl_3$ (2.29, 2.52 Å),[26] both of which showed agostic interactions with the titanium.

The Ti–Rh bond length of 2.835(1) Å is sufficiently short such that some direct metal-metal interaction is possible. For example, the Ti–Rh distance is 2.68 Å in an alloy of the two metals[3a] and the Ti–Rh distance in a highly

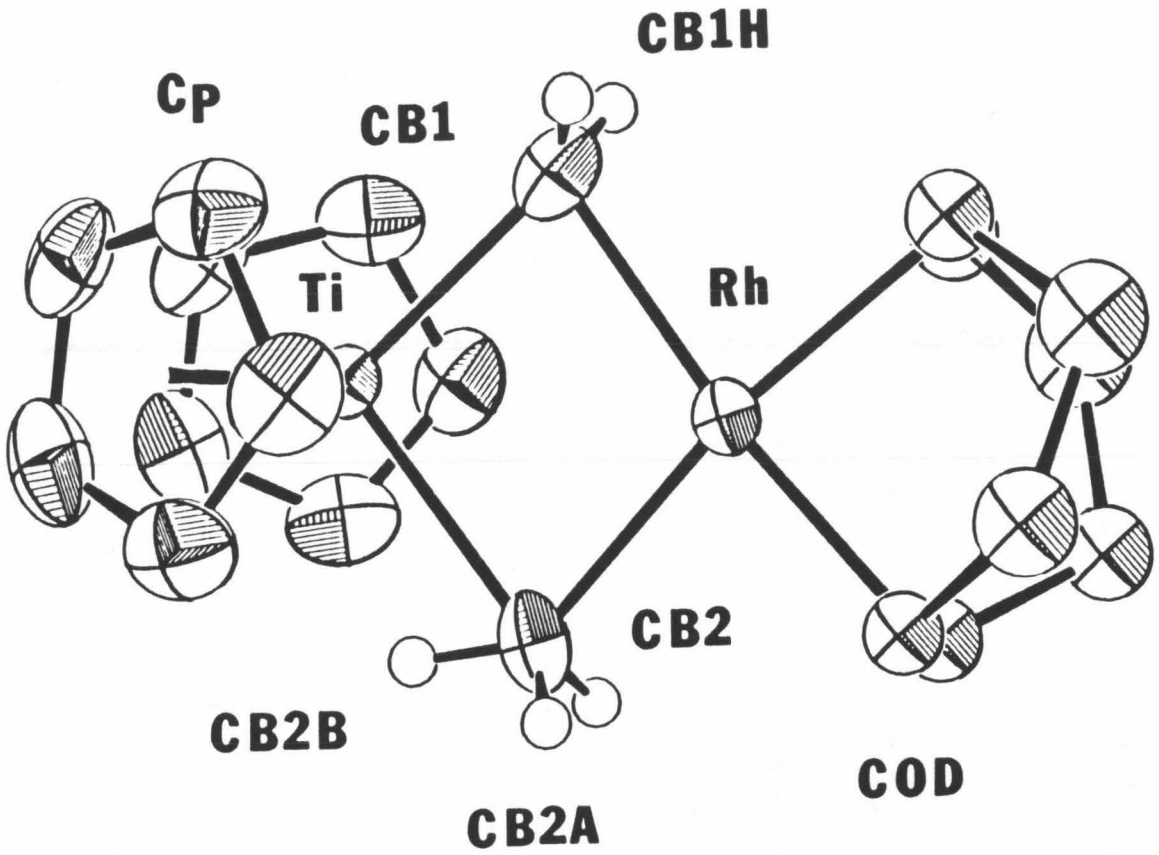

Figure 1. ORTEP diagram of $Cp_2TiRh(COD)(\mu\text{-}CH_2)(\mu\text{-}CH_3)$. The ellipsoids are drawn at the 50% probability level except for the hydrogen atoms. The hydrogen atoms of the cyclopentadienyl rings and 1,5-cyclooctadiene are omitted for clarity.

reduced rhodium and titania is 2.55 Å.[27] The Ti–Rh bond of complex **4a** is also 0.15 Å shorter than that of the corresponding μ-CH_2, μ-Cl analogue.[9b] The better electron donating ability of the C–H bond to titanium was responsible for the stronger metal-metal interaction in μ-CH_3 complex than that in μ-Cl complex as demonstrated in the Pt analogue. The presence of the Ti–Rh bond is reflected in the narrow Ti–CB1–Rh angle (83.9(2) Å); the magnitude of this angle is typical of binuclear μ-methylene complexs with a metal-metal bond.[4c]

The Ti–CH_2 distance (2.147(5) Å) is similar to that in $Cp_2\overline{TiCH_2C(Me)_2CH_2}$ (2.16 Å),[28] but much longer than both the distance in μ-Cl analogue (2.02 Å) and the calculated distance for the Ti=CH_2 double bond (1.85-1.88 Å).[29] This long distance can be attributed to the stronger π-back donation from an occupied d orbital on rhodium to the π* orbital of the "titanaolefin" group which localized on the electropositive titanium atom. (See ref. 10b for further discussion.)

IR. Agostic hydrogens also exibit characteristic IR absorbance bands between ca. 2700 and 2350 cm^{-1}. Complex **4a** (**4b**) displayed a weak absorbance at 2460 (2506) cm^{-1}. Upon deuteration of the methyl group, **4a-CD_3** showed new absorbances at 2196, 2110, and 1845 cm^{-1} with disappearance of absorbance at 2460 cm^{-1}, concurrently. The first two absorbances are assigned to the stretching mode of the nonagostic C–D bonds and the latter absorbance to the stretching mode of the agostic C–D bond. The abnormally large chemical shift changes upon partial deuteration of the μ-CH_3 group in the ^1H NMR were attributed to these low stretching frequencies for the agostic C–H bond. The approximate equilibrium constant can be calculated based on the IR data with a few of assumptions.

Partial Deuteration. As suggested by Shapley,[30] the μ-CH_3 group was

partially deuterated by using a mixture of CH_3Li, CH_2DLi, and CHD_2Li (mole ratio; 0.12 : 0.73 : 0.16) to metathesize the μ-Cl group of complex **3a**. Three broad peaks were observed at room temperature in the ^1H NMR. Relatively sharper peaks at –3.10, –3.26, and –3.42 ppm corresponding to μ-CH_3, μ-CH_2D, and μ-CHD_2 group were obtained at a higher temperature of 80 °C. The equilibrium constant was calculated by applying the chemical shift changes and the known chemical shifts of the terminal proton ($^t\delta$) and the bridging proton ($^b\delta$) to eq 6, 7. The calculated equilibrium constant of 1.11 at 80 °C is relatively small in comparison with those of related Os and Mn clusters (1.25 at 25 °C for Os cluster[30]; 1.35 at 44 °C for Mn cluster[23b]).

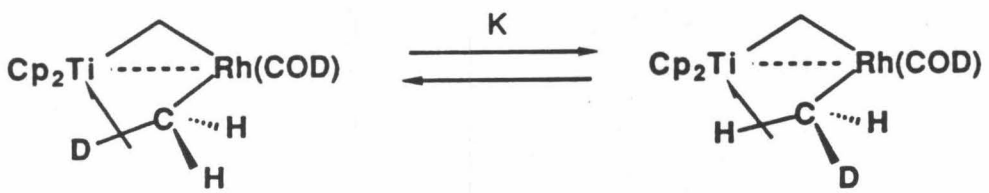

(5)

$$^{av}\delta(\mu\text{-}CH_2D) = \frac{^t\delta}{2K+1} + \frac{K(^t\delta + {}^b\delta)}{2K+1} \qquad (6)$$

$$^{av}\delta(\mu\text{-}CHD_2) = \frac{2\,^t\delta}{K+2} + \frac{K\,^b\delta}{K+2} \qquad (7)$$

$^t\delta$ = 1.44 ppm, $^b\delta$ = – 12.17 ppm

C–H Bond Activation.[31] The existence of both a μ-methylene and μ-methyl ligand in this molecule raised the intriguing possibility of a hydrogen-transfer reaction between the bridging alkyl ligands. Indeed, when the ^{13}C-labeled complex **4a-$^{13}CH_3$** was allowed to react above room

temperature, the ^{13}C label was incorporated into the μ-methylene position (eq 8). Also, the same type of equilibration observed in **4b-$^{13}CH_3$** suggested the generality of the reaction.

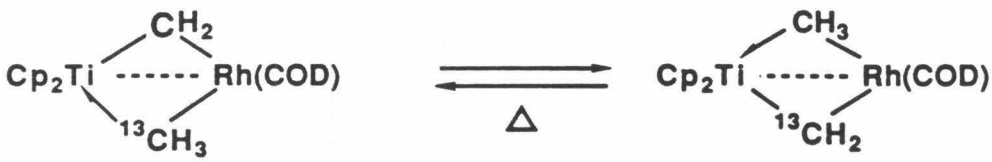

(8)

4a-$^{13}CH_3$

The reaction was not catalyzed by either acids (e.g., acetic acid, Ph_3CBF_4) or base (e.g., Et_3N). But a stronger acid such as dry hydrogen chloride gave only decomposition products and ultimately Cp_2TiCl_2 plus a rhodium complex. Neither new esr signal with a radical trap *N-tert*-butyl-α-phenylnitrone (PBN), nor change of rate constant of the C–H bond activation was observed. The apparent rate constant of the reaction at 75 °C was not changed by the concentration, which is characteristic of a unimolecular reaction. The rate constants of the reaction from 45 to 110 °C were measured to elucidate kinetic behaviour of the reaction.

Rate Constants of C–H Bond Activation (k_H). Relative peak heights[32] of μ-$^{13}CH_2$ and μ-$^{13}CH_3$ of **4a** in $^{13}C\{^1H\}$ NMR spectra were measured in order to obtain kinetic rate constants of the C–H bond activation (k_H). For the unimolecular equilibrium reaction, the rate equation is expressed as shown below in eq 9.[33] Good linearity between ln $[x_e/(x_e - x)]$ and time assured the unimolecularity of the C–H bond activation. (From the slope ($2k_H$) the rate of the reaction can be calculated.) The reaction was followed longer than three

half-lives except at 45 °C, where the rate was followed until two half-lives due to the slowness of the reaction. Individual rate constants (k_H) at different temperatures are shown in Table IV. An Eyring plot (ln (k/T) vs. 1/T) of k_H is shown in Figure 2. The deviation from the expected linearity in the low temperature region (45-75 °C) is conspicuous. Measuring the rate constants over a wider temperature region was prohibited by rapid decomposition of the complex at high temperatures over 110 °C and extremely slow reaction below 45 °C.

$$\mathbf{A} \underset{k'}{\overset{k}{\rightleftharpoons}} \mathbf{B}$$

$$\ln\,[x_e / (x_e - x)] = (k + k')\,t\,, \qquad (9)$$

where x is the extent of the reaction, and x_e is the value at the equilibrium.

Rate constants of C–D Activation. Two types of labelled molecules $Cp_2TiRh(COD)(\mu\text{-}CH_2)(\mu\text{-}^{13}CD_3)$ and $Cp_2TiRh(COD)(\mu\text{-}CH_2)(\mu\text{-}CD_3)$ were prepared to measure the rate constant of C–D activation (k_D). Utilization of $^{13}C\{^1H\}$ NMR to follow the reaction for the measurement of k_D was complicated by the multiplicities of $\mu\text{-}^{13}CD_2$ and $\mu\text{-}^{13}CD_3$ groups. Employing ^2H NMR to follow the relative peak heights of $\mu\text{-}CD_2$ and $\mu\text{-}CD_3$ was more successful. Only the early stage ($x < 10\%$) of the reaction was considered so as to avoid complications coming from the involvement of $\mu\text{-}CH_2$ hydrogens. The kinetic isotope effect (k_H/k_D) was calculated based on the measured rate constant (k_D). (See Table V for the k_D.) The kinetic isotope effect increased

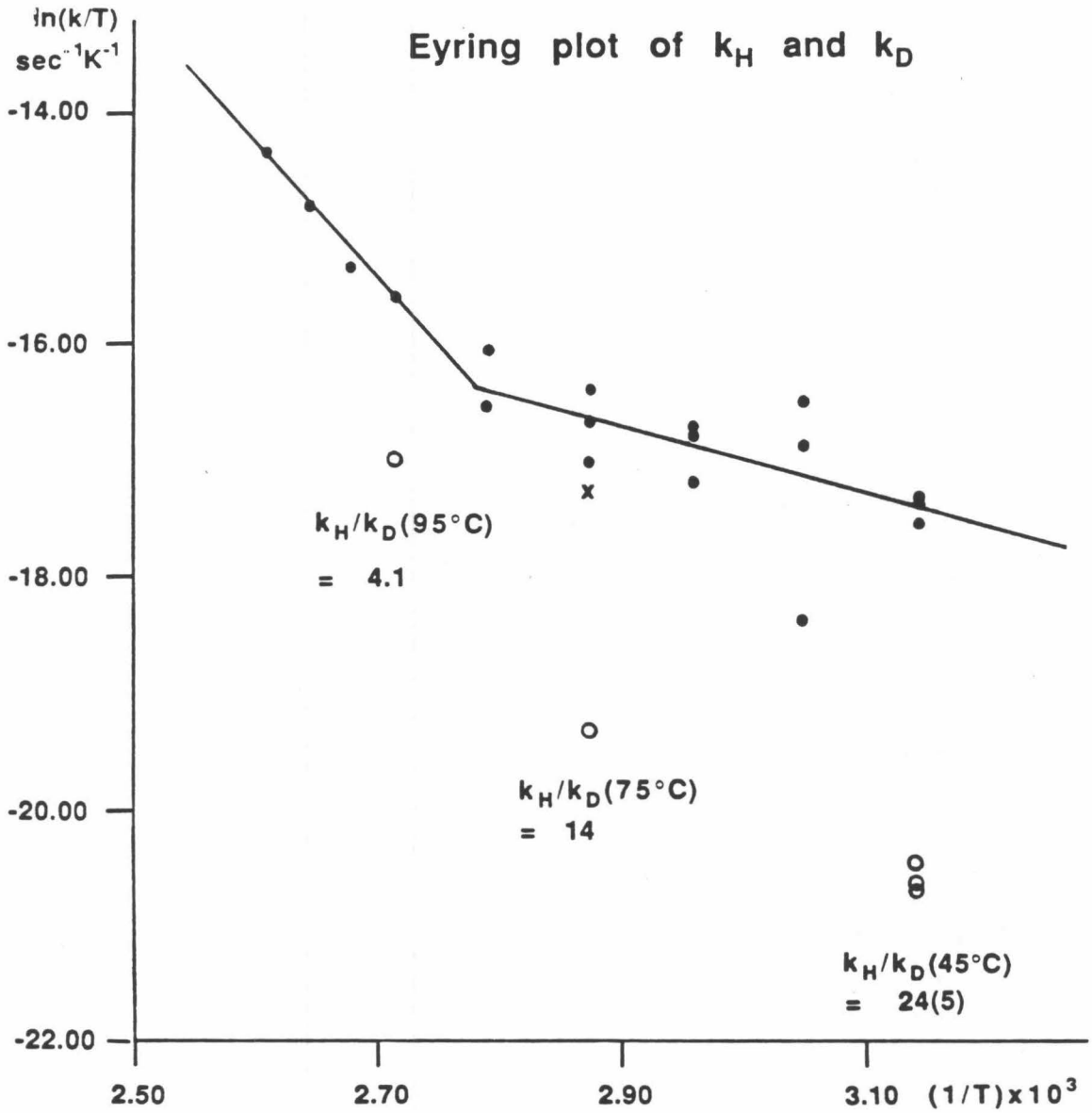

Figure 2. Plot of ln (k_{obsd}/T) versus 1/T and kinetic isotope effects (k_H/k_D) at 95, 75, and 45 °C.

sharply from 4.1 to 24(5)[34] upon decreasing the temperature from 95 °C to 45 °C. This unusual behavior can be explained by either existence of two different mechanisms at two temperature regions or a mechanism involving quantum-mechanical tunneling. After two temperature regions were divided, the data were fitted on the two straight lines to get two sets of activation enthalpy ($\Delta H^{\neq}$) and entropy ($\Delta S^{\neq}$). At high (110-85 °C) and low (85-45 °C) temperature regions, these were 24(4) Kcal/mol, –13(6) eu, 5.5(1) Kcal/mol, –64(3) eu, respectively. Such a large negative activation entropy prompted the running of a cross-over experiment in order to reasssure the unimolecularity, even though good linearity of ln $[x_e(x_e - x)]$ vs. time was observed through the whole temperature region.

Cross-over Experiment. A mixture of two complexes, $Cp_2TiRh(COD)$-(μ-CH_2)(μ-$^{13}CH_3$) and $Cp_2TiRh(COD)$(μ-CX_2)(μ-CX_3) (X = H or D) which was prepared from **4a-CD$_3$**, were heated at both temperature extremes (105, 45 °C) (eq 10). The region of μ-CH_3 and μ-CH_2 groups in the ^{13}C NMR was observed after the sealed NMR tube was heated for longer than $2t_{1/2}$ (47 days for 45 °C). (Half-life ($t_{1/2}$) can be estimated from k_D, the rate constant of the C–D activation.) The intactness of the doublets for the μ-$^{13}CH_3$ group in the $^{13}C\{^1H\}$ NMR was observed as a evidence for the absence of cross-over between the two types of molecule even at the low temperature extreme. This result confirmed the unimolecularity of the reaction over the whole temperature region.

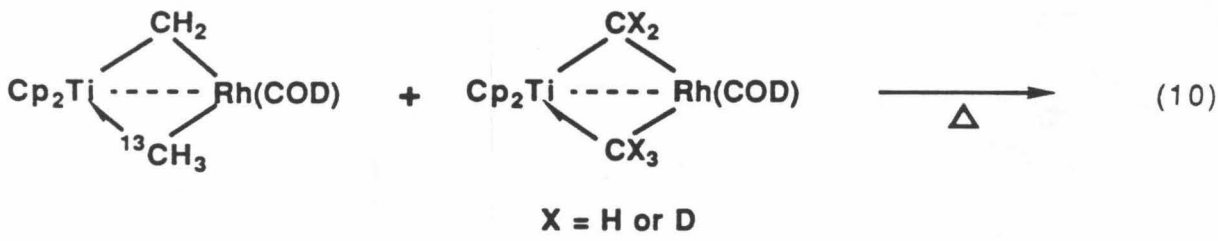

(10)

Quantum-mechanical Tunneling. Three observed features for the reaction were characteristic of quantum-mechanical tunneling.[35] These three are as follows: (1) non-linear Arrhenius plot, (2) unusually large kinetic isotope effect at low temperature, (3) low apparent activation enthalpy ($\Delta H^{\neq}$) and large negative activation energy ($\Delta S^{\neq}$). The theoretical rate constants (k_H, k_D) were calculated with the program based on the truncated parabolic (or Bell type)[36] barrier, and the rate equation is expressed by the equation shown below.

$$k = Q(T)\, A \exp(-E/RT), \qquad (11)$$

where

$$Q = [e^{b}/(c-b)]\,(ce^{-b} - be^{-c})$$

$$b = E/RT$$

$$c = [2\pi^2 a(2mE)^{1/2}]/h$$

$$2a = \text{barrier width}$$

$$E = \text{energy barrier}$$

The activation energy of 24 Kcal/mol was deduced from the activation enthalpy at the high temperature region. The other two parameters, tunneling width (2a) and preexponetial factor (A), were varied to optimize the fit of the calculated values and the observed values. The rate constants of C–D activation (k_D) were calculated with the parameters fixed for k_H. As shown in Figure 3, the calculated value agreed moderately well with the observed rate constants, and showed curvature even at 110-45 °C region. No curvature for the calculated k_D is characteristic of the Bell type barrier. Better fitting for k_D was presumed with more sophisticated types of barrier. A preexponetial factor of 1.0×10^9 is reasonable, and a tunneling width of 1.00 Å can be explained

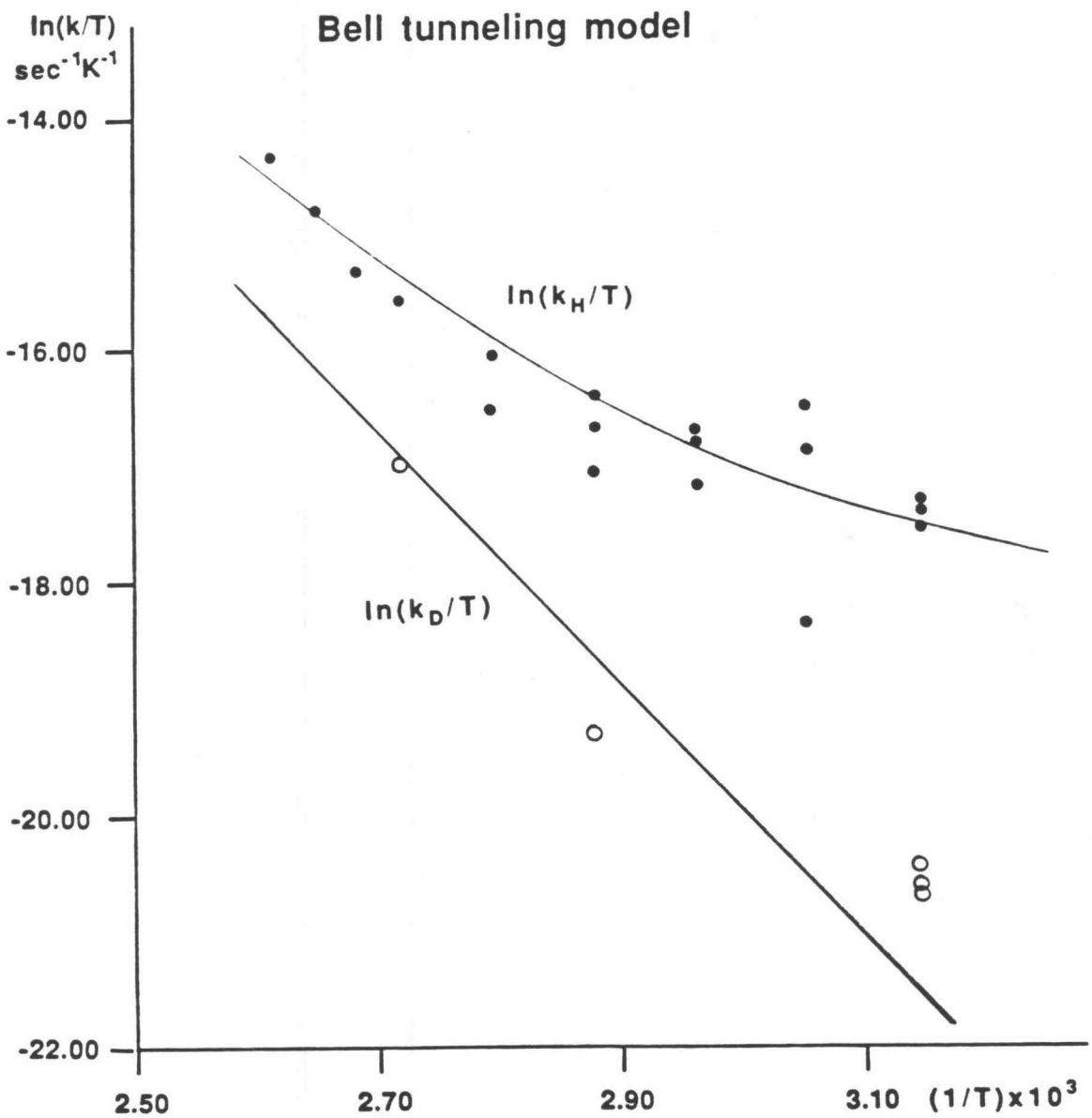

Figure 3. Plot of ln (k_{calcd}/T) versus 1/T. The solid line represents calculated rate constants based on the three parameters in the Bell tunneling model (2a = 1.00Å, A = 1.0 x 10^9, and E = 24 Kcal/mol); closed and open circles represent the observed value of k_H and K_D, respectively.

through the conformational change of μ-CH_3 group prior to the C–H activation step. One speculative conformational change to satisfy tunneling width of 1.00 Å is shown Scheme I. This quantum-mechanical tunneling effect explained the nonlinear Arrhenius plot and the apparent rapid increase of the kinetic isotope effect upon decreasing the reaction temperature.

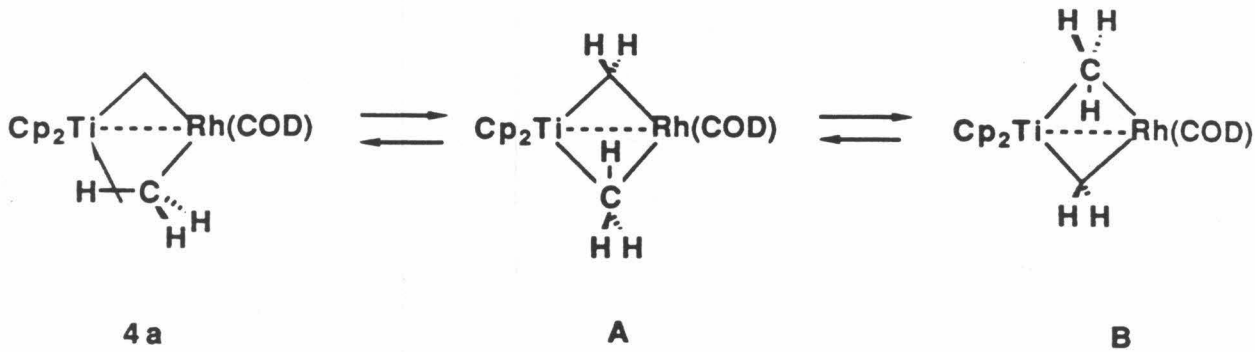

Scheme I. Geometrical change of μ-CH_3 group before hydrogen atom transfer. Hydrogen atom of μ-CH_3 group moves 1.3 Å when the equilibration goes through the intermediate **A** and **B**.

Mechanism. Three mechanisms can be conceived : (1) 4e-4c concerted mechanism (maybe after preconformational change),[37] (2) oxidative addition of C–H bond on titanium center,[12,38] and (3) α-elimination on rhodium[39] and hydride-carbene insertion[40] (Scheme II). Mechanism 2 is attractive in the sense that formation of an agostic bond with electron-deficient titanium is the intermediate stage of the C–H bond activation. But the geometry of Cp_2MX_3 was generated after C–H bond activation, so difficulty is unavoidable in rearranging the geometry for the α-addition on the μ-methylene group. Mechanism 3 was disfavored by the fact that α-elimination is less frequently observed in the late transition metal and the observation that the iridium

analogue has the same rate constant (k_H at 75 °C = 1.07 x 10^{-5} sec^{-1}) of the C–H activation. Observed parameters ($\Delta H^{\neq}$, $\Delta S^{\neq}$) of our system agreed well with the 4e-4c concerted mechanism (also known as σ bond metathesis). Additionally, mechanism 1 does not contradict with the calculated tunneling width. In conclusion, 4e-4c mechanism (or σ bond metathesis) with the character of quantum-mechanical tunneling is most plausible.

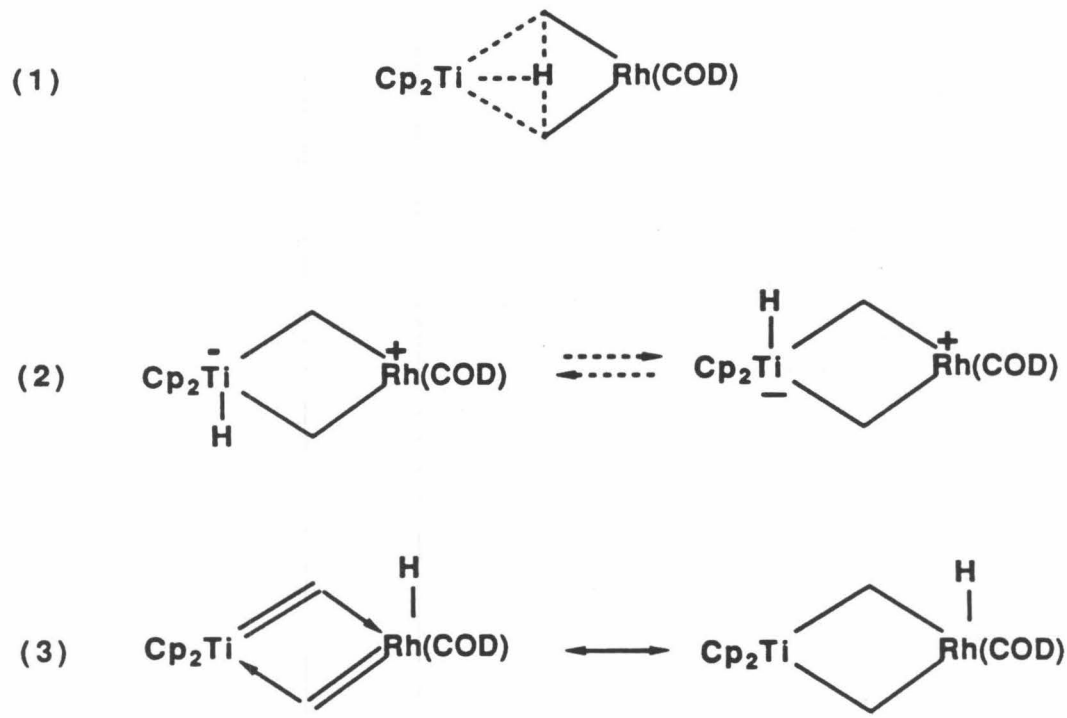

Scheme II. Three mechanisms of the equilibration between μ-CH_2 and μ-CH_3 groups in the complex **4a**. (1) 4e-4c concerted mechanism, (2) oxidative addition of C–H bond on titanium center, and (3) α-elimination on rhodium and hydride-carbene insertion.

Reaction of 3a and 4a with Carbon Monoxide. A ligand of the rhodium atom, 1,5-cyclooctadiene, was easily displaced by the carbon monoxide at low temperature. The product could not be isolated due to its thermal instability. The product was identified by its ^{13}C NMR, where two new resonances of carbon monoxide having ^{103}Rh-^{13}C coupling along with free COD were observed (eq 12).

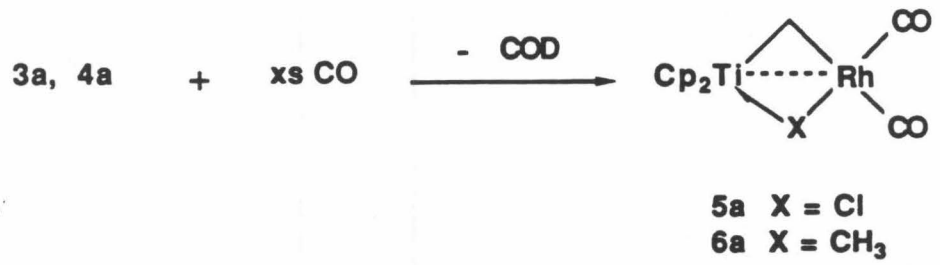

(12)

Complex transformations were observed with ^{1}H, ^{13}C NMR when trimethylphosphine was allowed to react with the complexes **5a, 6a**. The product distribution was dependent on the concentration of trimethylphosphine. Insertion of carbon monoxide in the μ-CH_3 and/or μ-CH_2 group and breaking of bridge between the chloride and rhodium for an additional ligand on rhodium[10b] can be presumed.

Table I. Rate Constant for the Rotation versus Temperature.

Temperature (°K)	Rate constant (sec^{-1})
313	9.09×10^5
303	5.56×10^5
293	2.99×10^5
283	1.71×10^5
273	1.03×10^5
233	3.13×10^3
223	1.46×10^3
212	5.00×10^2
202	2.11×10^2

Table V. Rate Constant (k_D) for the C–D Activation in Complex **4a**.

Temperature (°K)	Rate Constant (sec^{-1})	Average rate constant (sec^{-1})
368	1.5×10^{-5}	1.5×10^{-5}
348	1.4×10^{-6}	1.4×10^{-6}
318	3.4×10^{-7}	3.6×10^{-7}
	4.1×10^{-7}	
	3.2×10^{-7}	

Table II. Selected Bond lengths and Angles

Distances (Å)		Angles (°)	
Rh–Ti	2.835(1)	Rh –CB1–Ti	83.9(2)
Rh –CB1	2.094(5)	Rh–CB2–Ti	80.0(2)
Rh –CB2	2.110(6)	CB1–Rh–CB2	101.7(2)
Rh–CD1	2.083(6)	CB1–Ti–CB2	94.4(2)
Rh–CD4	2.087(8)	Rh–CB1–CB1H	105(2)
Ti–CB1	2.147(5)	Rh–CB2–CB2B	141(3)
Ti–CB2	2.294(6)	Rh–CB2–CB2A	100(3)
Ti–CB2B	2.01(5)	Ti–CB1–CB1H	123(2)
Ti–Cp	2.076(4)	Ti–CB2–CB2B	61(3)
CB1–CB1H	0.91(3)	Ti–CB2–CB2A	124(3)
CB2–CB2A	0.98(4)	CD1–Rh–CD4	86.0(3)
CB2–CB2B	0.92(5)	CB1H–CB1–CB1H	108(3)
		CB2B–CB2–CB2A	102(5)
		CB2A–CB2–CB2A	110(4)

Table III. Crystal and Intensity Collection Data.

Formula : $C_{20}H_{27}RhTi$ Formula Weight : 418.24

Crystal Color : Yellow

a = 8.219(1) Å

b = 16.330(2) Å

c = 12.613(2) Å

V = 1692.9(7) $Å^3$ Z = 4

λ = 0.7107 Å T : 21°

Space group : *Pbcm* (#57)

Crystal Size : 0.11 x 0.14 x 0.26 mm

CAD-4 Diffractometer

Number reflections measured : 7298

Number of independent reflections : 1560

Number with $F_o^2 > 0$: 1434

Number with $F_o^2 > 3\sigma(F_o^2)$: 1274

Final R-index : 0.032 (0.025 for $F_o^2 > 3\sigma(F_o^2)$)

Final goodness of fit : 1.98 for 1560 data and 134 parameters.

Table IV. Rate Constant (k_H) for the C–H Activation in Complex **4a**.

Temperature (°K)	Rate constant (sec^{-1})	Average rate constant (sec^{-1})
383	2.24×10^{-4}	2.24×10^{-4}
378	1.39×10^{-4}	1.39×10^{-4}
373	8.05×10^{-5}	8.05×10^{-5}
368	6.11×10^{-5}	6.11×10^{-5}
358	3.75×10^{-5}	3.06×10^{-5}
	2.37×10^{-5}	
348	2.62×10^{-5}	2.00×10^{-5}
	1.40×10^{-5}	
	1.98×10^{-5}	
338	1.81×10^{-5}	1.55×10^{-5}
	1.15×10^{-5}	
	1.69×10^{-5}	
328	3.40×10^{-6}	1.36×10^{-5}
	1.53×10^{-5}	
	2.20×10^{-5}	
318	9.43×10^{-6}	8.56×10^{-5}
	7.68×10^{-6}	

EXPERIMENT

General. All manipulation of air and/or moisture sensitive compounds were carried out with use of standard Schlenk or vacuum line techniques. Argon was purified by passage through columns of BASF RS-11 catalyst (Chemalog) and Linde 4 Å molecular sieves. Solids were transferred and stored in a N_2-filled Vacuum Atmosphere glove box equipped with a MO-40-1 purification train and a DK-3E Dri-Kool conditioner, and Dri-Cold Freezer.

Toluene, benzene, diethyl ether, and tetrahydrofuran were stirred over CaH_2, then transferred to purple sodium-benzophenone ketyl. Pentane and hexane were stirred over concentrated H_2SO_4, washed with H_2O, dried over CaH_2, then transferred over P_2O_5 or CaH_2 and degassed by freeze-pump-thaw cycles. Dried degassed solvents were vacuum-transferred into dry glass vessels equipped with Teflon valve closures and stored under argon. Benzene-d_6, toluene-d_8, and tetrahydrofuran-d_8 (Cambridge Isotope) were dried and vacuum-transferred from purple sodium-benzophenone ketyl. Dichloromethane-d_2 (Cambridge Isotope, Norell) was dried over CaH_2 or Na-Pb alloy and degassed by several freeze-pump-thaw cycles. Carbon monoxide (Matheson), etheral solution of MeLi (Aldrich) and MeMgBr (Aldrich) were used as received. Tebbe's reagent[4e,41] and β,β-dimethyltitanacyclobutane **1**[28] were prepared as previously described.

NMR spectra were recorded on Varian EM-390 (90 MHz, ^1H), JEOL FX-90Q (89.60 MHz, ^1H; 22.53 MHz, ^{13}C; 36.27 MHz, ^{31}P), and JEOL GX-400 (399.65 MHz, ^1H; 100.4 MHz, ^{13}C) spectrometers. Chemical shifts are reported in δ, referenced to residual solvent signals. $^{31}P\{^1H\}$ NMR data are referenced

externally to 85% H_3PO_4 (downfield positive). Infrared spectra were recorded on a Mattson Sirius 100 FT-IR spectrometer and Perkin-Elmer 1720 (FT) spectrometer. UV-vis spectra were measured on a Hewelett Packard 8415A diode array spectrophtometer. Elemental analyses (C,H,N) were performed by the California Institute of Technology Analytical Services.

Preparation of 3a. The compound was prepared by the known method.[9] The starting material, $[Rh(COD)Cl]_2$ was purchased or synthesized from rhodium trichloride hydrate (Strem) by the literature method.[42] A mixture of β,β-dimethyltitanocene cyclobutane (0.40 g, 1.61 mmol) and $[Rh(COD)Cl]_2$ (0.40 g, 0.81 mmol) was dissolved in toluene (30 mL) at room temperature, and stirred for 10 min. (The yield was 60% based on the integration in the ^1H NMR compared with that of internal standard, previously calibrated with the pure compound.) The resulting solution was concentrated in a vacuum at room temperature to yield red powders. This material was used without further purification. ^1H NMR (C_6D_6, r.t.) δ 7.48 (s, 2H, μ-CH_2), 5.50 (s, 10H, Cp), 4.97 (m, 2H, olefinic COD), 3.95 (m, 2H, olefinic COD), 2.4-1.3 (m, 8H, COD). ^{13}C NMR (C_6D_6, r.t.) δ 186.5 (td, J_{CH} = 128 Hz, J_{CRh} = 20Hz, μ-CH_2), 107.9 (dm, J_{CH} = 173 Hz, Cp), 89.5(dd, J_{CH} = 155 Hz, olefinic COD) 77.1 (dd, J_{CH} = 155 Hz, J_{CRh} = 16 Hz, olefinic COD), 33.0 (t, J_{CH} = 128 Hz, COD), 29.9 (t, J_{CH} = 128 Hz, COD). λ_{max} (THF) = 392, 486 nm.

Preparation of 4a. A mixture of crude **3a** prepared by the above procedure and dry MeLi (81 mg, 3.21 mmol, activity = 0.87) was dissolved in toluene (30 mL) and diethyl ether (30 mL) at room temperature, and stirred for 2 hours. (The total yield was 31% based on the integration in the ^1H NMR compared with that of internal standard, previously calibrated with the pure compound.) After the mixture was evaporated to dryness, the residue was

extracted with toluene (30 mL). Evaporation of the toluene solution to dryness was followed by extraction with diethyl ether (50 mL). The diethyl ether solution was concentrated to half of its volume at room temperature. Three consecutive recrystallizations at –50 °C gave 60-90 mg (9-13%) of red crystals, suitable for single X-ray crystallography. ^{1}H NMR(tol-d_8/THF-d_8 = 3/1, r.t.) δ 7.24 (s, 2H, μ-CH_2), 5.30 (s, 10H, Cp), 4.13-4.09 (m, 4H, olefinic COD), 2.18-2.08 (m, 4H, COD), 2.02-1.98 (m, 4H, COD), -3.13 (br, 3H, μ-CH_3); ^{1}H NMR at – 92 °C δ 1.28 (d, 2H, J = 12.8 Hz, terminal ^{1}H of μ-CH_3), -12.15 (t, 1H, J = 12.8 Hz, bridging ^{1}H of μ-CH_3); ^{13}C NMR (tol-d_8/THF-d_8 = 3/1, r.t.) δ 185.4 (dt, J_{CH} = 129 Hz, J_{CRh} = 24 Hz, μ-CH_2), 104.7 (dm, J_{CH} = 172 Hz, Cp), 84.1 (d, J_{CH} = 151 Hz, olefinic COD), 82.9 (d, J_{CH} = 158 Hz, olefinic COD) , 49.7 (dq, J_{CH} = 114 Hz, J_{CRh} = 29 Hz, μ-CH_3), 32.4 (t, J_{CH} = 126 Hz, COD), 31.6 (t, J_{CH} = 128 Hz, COD); ^{13}C NMR at – 92 °C δ 51.1 (ddt, $^bJ_{CH}$ = 87.7 Hz, $^tJ_{CH}$ = 126.7 Hz, J_{CRh} = 29.9 Hz, μ-CH_3); Anal. Calcd for $C_{20}H_{27}RhTi$: C, 57.44; H, 6.51. Found: C, 61.82: H, 6.42. IR (KBr): 3030, 3018, 2999, 2959, 2924, 2874, 2868, 2820, 2496 (ν_{CH} of the agostic hydrogen), 1488, 1446, 1439, 1426, 1331, 1176, 1029, 1024, 1013, 799, 790, 767 cm^{-1}. λ_{max} (THF) = 430, 486 nm.

Preparation of 3b. A procedure similar to that used to prepare **3a** was followed. A starting material [Ir(COD)Cl]$_2$ (Strem) was used as received. ^{1}H NMR (C_6D_6, r.t.) δ 7.95 (s, 2H, μ-CH_2), 5,42 (s, 10H, Cp), 4.57 (m, 2H, olefinic COD), 3.71 (m, 2H, olefinic COD), 2.4-1.3 (m, 8H, COD). ^{13}C NMR (C_6D_6, r.t.) δ 180.7 (t, J_{CH} = 132 Hz, μ-CH_2), 107.2 (dm, J_{CH} = 174 Hz, Cp), 70.4 (d, J_{CH} = 153 Hz, olefinic COD), 62.1 (d, J_{CH} = 156 Hz, olefinic COD), 33.0 (t, J_{CH} = 134 Hz, COD), 30.4 (t, J_{CH} = 134 Hz, COD).

Preparation of 4b. A procedure similar to that used to prepare **4a** was followed, except that two equivalents of MeMgBr were used intead of MeLi.

(The total yield was 49% based on the integration in the ^{1}H NMR compared with that of internal standard, previously calibrated with the pure compound.) ^{1}H NMR (tol-d_8, r.t.) δ 7.46 (s, 2H, μ-CH_2), 5.17 (s, 10H, Cp), 3.90(m, 2H, olefinic COD), 3.76 (m, 2H, olefinic COD), 2.06 (m, 4H, COD), 1.85 (m, 4H, COD), –2.93 (br, 3H, μ-CH_3); ^{1}H NMR at –92 °C δ 1.14 (d, 2H, terminal ^{1}H of μ-CH_3), –11.5 (t, 1H, bridging ^{1}H of μ-CH_3); ^{13}C NMR (tol-d_8, r.t.) δ 177.2 (t, J_{CH} = 132 Hz, μ-CH_2), 104.3 (dm, J_{CH} = 173 Hz, Cp), 69.0 (s, J_{CH} = 159 Hz, olefinic COD), 68.5 (s, J_{CH} = 156 Hz, olefinic COD), 48.5 (q, J_{CH} = 115 Hz, μ-CH_3), 32.1 (t, J_{CH} = 128 Hz, COD), 31.5 (t, J_{CH} = 126 Hz, COD); ^{13}C NMR at –92 °C δ 49.6 (dt, $^bJ_{CH}$ = 91.0 Hz, $^tJ_{CH}$ = 127.3 Hz, μ-CH_3). Anal. Calcd for $C_{20}H_{27}IrTi$: C, 47.33; H, 5.36. Found: C, 47.03; H, 5.29. IR (KBr): 3001, 2929, 2881, 2869, 2852, 2823, 2506 (ν_{CH} of the agostic hydrogen), 2023, 1956, 1462, 1448, 1440, 1375, 1328, 1030, 1024, 1013, 804, 791 cm^{-1}.

Complete Line-Shape Analysis. A Nicolet 1280 computer and Nicolet NMC software were used to simulate two-site exchange in the ^{1}H NMR. The equation used to calculate the exchange simulation is

```
y(x) = K * [P * (1 + T * C) + Q * R] / [P ** 2 + R ** 2]
```

where

```
P = T * [J – E ** 2 + B ** 2] + G
G = T * (E – D)
R = E * {1 + T * [W(1) + W(2)]} + D + T * B * [W(2) – W(1)]
```

and

```
A = pi * [F(1) + F(2)]
B = pi * [F(1) – F(2)]
C = N(1) * W(2) + N(2) * W(1)
G = N(1) * W(1) + N(2) * W(2)
D = B * [N(1) – N(2)]
E = A – x
F(1) = "FREQ(A)"
F(2) = "FREQ(B)"
J = W(1) * W(2)
K = "SCALE(Y)"
N(1) = "FRACTION(A)"
N(2) = 1 – N(1)
T = "TAU" = 1/(exchange rate)
W(1) = pi * "LINE WIDTH(A)"
W(2) = pi * "LINE WIDTH(B)"
```

Partial Deuteration. A mixture of CHD_2Li, CH_2DLi, and CH_3Li (mole ratio = 0.73: 0.16: 0.12) was obtained through four steps: (1) reduction of *n*-butyl formate with $LiAlD_4$ to make CHX_2OH (X = H or D) (Y = 31-68%),[43] (2) tosylation with tosyl cholride to generate CHX_2OTs (Y = 37-69%),[44] (3) substitution of the tosylate group by a potassium iodide (Y = 77-91%),[45] and (4) reaction of CHX_2I with lithium metal (Y = 84%).[46] $^{13}C\{^1H\}$ NMR (THF-d_8) δ –15.9 (quintet); isotopic impurities were observed as well. A mixture of $Cp_2TiRh(COD)(\mu\text{-}CH_2)(\mu\text{-}CHX_2)$ (X = H or D) was obtained by the procedure similar to that for the preparation of **4a**. Chemical shifts of $\mu\text{-}CH_3$, $\mu\text{-}CH_2D$, and $\mu\text{-}CHD_2$ groups were measured on a JEOL FX-90Q spectrometer at temperatures between 20 and 70 °C.

Preparation of $Cp_2TiRh(COD)(\mu\text{-}CX_2)(\mu\text{-}CX_3)$ (X = H or D). Crystalline $Cp_2TiRh(COD)(\mu\text{-}CH_2)(\mu\text{-}CD_3)$ (**4a-CD_3**) (95mg, 0.23 mmol) was prepared from β,β-dimethyltitanocene cyclobutane **1** and $[Rh(COD)Cl]_2$ (0.40 g, 0.81 mmol), and two equivalents of CD_3Li. After the solution of **4a-CD_3** was heated in toluene (1.5mL) at 75 °C for 8 days, black metallic precipitates were separated by the filtration. The slow cooling of the double layer (pentane (7 mL)/toluene(2.5 mL)) gave a recrystallized title compound (43 mg, 0.10 mmol). ^1H and ^2H NMR showed that the deuterium content was 47% in the bridging methylene position and 69% in the bridging methyl position.

Cross-over Experiment. To find the molecularity of the reaction, $Cp_2TiRh(COD)(\mu\text{-}CH_2)(\mu\text{-}^{13}CH_3)$ (**4a-$^{13}CH_3$**) (7.0 mg) prepared from **3a** and $^{13}CH_3Li$ was mixed with $Cp_2TiRh(COD)(\mu\text{-}CX_2)(\mu\text{-}CX_3)$ (X = H or D) (7.0 mg) in a NMR tube. The NMR tube was flame sealed after dissolving in tol-d_8 (400 μL) and THF-d_8 (20μL). The regions of $\mu\text{-}CH_3$ and $\mu\text{-}CH_2$ groups in the ^{13}C NMR was observed after heating the sealed NMR tube for $2t_{1/2}$ at both

extreme temperatures (105, 45 °C). (Half-life $t_{1/2}$ can be estimated from k_D, the rate constant of the C–D activation.)

Kinetics. $Cp_2TiM(COD)(\mu\text{-}CH_2)(\mu\text{-}^{13}CH_3)$ (M = Rh, Ir) were prepared by a method similar to that of **4a**, **4b**, $^{13}CH_3Li$ or $^{13}CH_3MgBr$ was synthesized from $^{13}CH_3I$ (Cambridge Isotope, ^{13}C, 99%). $Cp_2TiM(COD)(\mu\text{-}CH_2)(\mu\text{-}^{13}CH_3)$ (M = Rh, Ir) (6 mg) was dissolved in tol-d_8 (400μL) and THF-d_8 (20 μL). After the NMR tube was sealed, several ^{13}C NMR spectra of heated samples over 45-110 °C were taken until three half-lives had elapsed. At least 700 scans were required for each $^{13}C\{^1H\}$ NMR spectra with a JEOL GX-400. The relative peak heights of $\mu\text{-}^{13}CH_2$ and $\mu\text{-}^{13}CH_3$ in the spectra were analyzed to obtain kinetic rate constants of C–H bond activation (k_H).* For the rate constants of C–D bond acivation (k_D), $^{13}C\{^1H\}$ NMR spectra of $Cp_2TiRh(COD)(\mu\text{-}CH_2)(\mu\text{-}^{13}CD_3)$ synthesized from $^{13}CD_3I$ (Cambridge Isotope, ^{13}C, 99%; ^1H, 99%) and ^2H NMR spectra of $Cp_2TiRh(COD)(\mu\text{-}CH_2)(\mu\text{-}CD_3)$ synthesized from CD_3I (Aldrich, ^2H, 99%) were measured. At three different temperatures (95, 75, 45 °C), k_D were measured by the same method as for the k_H except that only the early stage of the reaction was followed to avoid complications coming from the involvement of bridging methylene hydrogens.

Crystal strucure Determination of 4a. A crystal of 0.11 x 0.14 x 0.26 mm of **4a**, obtained through a slow cooling of the etheral solution at –50 °C, was mounted in a glass capillary under N_2. Oscillation and Weisenberg photographs indicated an orthorhombic crystal. The crystal was centered on a Nonius CAD-4 diffractometer and cell dimensions plus an orientation matrix were obtained from the setting angles of 25 reflections with $40^o < 2\theta < 46^o$. Altogether 7,298 reflections were scanned in four octants h, ±k, ±l with $0^o < 2\theta < 50^o$ (MoK_α) and in two octants ±h, k, l with $0^o < 2\theta < 25^o$, including three

check reflections measured every 5,000 seconds of X-ray exposure. The check reflections showed no fluctuations greater than those expected from counting statistics. A θ-2θ scan was used at 2° (2θ) per minute, covering the $K\alpha_1$ and $K\alpha_2$ components. Backgrounds were measured for each reflection at each end of the scan; an average background as a function of 2θ was calculated and was used to correct the measured scan counts. After deleting space group absences and merging equivalent reflections, 1,560 independent reflections remained, of which 1,434 had $F_o^2 > 0$ and 1,274 had $F_o^2 > 3\sigma (F_o^2)$. The data were corrected for Lorentz and polarization factors, but not for absorption; μr_{max} is 0.23, and the several forms of the data averaged together within their expected deviations. Variances of the individual reflections were assigned based on counting statistics plus an additional term, $0.014I^2$. Variances for the merged reflections were determined by standard propagation of error plus another additional term, $0.014\langle I\rangle^2$.

The coordinates of the rhodium atom were obtained from a Patterson map and the rest of the structure was determined by successive structure factor-Fourier calculations. The systematic absences, $0\underline{k}\underline{l}$ with $\underline{k}$ odd and $\underline{h}0\underline{l}$ with $\underline{h}$ odd indicated space group *Pbcm* or $Pbc2_1$. Intensity statistics favored the centric space group and a model was developed with the rhodium, titanium and bridging atoms lying in the mirror plane. The cyclooctadiene ligand showed high apparent thermal motion and it was finally represented as two disordered groups of four carbon atoms each, the other four being generated by the mirror plane. This disorder can be removed by going to noncentro-symmetric space group Pbc_1, but because the overall structure is still nearly centric, the refinement in that space group was unsatisfactory. The same final R-index and goodness of fit were obtained, but the molecular geometry of

the ligands was worse and esd's in all the bond distances were 2.5-3 times larger. Hydrogen atoms could not be refined in $Pbc2_1$, but they behaved satisfactorily in *Pbcm*. Thus the reported structure is based on the space group *Pbcm* with a disordered COD ligand. The rhodium, titanium, bridging carbon, and Cp carbon atoms were given anisotopic thermal parameters; the disordered COD carbon atoms and all hydrogen atoms were treated isotropically. The half-hydrogen atoms on the COD ligand were placed at calculated positions 0.95 Å from the half-carbon atoms and were not refined; all the rest of the positional and thermal parameters, plus a scale factor and a secondary extinction parameter (Larson, E. C. *Acta Cryst.* **1967**, *23*, 664, eq 3) were refined in one matrix. All 1,560 reflections were used in the refinement; at convergence the R-index was 0.032 for the 1,434 reflections with $F_o^2 > 0$ ($R = \Sigma | F_o - |F_c| | / \Sigma F_o$) and 0.025 for the 1,274 strong reflections. The goodness of fit (= $[\Sigma(F_o^2 - F_c^2)^2/(n-p)]^{1/2}$) is 1.98 for 1,560 data and 134 parameters. The secondary extinction parameter refined to $0.29(4) \times 10^{-6}$.

Preparation of 5a. A NMR tube with **3a** (20 mg) in tol-d_8 was cooled to –78 °C. The color of the solution changed from red to orange with excess carbon monoxide injected through a syringe. Free COD and complex **5a** which is stable only below –70 °C were identified by the NMR. ^{1}H NMR(tol-d_8, –72 °C) δ 7.02 (s, 2H, μ-CH_2), 4.99 (s, 10H, Cp); ^{13}C NMR (tol-d_8, –72 °C), δ 191.2 (d, J_{CRh} = 86.8 Hz, CO), 186.1 (d, J_{CRh} = 62.8 Hz, CO), 158.0 (dt, J_{CH} = 134 Hz, J_{CRh} = 15.0 Hz, μ-CH_2), 116.6 (dm, Cp).

Preparation of 6a. A NMR tube with **4a** (20 mg) in tol-d_8 was cooled down to –78 °C. The color of the solution changed from orange to yellow with excess carbon monoxide injected through a syringe. Complex **6a** which is stable only below –50 °C was identified by the NMR. ^{1}H NMR (tol-d_8, –80 °C) δ 7.32

(s, 2H, μ-CH_2), 4.80 (s, 10H, Cp), 1.87 (d, 2H, $^2J_{HH}$ = 12 Hz, terminal ^{1}H of μ-CH_3), –12.2 (t, 1H, $^2J_{HH}$ = 12 Hz, bridging ^{1}H of μ-CH_3); ^{13}C NMR (tol-d_8, –80 °C), δ 195.4 (br, CO), 192.8 (br, CO), 169.6 (dt, J_{CH} = 134 Hz, J_{CRh} = 18 Hz, μ-CH_2), 116.7 (d, Cp), 49.1 (ddt, J_{CRh} = 21 Hz, μ-CH_3).

REFERENCES AND NOTES

(1) (a) Jacobson, E. N.; Goldberg, K. I.; Bergman, R. G. *J. Am. Chem. Soc.* **1988**, *110*, 3706-3707. (b) White, G. S.; Stephan, D. W. *Organometallics* **1988**, *7*, 903-910. (c) Gelmini, L.; Stephan, D. W. *Ibid.* **1988**, *7*, 849-855. (d) Sternal, R. S.; Sabat, M.; Marks, T. J. *J. Am. Chem. Soc.* **1987**, *109*, 7920-7921. (e) Sternal, R. S.; Marks, T. J. *Organometallics* **1987**, *6*, 2621-2623. (f) Casey, C. P.; Palermo, R. E.; Rheingold, A. L. *J. Am. Chem. Soc.* **1986**, *108*, 549-550. (g) Choukroun, R.; Gervais, D.; Jaud, J.; Kalck, P.; Senocq, F. *Organometallics* **1986**, *5*, 67-71. (h) Tso, C. T.; Cutler, A. R. *J. Am. Chem. Soc.* **1986**, *108*, 6069-6071. (i) Ferguson, G. S.; Wolczanski, P. T. *Organometallics* **1985**, *4*, 1601-1605. (j) Barger, P. T.; Bercaw, J. E. *Ibid.* **1984**,*3*, 278-284.

(2) Bullock, R. M.; Casey, C. P. *Acc. Chem. Res.* **1987**, *20*, 167-173.

(3) (a) Tauser, S. J. *Acc. Chem. Res.* **1987**, *20*, 389-394. (b) Baker, R. T. K.; Tauser, S. J.; Dumestic, J. A. Eds. *Strong Metal-Support Interaction;* American Chemical Society: Washington, DC, 1986. (c) Imelik, B.; Naccache, C.; Coudurier, G.; Praliaud, H.; Meriaudeau, P.; Gallezot, P.; Martin, G. A.; Verrine, J. C. Eds. *Strong Metal-Support and Metal-Additive Effects in Catalysis;* Elsevier: New York, 1982. (d) Tauster, S. J.; Fung, S. C.; Baker, R. T. K.; Horsley, T. A. *Science* **1981**, *211*, 1121-1125. (e) Doi, Y.; Miyake, H.; Soga, K. *J. Chem. Soc., Chem. Commun.* **1987**, 347-349. (f) Rieck, J. C.; Bell, A. T. *J. Catal.* **1986**, *99*, 267-277.

(4) (a) Smith, G. M.; Sabat, M.; Marks, T. J. *J. Am. Chem. Soc.* **1987**, *109*, 1854-1856. (b) Casey, C. P.; Audett, J. D. *Chem. Rev.* **1986**, *86*, 339-352. (c) Herrmann, W. A. *Adv. Organomet. Chem.* **1982**, *20*, 159-263. (d) Holton, J.; Lappert, M. F.; Pearce, R.; Yarrow, P. I. W. *Chem. Rev.* **1983**, *83*, 135-201.

(e) Tebbe, F. N.; Parshall, G. W.; Reddy, G. S. *J. Am. Chem. Soc.* **1978**, *100*, 3611-3613.

(5) (a) Collman, J. P.; Hegedus, L. S.; Norton, J. R.; Finke, R. G. *Principles and Applications of Organotransition Metal Chemistry;* University Science, Mill Valley, California, 1987, p 653. (b) Herrmann, W. A. *Angew. Chem. Int. Ed. Engl.* **1982**, *21*, 117-130. (c) Masters, C. *Adv. Organomet. Chem.* **1979**, *17*, 61-103.

(6) For existing models, see (a) Saez, I. M.; Meanwell, N. J.; Taylor, B. F.; Mann, B. E.; Maitlis, P. M. *J. Am. Chem. Soc., Chem. Commun.* **1987**, 361-363. (b) Saez, I. M.; Meanwell, N. J.; Nutton, A.; Isobe, K.; Vázquez de Miguel, A.; Bruce, D. W.; Okeya, S.; Andrew, D. G.; Ashton, P. R.; Johnstone, I. R.; Maitlis, P. M. *J. Chem. Soc. Dalton Trans.* **1986**, 1565-1575. (c) Toreki, R.; LaPointe, R. E.; Wolczanski, P. T. *J. Am. Chem. Soc.* **1987**, *109*, 7558-7560.

(7) (a) Ansyln, E. V.; Grubbs, R. H. *J. Am. Chem. Soc.* **1987**, *109*, 4880-4890. (b) Lee, J. B.; Gajda, G. J.; Schaefer, W. P.; Howard, T. R.; Ikariya, T.; Straus, D. A.; Grubbs, R. H. *J. Am. Chem. Soc.* **1981**, *103*, 7358-7361.

(8) (a) Tebbe, F. N.; Parshall, G. W.; Ovenall, D. W. *J. Am. Chem. Soc.* **1979**, *101*, 5074-5075. (b) Klabunde, U.; Tebbe, F. N.; Parshall, G. W.; Harlow, R. L. *J. Mol. Catlal.* **1980**, *8*, 37-51.

(9) (a) Mackenzie, P. B.; Ott, K. C.; Grubbs, R. H. *Pure and Appl. Chem.* **1984**, *56*, 59-61. (b) Mackenzie, P. B.; Coots, R. J.; Grubbs, R. H. submitted for publication in *Organometallics.*

(10) (a) Park, J. W.; Mackenzie, P. B.; Schaefer, W. P.; Grubbs, R. H. *J. Am. Chem. Soc.* **1986**, *108*, 6402-6404. (b) Fumiyuki, O.; Park, J. W.; Mackenzie, P. B.; Schaefer, W. P.; Henling, L. M.; Grubbs, R. H. submitted for

publication in *J. Am. Chem. Soc.*

(11) (a) Bleeke, J. R.; Kotyk, J. J.; Moore, D. A.; Rauscher, D. J. *J. Am. Chem. Soc.* **1987**, *109*, 417-423. (b) Brookhart, M.; Noh, S. K.; Timmers, F. J. *Organometallics* **1987**, *6*, 1829-1831. (c) Vites, J. C.; Jacobsen, C.; Dutta, T. K.; Fehlner, T. P. *J. Am. Chem. Soc.* **1985**, *107*, 5563-5565. (d) Dutta, T. K.; Vites, J. C.; Jacobsen, G. B.; Fehlner, T. P. *Organometallics*, **1987**, *6*, 842-847. (e) Jensen, J. A.; Wilson, S. R.; Schultz, A. J.; Girolami, G. S. *J. Am. Chem. Soc.* **1987**, *109*, 8094-8096. (f) Brookhart, M.; Green, M. L. H. *J. Organomet. Chem.* **1983**, *250*, 395-408, and references cited therein.

(12) (a) Crabtree, R. H. *Chem. Rev.* **1985**, *85*, 245-269. (b) Bergman, R. G. *Science*, **1984**, *223*, 902-908. (c) Parshall, G. W. *Chemtech* **1984**, 628-638. (d) Somorjai, G. A.; Davis, S. M. *Chemtech* **1983**, 502-511. (e) Muetterties, E. L.; Rhodin, T. L.; Band, E.; Brucker, C. F.; Pretzer, W. R. *Chem. Rev.* **1979**, *79*, 91-137.

(13) (a) Saillard, J.-Y.; Hoffman, R. *J. Am. Chem. Soc.* **1984**, *106*, 2006-2026. (b) Eisenstein, O.; Jean, Y. *J. Am. Chem. Soc.* **1985**, *107*, 1177-1186. (c) Johnson, C. E.; Eisenberg, R. *J. Am. Chem Soc.* **1985**, *107*, 3148-3160. (d) Lichtenberger, D. L.; Kellog, G. E. *J. Am. Chem. Soc.* **1986**, *108*, 2560-2567. (e) Harlow, R. L.; Mckinney, R. J.; Ittel, S. D. *J. Am. Chem. Soc.* **1979**, *101*, 7496-7504. (f) Koga, N.; Obara, S.; Morokuma, K. *J. Am. Chem. Soc.* **1984**, *106*, 4625-4626. (g) Bursten, B. E.; Cayton, R. H. *Organometallics* **1986**, *5*, 1051-1053.

(14) (a) Kubas, G. J. *Acc. Chem. Res.* **1988**, *21*, 120-128. (b) Crabtree, R. H.; Hamilton, D. G. *Adv. Organomet. Chem.* **1988**, *28*, 299-338.

(15) (a) Sinfelt, J. H. *Acc. Chem Res.* **1987**, *20*, 134-139. (b) Sinfelt, J. H. *Bimetallic Catalysts: Discoveries, Concepts, and Applications;* Wiley: New

York, 1983.

(16) COD represents 1,5-cyclooctadiene.

(17) Part of this chapter was presented in *J. Am. Chem. Soc.* (ref. 10a), and at the 195th ACS National Meeting of the American Chemical Society, Toronto, Canada, June, 1988; paper INOR 217.

(18) (a) Paramagnetic species from the decomposition were the major by-product. (b) Poorer yield was obtained with a alternative route utilizing $[Rh(COD)(\mu\text{-}CH_3)]_2$ and β,β-dimethyltitanacyclobutane.

(19) Bursten, B. E.; Cayton, R. H. *Organometallics* **1986**, *5*, 1051-1053.

(20) (a) Waymouth, R. M.; Santarsiero, B. D.; Coots, R. J.; Bronikowski, M. J.; Grubbs, R. H. *J. Am. Chem. Soc.* **1986**, *108*, 1427-1441. (b) Waymouth, R. M.; Santarsiero, B. D.; Grubbs, R. H. *J. Am. Chem. Soc.* **1984**, *106*, 4050-4051. (c) Watson, P. L. *J. Am. Chem. Soc.* **1983**, *105*, 6491-6493.

(21) Silverstein, R. M.; Bassler, G. C.; Morrill, T. C. *Spectrometric Identification of Organic Compounds*, 4th ed.; Wiley: New York, 1981.

(22) Schmidt, G. F.; Muetterries, E. L.; Beno, M. A. Williams, J. M. *Proc. Natl. Acad. Sci. U. S. A.* **1981**, *78*, 1318-1320.

(23) (a) Martin, M. L.; Martin, G. J.; Delpuech, J. J. *Practical NMR Spectroscopy;* Heyden & Sons: London, 1980; p 339. $\Delta G^{\neq} = [45.45 - 1.98\log(\Delta\nu/T_c)]T_c$, $\Delta\nu$ in Hz, T_c in absolute temperature. (b) For agostic bonds with manganese, rotational activation-energy of 8.3 Kcal/mol was observed. See ref. 11f and Brookhart, M.; Lamanna, W.; Humphrey, M. B. *J. Am. Chem. Soc.* **1982**, *104*, 2117-2126.

(24) The uncertainty can be ascribed to the possible existence of steric hindrance, inherent rotational energy. Also, mechanisms of the rotation, which can be either rotation through the state having agostic interactions

between two hydrogens and a metal or rotation with discrete formation and breaking of the agostic bond, affect the interpretation.

(25) (a) Binsch, G.; Kessler, H. *Angew. Chem. Int. Ed. Engl.* **1980**, *19*, 411-494. (b) Jesson, J. P.; Meakin, P. *Acc. Chem Res.* **1973**, *6*, 269-275. (c) Campbell, I. D.; Dobson, C. M.; Ratcliffe, R. G.; Williams, R. J. P. *J. Magn. Reson.* **1978**, *29*, 397-417.

(26) Dawoodi, Z.; Green, M. L. H.; Mtetwa, V. S. B.; Prout, K. *J. Chem. Soc., Chem. Commun.* **1982**, 802-803.

(27) Sakellson, S.; McMillan, M.; Haller, G. L. *J. Phys. Chem.* **1986**, *90*, 1733-1736.

(28) (a) Straus, D. A.; Grubbs, R. H. *Organometallics* **1982**, *1*, 1658-1661. (b) Straus, D. A. Ph. D. Thesis, California Institute of Technology, Pasadena, California, 1983.

(29) Upton, T. H.; Rappé, A. K. *J. Am. Chem. Soc.* **1985**, *107*, 1206-1218.

(30) (a) Calvert, R. B.; Shapley, J. R. *J. Am. Chem. Soc.* **1978**, *100*, 7726-7727. (b) Calvert, R. B.; Shapley, J. R.; Schultz, A. J.; Williams, J. M.; Suib, S. L.; Stucky, G. D. *Ibid.* **1978**, *100*, 6240-6241.

(31) For examples of C–H bond activation in the dinuclear system, see ref. 1a. See also, (a) McGhee, W. D.; Bergamn, R. G. *J. Am. Chem. Soc.* **1986**, *108*, 5621-5622. (b) Berry, D. H.; Eisenberg, R. *J. Am. Chem. Soc.* **1985**, *107*, 7181-7183. (c) Nubel, P. O.; Brown, T. L. *J. Am. Chem. Soc.* **1984**, *106*, 644-652. (d) Fryzuk, M. D.; Jones, T.; Einstein, F. W. B. *Organometallics* **1984**, *3*, 186-191.

(32) Spin-lattice relaxation times (T_1) of ^{13}C nucleus of μ-CH_2 and μ-CH_3 group in **4a** were measured by the inversion-recovery method with a Jeol supplied program on JEOL GX-400. Similar T_1 values (890 msec for

μ-CH_2; 860msec for μ-CH_3) and the fact that the same peak heights were achieved after prolonged heating supported the suitability of using the relative peak heights for the rate constant measurement without any adjustment.

(33) Moore, J. W.; Pearson, R. G. *Kinetics and Mechanism*, 3rd ed., John Wiley & Sons, New York: 1981, p 304.

(34) For examples of large kinetic isotope effect involving metal atom, see (a) Roecker, L.; Meyer, T. J. *J. Am. Chem. Soc.* **1987**, *109*, 746-754. (b) Bruno, J. W.; Smith, G. M.; Marks, T. J.; Fair, C. K.; Schultz, A. J.; Williams, J. M. *Ibid.* **1986**, *108*, 40-56.

(35) (a) Brunton, G.; Griller, D.; Barclay, L. R. C.; Ingold, K. U. *J. Am. Chem. Soc.* **1976**, *98*, 6803-6811. (b) Caldin, E. F. *Chem. Rev.* **1969**, *69*, 135-156. (c) Bell, R. P. *Chem. Soc. Rev.* **1974**, *3*, 513-544. (d) Harmony, M. D. *Chem. Soc. Rev.* **1972**, *1*, 211-228.

(36) Bell, R. P. *The Tunnel Effect in Chemistry*; Chapman and Hall: New York, 1980.

(37) (a) Rothwell, I. P. *Acc. Chem. Res.* **1988**, *21*, 153-159. (b) Bruno, J. W.; Smith, G. M.; Marks, T. J.; Fair, C. K.; Schultz, A. J.; Williams, J. M. *J. Am. Chem. Soc.* **1986**, *108*, 40-56. (c) Fendrick, C. M.; Marks, T. J. *J. Am. Chem Soc.* **1986**, *108*, 425-437. (d) Watson, P. L. *J. Am. Chem. Soc.* **1983**, *105*, 6491-6493. (e) Thompson, M. E.; Baxter, S. M.; Bulls, A. R.; Burger, B. J.; Nolan, M. C.; Santarsiero, B. D.; Schaefer, W. P.; Bercaw, J. E. *J. Am. Chem. Soc.* **1987**, *109*, 203-219. (f) Rabaâ, H.; Saillard, J.-Y.; Hoffmann, R. *J. Am. Chem. Soc.* **1986**, *108*, 4327-4333.

(38) (a) Crespo, M.; Puddephatt, R. J. *Organometallics*, **1987**, *6*, 2548-2550. (b) Stille, J. K.; Lau, K. S. Y. *Acc. Chem. Res.* **1977**, *10*, 434-442.

(39) (a) Schrock, R. R. *Acc. Chem. Res.* **1979**, *12*, 98-104. (b) Churchill, M. R.; Wasserman, H. J.; Turner, H. W.; Schrock, R. R. *J. Am. Chem. Soc.* **1982**, *104*, 1710-1716.

(40) Carter, E. A.; Goddard III, W. A. *Organometallics,* **1988**, *7*, 675-686.

(41) Lee, J. B.; Ott, K. C.; Grubbs, R. H. *J. Am. Chem. Soc.* **1982**, *104*, 7491-7496.

(42) Giodano, G.; Crabtree, R. H. *Inorg. Synth.* **1979**, *19*, 218-220.

(43) (a) Nystrom, R. F.; Yanko, W. H.; Brown, W. G. *J. Am. Chem. Soc.* **1948**, *70*, 441. (b) Hochstein, F. A. *J. Am. Chem. Soc.* **1949**, *71*, 305-307. (c) Nystrom, R. F.; Brown, W. G. *Ibid.* **1947**, *69*, 1197-1199.

(44) (a) Edgell, W. F.; Parts, L. *J. Am. Chem. Soc.* **1955**, *77*, 4899-4902. (b) Fieser L. F.; Fieser, M. *Reagents for Organic Synthesis;* Wiley:New York, 1967, vol. 1, 1179-1181.

(45) Drahowzal, F.; Klamann, D. *Monatsh. Chem.* **1951**, *82*, 970-977.

(46) Wakefield, B. J. *The Chemistry of Organolithium Compounds,*Pergamon: Oxford, New York, 1974.

CHAPTER 2

Structure of Titanium–Rhodium Heterobinuclear Complexes with μ-Phenyl Ligand Retaining *ipso* Interaction

ABSTRACT

The heteronuclear μ-methylene μ-phenyl complexes, $Cp_2TiRh(1,5\text{-}COD)(\mu\text{-}CH_2)(\mu\text{-}p\text{-}(CH_3)_2NC_6H_4)$ (**3b**), $Cp_2TiRh(1,5\text{-}COD)(\mu\text{-}CH_2)(\mu\text{-}o\text{-}MeOC_6H_4)$ (**3c**) were synthesized from the $Cp_2TiRh(1,5\text{-}COD)(\mu\text{-}CH_2)(\mu\text{-}Cl)$ (**1**) with appropriate lithium compounds. The structure of **3b** has been determined by single crystal X-ray crystallography. The two metal atoms are bridged by the methylene carbon and the *ipso* carbon of the *p-N,N*-dimethylaminophenyl group. Complex **3b** crystallizes in the triclinic system, in space group *P1* (#2), with a = 8.988(1) Å, b = 10.169(1) Å, c = 13.707(2) Å, α = 102.85(1)°, β = 103.47(1)°, γ = 101.36(1), and V = 1145.6(3) $Å^3$; Z = 2. The analogous structure of **3c** has been verified by the differential NOE. The aromaticity of the phenyl group in **3b** observed by ^1H NMR, was confirmed by the comparison of the C-C bond lengths in the crystallographic structure. The unusual downfield shifts of the *ipso* carbon of **3b** and **3c** in the ^{13}C NMR are assumed to be an indication of the interaction between the *ipso* carbon and electron-deficient titanium.

INTRODUCTION

Many examples of arene bonding modes have been characterized in organometallic chemistry.[1] One type involves a bridging *ipso* carbon atom between two metal centers.[2] The structures of these compounds with bridging phenyl group have been characterized by spectroscopy and/or single crystal X-ray crystallography.[3] This type of structure has been suggested as an intermediate of bimolecular aryl exchange reactions.[4] Crystallography showed unambiguously the bridging structure between the transition-metals, or between the transition metal and the main-group-metal. No crystallographic structure with a bridge between two different transition metals, which manifests an asymmetrical bridging phenyl structure, was known. The bridging phenyl structure is analogous to that of some early transition-metal complexes with benzyl ligand. The latter showed an η^2-interaction through both the methylene carbon and the phenyl π-system.[5] The structure is also reminiscent of the arometic σ-complexes, the Wheland intermediate, in aromatic electrophilic substitution.[6]

RESULTS AND DISCUSSION

The heteronuclear μ-methylene complex $Cp_2TiRh(1,5\text{-}COD)(\mu\text{-}CH_2)(\mu\text{-}Cl)$[7] reacted with phenyl lithium to give an interesting heteronuclear μ-methylene μ-phenyl complex which is not thermally stable enough to be isolated for the full characterization. The formation of the agostic bond to satisfy the electron deficiency on the titanium center of the $Cp_2TiRh(1,5\text{-}COD)\text{-}(\mu\text{-}CH_2)(\mu\text{-}CH_3)$[8] prompted the addition of an electron donating group on the phenyl ring to stabilize the heteronuclear μ-methylene μ-phenyl complex. As expected, substitution of *ortho* or *para* position of the phenyl ring with methoxy or *N,N*- dimethylamino group increased the thermal stability substantially (eq 1). The half-lives of the complexes, **3b** and **3c**, are 24 and 8 hours in the hydrocarbon solution, respectively, at room temperature.

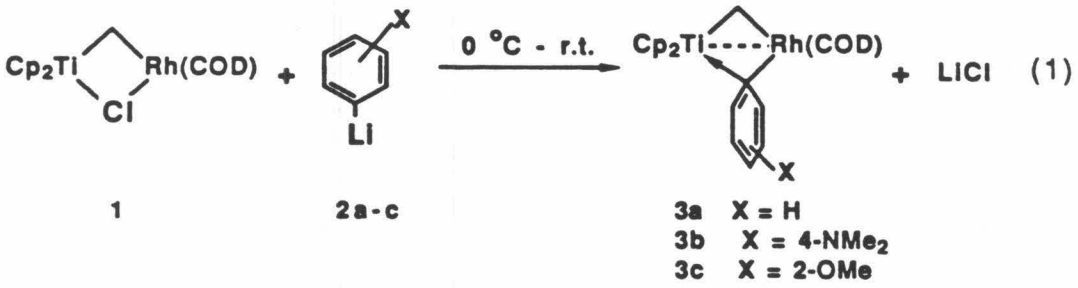

The yields determined by ^1H NMR, based on mesitylene which was calibrated with the pure product, are 33% for **3b** and 58% for **3c**. A single crystal of **3b** suitable for X-ray crystallography was obtained through several recystallizations at –50 °C. (The yield was approximately 10%.)

The X-ray crystal structure of **3b** was determined, and an ORTEP

diagram is shown in Fig. 1. The selected distances and angles are shown in Table I. Table II lists the data collection details. The molecule contains no crystallographic symmetry-elements. The two cyclopentadienyl rings are coordinated to the titanium atom with Ti-ring centroid distances of 2.115(4) and 2.092(4) Å. The cyclopentadiene ligand is coordinated to the rhodium atom with Rh-double bond centroid distances of 2.076(4) and 2.055(4) Å. The titanium atom has a pseudotetrahedral structure, while the rhodium maintains a pseudosquare-planar structure. All internal organic bond lengths and angles are normal.

The two metal atoms are separated by 2.827(1) Å and bridged by the methylene carbon CB and the carbon C_i of the *N,N*-dimethylaminophenyl group. The distance between the two metal atoms is comparable with that of μ-methylene μ-methyl analogue (2.835(1) Å),[8] and is shorter than that of μ-methylene μ-chloride analogue (2.986(1) Å).[7b] The Ti-Rh bond length of 2.827(1) Å is sufficiently short such that direct metal-metal interaction is possible. For example, the Ti-Rh distance is 2.68 Å in an alloy of the two metals,[9] and the Ti-Rh distance in a highly reduced Rh on titania is 2.55 Å.[10] The Ti-CB bond length of 2.076(4) Å is shorter than that of the μ-methylene μ-methyl analogue (2.147(5) Å), and is longer than that of the μ-methylene μ-chloride analogue (2.015(2) Å). However, all of the J_{CH} values for the μ-methylene are 129, 128 Hz, which reflects very similar bonding character of the μ-methylene in those complexes. (See Ref. 7b, 11 for the further discussion.) The calculated bond length for a Ti=CH_2 double bond is 1.85-1.88Å,[12] and the Ti-C distance in β,β-dimethyltitanocene cyclobutane is 2.15 Å. The observed bond length of 2.076(4) Å suggests some residual multiple bonding character between the Ti and CH_2 group in the complex. The Rh–C_i

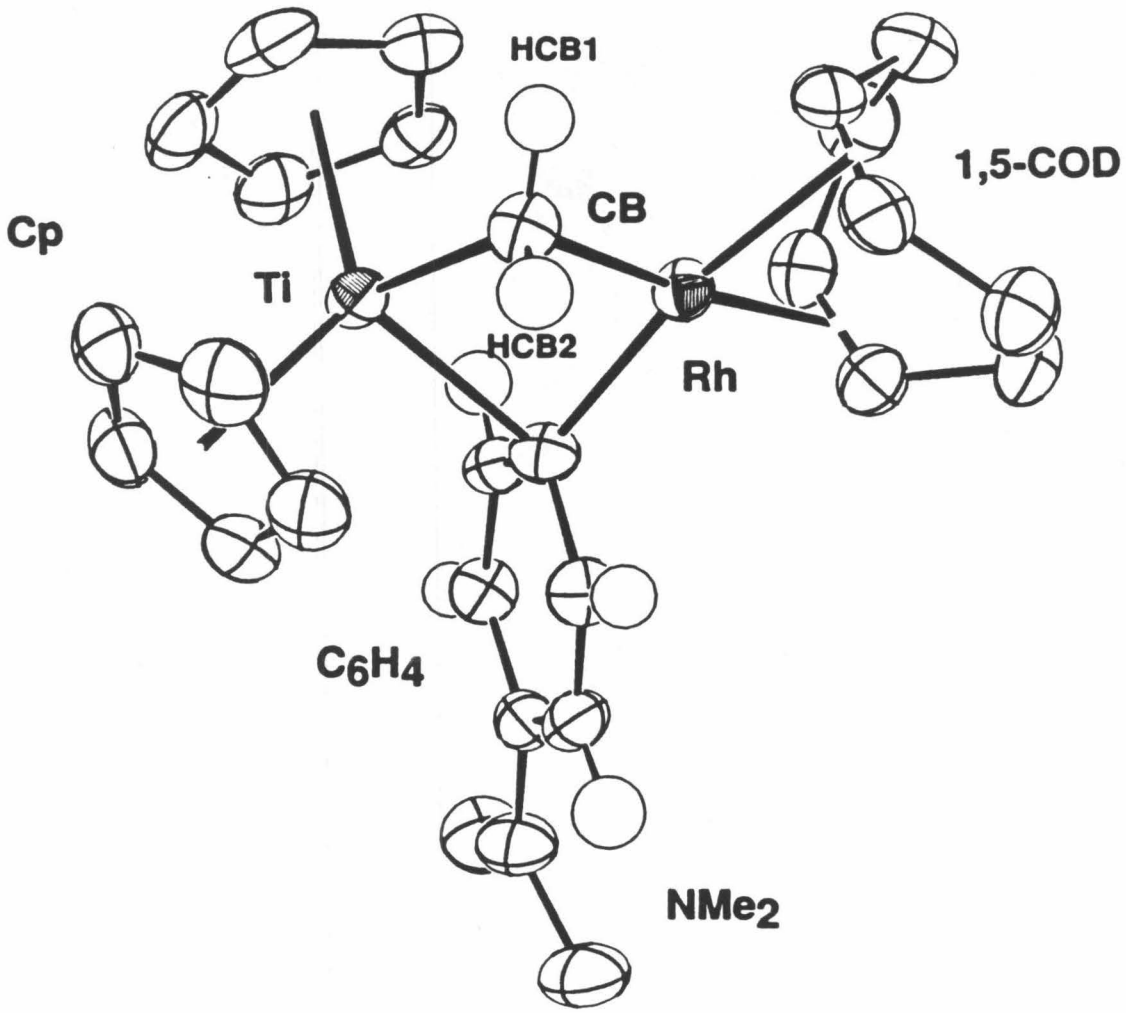

Figure 1. ORTEP diagram of complex **3b**. The ellipsoids are drawn at 50% probability level except for the hydrogen atoms. Only the two methylene hydrogens and four phenyl aromatic hydrogens are shown.

bond length of 2.122(4) Å is comparable with that of the μ–methylene μ-methyl analogue (2.110(6) Å). However, the Ti–C_i bond length of 2.403(4) Å is significantly longer than that of μ-methylene μ-methyl analogue (2.294(6) Å) which retains the strong interaction between a C–H bond and the titanium. The four central atoms are not coplanar; the dihedral angle between the planes of Rh, Ti, CB and Rh, Ti, C_i is 145(6)°. The plane of the phenyl ring is 16(4) from being perpendicular to the Rh, Ti, C_i plane and the Rh-C_i-C_p angle is 148.6(2)°. The two hydrogen atoms of the bridging methylene group are tilted slightly toward the rhodium atom so that the average Ti-CB-HCB angle is 119(2) and the average Rh-CB-HCB angle is 111(2)°. The dihedral angle between the Ti, CB, Rh plane and HCB1, CB, HCB2 plane is 94(6)°.

The C-C bond lengths of the phenyl group were analyzed in order to estimate the relative contribution of the two resonance structures A and B in Fig. 2.[14] The resonance form B is believed to have alternating bond lengths. The average C-C bond distance of C_i-C_o, C_m-C_p (= d1) is 1.408 Å, and that of C_o-C_p (= d2) is 1.376 Å. These values more closely resemble those of *p-N,N*-dimethyl-aminobenzoic acid (d1 = 1.406Å, d2 = 1.381 Å)[15] than those of *p*-nitroso-*N,N*-dimethylaniline (d1 = 1.404 Å, d2 = 1.348 Å) which is believed to have a significant amount of quinoid structure with charge-transfer character. This analysis agrees with the retention of aromaticity shown in the ^{1}H NMR.

A space-filling model based on the X-ray crystallographic data was drawn by Biograf software using an Evans and Sutherland PS 340 system. As shown in Fig. 3, the rotation of the *N,N*-dimethylaminophenyl group is inhibited by the steric hindrance together with the energy barrier imposed by the breaking of the interaction with the titanium center. However, very fast vertical movement of the phenyl ring is proposed to explain the single peaks of

cyclopentadienyl protons and μ-methylene protons in the ^{1}H NMR even at –80 ^oC.[17]

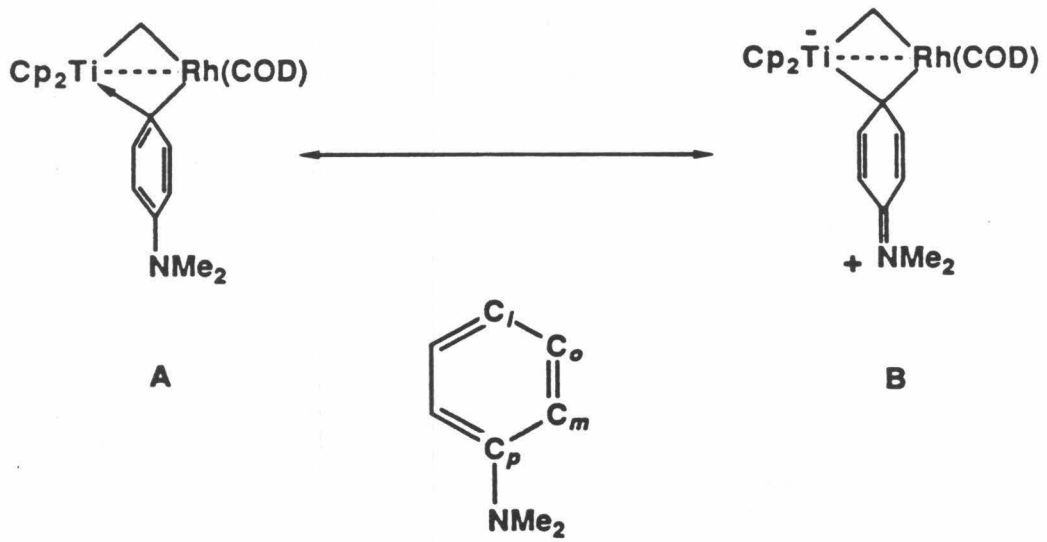

Figure 2. Two resonance structures of complex **3b** and the phenyl group showing the numbering system. The form A is more likely to represent the real structure of the complex.

In comparison with **3b**, **3c** gave two singlets for the cyclopentadienyl protons and μ-methylene, respectively, in the ^{1}H NMR due to the asymmetry imposed by the methoxy group on the phenyl ring. The differential NOE was used to confirm the molecular structure in the solution state. The irradiation of methoxy protons induced larger NOE for H_2 than that for H_1. (See Table III and Figure 4.) The C-H correlated two-dimensional NMR (Figure 5) was employed to assign the peaks in the ^{13}C NMR unambiguously.

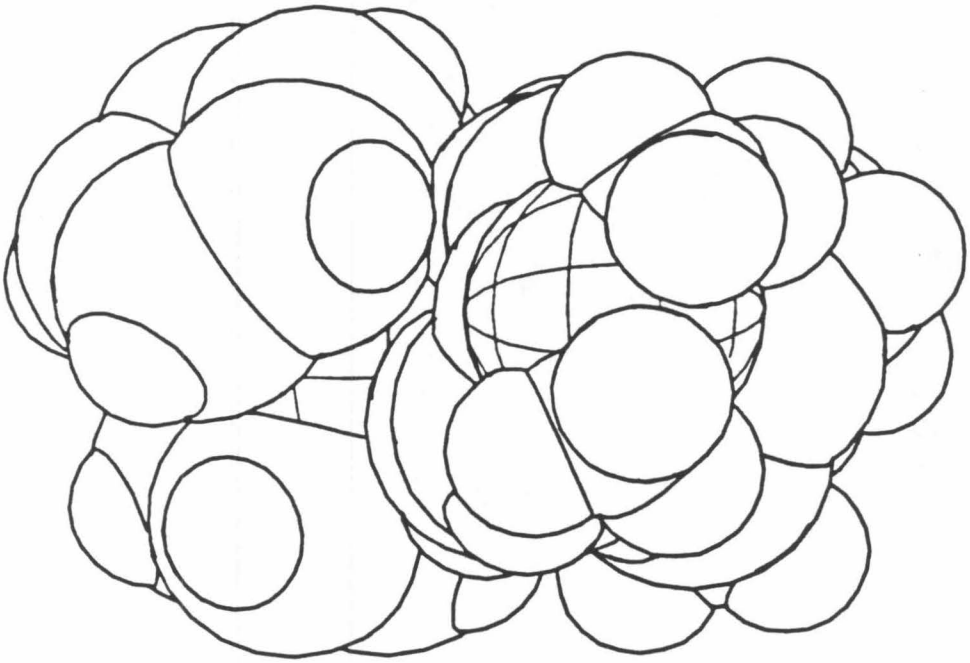

Figure 3. Space-filling model of complex **3b** generated by Biograf software using an Evans and Sutherland PS 340 system. The five-membered rings in the left side are the cyclopentadienyl groups. A shaded area represents the nitrogen atom.

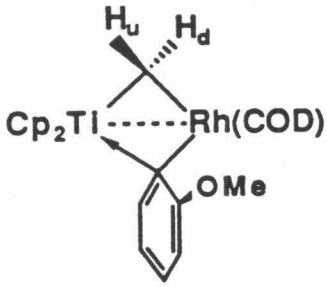

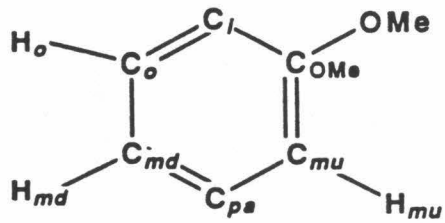

Figure 4. The numbering system for the complex **3c**, H_{up} and Cp_{up} represent the μ-methylene proton and the cyclopentadienyl protons with the same side of methoxy group.

The chemical shift of *ipso* carbon (C_i) of **3b** in the ^{13}C NMR is 156.7 ppm, which shifts downfield relative to that of *N,N*-dimethylaniline (117.2 ppm).[18] For **3c**, the same downfield shift was observed relative to the chemical shift of *ipso* carbon of methoxybenzene (175.1 ppm vs. 113.2 ppm).[19] This downfield shift is in contrast with the upfield shift[5a,b] or insensitivity[5c] of the resonances for the *ipso* carbon of the η^2-benzyl transition-metal complexes. These unusual downfield shifts of the *ipso* carbon in the ^{13}C NMR are assumed to be an indication of the interaction between the *ipso* carbon and the electron-deficient titanium.

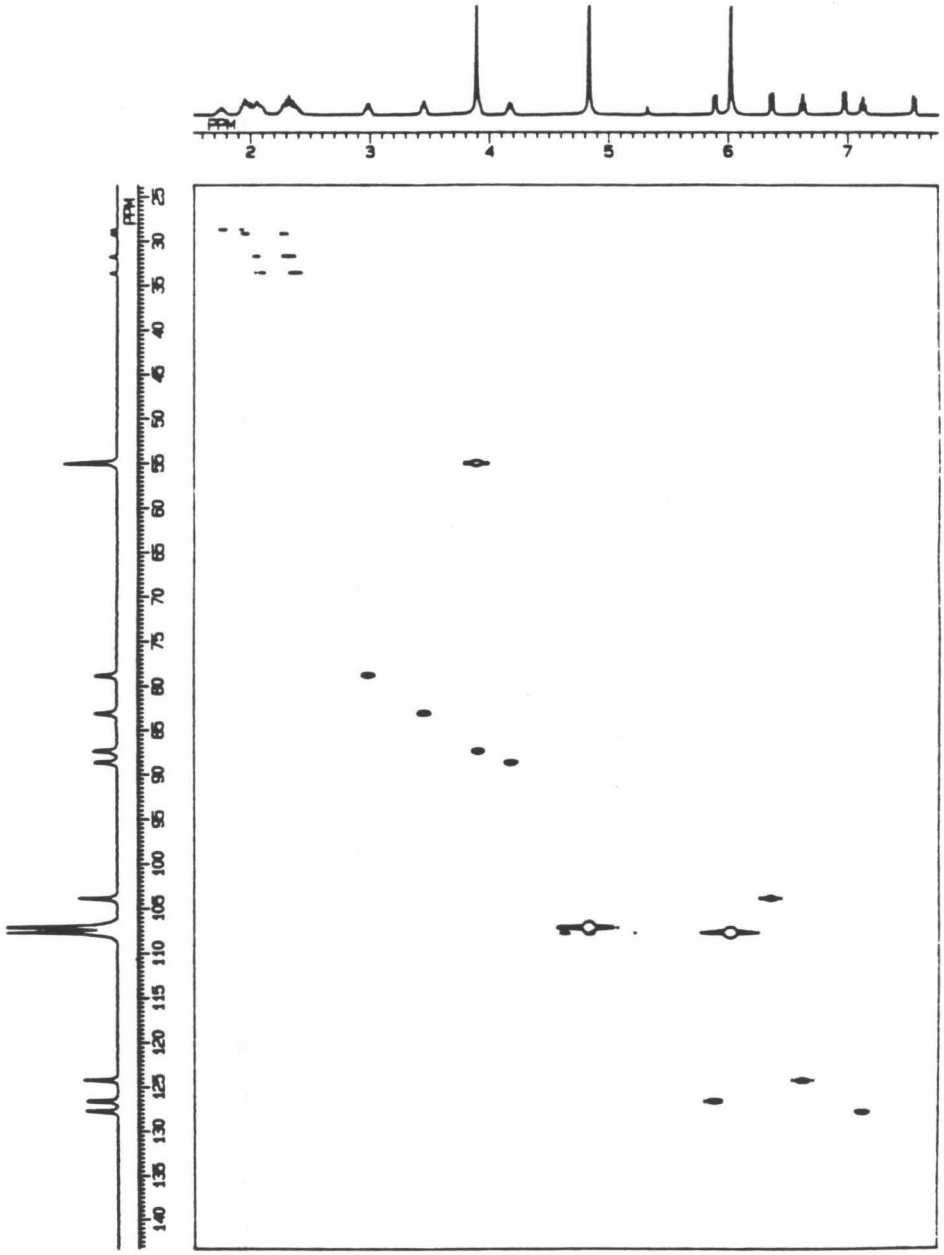

Figure 5. The heterocorrelated two-dimensional NMR of complex **3c**. ^{1}H NMR and ^{1}H-decoupled ^{13}C NMR are shown in x and y axis, respectively.

Table I. Selected Distances and Angles.

distance (Å)		angle (°)	
Rh–Ti	2.827(1)	HCB1–CB–HCB2	110.1(27)
Rh–C_i	2.122(4)	Ti–CB–HCB1	121.7(18)
Rh–CB	2.131(4)	Ti–CB–HCB2	115.8(20)
Rh–COD1	2.204(4)	Rh–CB–HCB1	109.2(18)
Rh–COD2	2.173(4)	Rh–CB–HCB2	112.5(20)
Rh–COD5	2.179(4)	Rh–CB–Ti	84.4(1)
Rh–COD6	2.153(4)	Rh–C_i–Ti	77.0(1)
Ti–CpA	2.115(4)	Rh–C_i–C_p	148.6(2)
Ti–CpB	2.092(4)	CB–Rh–C_i	96.6(5)
Ti–C_i	2.403(4)	CB–Ti–C_i	89.9(1)
Ti–CB	2.076(4)		
C_p–NPh	1.377(5)		
CB–HCB1	0.99(3)		
CB–HCB2	0.98(3)		

Table III. Differential Nuclear Overhaus Effect for Complex **3c**.

Irradiation	differential nOe(%)	
Cp_{down}	H_o	3.7
Cp_{up}	H_{m2}	1.9
	OMe	0.8
OMe	H_u	0.50
	H_d	0.25
	H_{mu}	3.1
H_o	H_{md}	2-3

Table II. Crystal and Intensity Collection Data for Complex **3b**.

Formula: $C_{27}H_{34}NRhTi$	Formula Weight: 523.38
Crystal Color: deep green	Habit: acicular
a = 8.988(1) Å	α = 102.85(1)°
b = 10.169(1) Å	β = 115.03(2)°
c = 13.707(2) Å	γ = 101.36(1)°
V = 1145.6(3) Å^3	Z = 2
λ = 0.71073 Å	T: 21 °C
Graphite monochromator	
Space group: *P1*	Absences: none
Crystal Size: 0.17 x 0.24 x 0.85 mm	μ = 7.09 cm^{-1} (μr_{max} = 0.32)
CAD-4 Diffractometer	θ-2θ scan
2θ range: 2° – 50°	Octants collected; ±h, ±k, ±l

Number of reflections measured: 8323

Number of independent reflections: 4031

Number with $F_o^2 > 0$: 3882

Number with $F_o^2 > 3\sigma(F_o^2)$: 3381

Goodness of fit for merging data: 1.14

Final R-index: 0.0370 (0.0302 for $F_o^2 > 3\sigma(F_o^2)$)

Final goodness of fit: 2.09

EXPERIMENT

General. All manipulations of air and/or moisture sensitive compounds were carried out with use of standard Schlenk or vacuum line techniques. Argon was purified by passage through columns of BASF RS-11 catalyst (Chemalog) and Linde 4 Å molecular sieves. Solids were transferred and stored in a N_2-filled Vacuum Atmospheres glove box equipped with a MO-40-1 purification train and a DK-3E Dri-Kool conditioner, and Dri-Cold Freezer.

Toluene, diethyl ether were stirred over CaH_2, then transferred to purple sodium-benzophenone ketyl. Dried solvents were vacuum-transferred into dry glass vessels equipped with Teflon valve closures and stored under argon. Toluene-d_8 (Cambridge Isotopes) were dried and vacuum-transferred from purple sodium-benzophenone ketyl. Dichloromethane-d_2 (Cambridge Isotopes and Norell, Inc.) was dried over CaH_2 or Na-Pb alloy and degassed by several freeze-pump-thaw cycles. Tebbe's reagent[20] and β,β-dimethyl-titanocene cyclobutane[13] were prepared as previously described.

NMR spectra were recorded on Varian EM-390 (90 MHZ, ^1H), JEOL FX-90Q (89.60 MHz, ^1H; 22.53 MHz, ^{13}C), and JEOL GX-400 (399.65 MHz, ^1H; 100.4 MHz, ^{13}C) spectrometers. Chemical shifts are reported in δ, referenced to residual solvent signals. Elemental analyses (C, H, N) were performed by the California Institute of Technology Analytical Services.

Synthesis of $Cp_2TiRh(1,5\text{-}COD)(\mu\text{-}CH_2)(\mu\text{-}p\text{-}Me_2NC_6H_4)$ A starting material, $Cp_2TiRh(1,5\text{-}COD)(\mu\text{-}CH_2)(\mu\text{-}Cl)$, was prepared with the known method.[7] A mixture of β,β-dimethyltitanocene cyclobutane (0.40 g, 1.61 mmol) and $[Rh(1,5\text{-}COD)Cl]_2$ (0.40 g, 0.81 mmol) was dissolved in 30 ml of toluene at

room temperature, and pumped off to yield red powders after stirring for 10 minutes. (The yield was 57% based on the integration in the ^{1}H NMR compared with that of internal standard, the pure compound.) *p*-Dimethylaminophenyl lithium (745 mg, 3.2 mmol) prepared by the known method was dissolved in 30 ml of diethyl ether. The solution of $Cp_2TiRh(1,5\text{-}COD)(\mu\text{-}CH_2)(\mu\text{-}Cl)$ in 30 ml of toluene was combined with the above etheral solution *via* cannula at 0 °C. ^{1}H NMR analysis with the internal standard showed that the yield for the second step was 33% after a stirring for an hour at 0 °C. Toluene (30 ml) was added at 0 °C to extract the product after a green resultant solution was evaporated to dryness. Evaporation to dryness after filter cannulation was followed by the extraction with 30 ml of diethyl ether. Several recrystallization in diethyl ether at –50 °C gave analytically pure dark green crystals suitable for X-ray crystallography. ^{1}H NMR (CD_2Cl_2, –20 °C) δ 7.46 (d, 2H, $C_6\underline{H}_4NMe_2$, J = 8.7 Hz), 6.92 (s, 2H, $\mu\text{-}CH_2$), 6.26(d, 2H, $C_6\underline{H}_4NMe_2$, J = 8.7 Hz), 5.53 (s, 10H, Cp), 3.87 (m, 2H, olefinic COD), 3.30 (m, 2H, olefinic COD), 2.90 (s, 6H, NMe_2), 2.27 (m, 2H, aliphatic COD), 2.13 (m, 2H, aliphatic COD), 1.90 (m, 2H, aliphatic COD), 1.82 (m, 2H, aliphatic COD); ^{13}C NMR (CD_2Cl_2, –10 °C) δ 189.4 (dt, 2C, J_{CH} = 129 Hz, J_{CRh} = 23.5, $\mu\text{-}CH_2$), 156.7 (d, 1C, J_{CRh} = 29.4Hz, C_i), 151.4 (s, 1C, C_p), 143.7 (d, 2C, J_{CH} = 156 Hz, C_o), 108.8 (d, 2C, J_{CH} = 157 Hz, C_m), 108.2 (s, 10C, J_{CH} = 173 Hz, Cp), 81.5 (d, 2C, J_{CH} = 156 Hz, olefinic COD), 81.4 (d, 2C, J_{CH} = 156 Hz, olefinic COD), 40.0 (quartet, 2C, J_{CH} = 136 Hz, NMe_2), 31.2 (t, 2C, J_{CH} = 126 Hz, methyleneic COD), 31.1 (t, 2C, J_{CH} = 126 Hz, methyleneic COD); Anal. Calcd for $C_{27}H_{34}NRhTi$: C, 61.96; H, 6.55; N, 2.68. Found: C, 61.82; H, 6.42; N, 2.78.

Synthesis of $Cp_2TiRh(1,5\text{-}COD)(\mu\text{-}CH_2)(\mu\text{-}o\text{-}MeOC_6H_4)$. A mixture of recrystallized $Cp_2TiRh(1,5\text{-}COD)(\mu\text{-}CH_2)(\mu\text{-}Cl)$ (0.50 g, 1.14 mmol) and

o-methoxy phenyl lithium (376 mg, 1.171 mmol) was dissolved in 15 ml of toluene and 15 ml of diethyl ether at room temperature. Toluene (15 ml) was added at 0 °C to extract the product after a green solution formed during the 30 minutes at room temperature was evaporated to dryness. (The yield was 58% based on the integration in ^{1}H NMR with that of internal standard.) Evaporation to dryness after filter cannulation was followed by the washing with 25 ml of diethyl ether. The remaining greenish solids were dissolved in 10 ml of toluene and filter cannulated. Pentane (20 ml) was added to make a double layer after the toluene solution was concentrated to 5 ml. The toluene and pentane two layer was cooled to –50 °C. Another recrystallization at –50 °C using toluene and pentane gave analytically pure dark green crystals. ^{1}H NMR (CD_2Cl_2, –10 °C) δ 7.58 (d, 1H, J_{CH} = 7.3 Hz, H_u), 7.13 (t, 1H, H_{pa}), 6.98 (d, 1H, J_{CH} = 7.3 Hz, H_d), 6.62(t, 1H, H_{md}), 6.36 (d, 1H, J_{CH} = 7.8 Hz, H_{mu}), 6.02 (m, 5H, Cp_{down}), 5.89 (d, 1H, J_{CH} = 6.8 Hz, H_{od}), 4.84 (m, 5H, Cp_{up}), 4.17 (m, 1H, olefinic COD), 3.89 (s, 3H, OMe), 3.89 (m, 1H, olefinic COD), 3.46 (m, 1H, olfinic COD), 2.99 (m, 1H, olefinic COD), 2.42-2.28 (m, 4H, methyleneic COD), 2.06-1.92 (m, 4H, methyleneic COD); ^{13}C NMR (CD_2Cl_2, –10 °C) δ 197.8 (dt, 1C, J_{CH} = 130 Hz, J_{CRh} = 22 Hz, μ-CH_2), 175.1 (d, 1C, J_{CRh} = 31.5 Hz, C_i), 171.7 (s, 1C, C_o), 127.8 (d, 1C, J_{CH} = 159 Hz, C_{pa}), 126.8 (d, 1C, J_{CH} = 156 Hz, C_{od}), 124.3 (d, 1C, J_{CH} = 162 Hz, C_{md}), 104.0 (d, 1C, J_{CH} = 157 Hz, C_{mu}), 107.8 (m, 5C, J_{CH} = 172 Hz, Cp), 107.2 (m, 5C, J_{CH} = 174 Hz, Cp), 88.7 (dd, 1C, J_{CH} = 157 Hz, J_{CRh} = 8.8 Hz, olefinic COD), 87.6 (dd, 1C, J_{CH} = 156 Hz, J_{CRh} = 8.1 Hz, olefinic COD), 78.9 (dd, 1C, J_{CH} = 149 Hz, J_{CRh} = 8.1 Hz, olefinic COD), 31.9 (t, 1C, J_{CH} = 128Hz, methyleneic COD), 29.9 (t, 1C, J_{CH} = 125 Hz, methyleneic COD), 29.4 (t, 1C, J_{CH} = 130 Hz, methyleneic COD), 28.9 (t, 1C, J_{CH} = 127 Hz, methyleneic COD). Anal. Calcd for $C_{26}H_{31}OTiRh$: C, 61.19; H, 6.12. Found: C, 61.35; H, 6.03.

Crystal Structure Determination of $Cp_2TiRh(1,5\text{-}COD)(\mu\text{-}CH_2)$-($\mu$-*p*-$Me_2NC_6H_4$). A dark green needle-like crystal of $Cp_2TiRh(1,5\text{-}COD)$-(μ-CH_2)(μ-*p*-$Me_2NC_6H_4$) was mounted in a capillary. Table II lists the data collection details. The rhodium atom was found from a Patterson map; the coordinates of the other non-hydrogen atoms were obtained by successive structure factor-Fourier calculations. Hydrogen atoms were placed by computation or difference maps and subsequently refined acceptably.

Calculations were done with programs of the CRYM Crystallographic Computing System and ORTEP. Scattering factors and corrections for anomalous scattering were taken from a standard reference (International Tables for X-ray Crystallography, Vol. IV, pp 71, 149; Birmingham, Kynoch, 1974). $R = \Sigma|F_o - |F_c||/\Sigma F_o$, for only $F_o^2>0$, and goodness of fit = $[\Sigma w(F_o^2-F_c^2)^2/(n-p)]^{1/2}$, where n is the number of data and p the number of parameters refined. The function minimized in least squares was $\Sigma w(F_o^2-F_c^2)^2$, where $w = 1/\sigma^2(F_o^2)$. Variances of the individual reflections were assigned based on counting statistics plus an additional term, $0.014I^2$. Variances of the merged reflections were determined by standard propagation of error plus another additional term, $0.014\langle I\rangle^2$. No absorption or secondary extinction corrections were required.

REFERENCES AND NOTES

(1) Collman, J. P.; Hegedus, L. S.; Norton, J. R.; Finke, R. G. *Principles and Applications of Organotransition Metal Chemistry*: University Science Books, Mill Valley, California, 1987; pp 158–164, references therein.

(2) Holton, J.; Lappert, M. F.; Pearce, R.; Yarrow, P. I. W. *Chem. Rev.* **1983**, *83*, 135–201.

(3) (a)–(j); bridging phenyl compounds through *ipso* carbon without *o*-chelation, (k)–(p); bridging phenyl compounds through *ipso* carbon with *o*-chelation.

(a) Bartlett, R. A.; Power, P. P.; Shoner, S. C. *J. Am. Chem. Soc.* **1988**, *110*, 1966–1968. (b) Khan, S. I.; Edwards, P. G.; Yuan, H. S.; Bau, R. *Ibid.* **1985**, *107*, 1682–1684. (c) Hope, H.; Oram, D.; Power, P. P. *Ibid.* **1984**, *106*, 1149–1150. (d) Hope, H.; Power, P. P. *Ibid.*, **1983**, *105*, 5320–5324. (e) Noltes, J. G.; ten Hoedt, R. W. M.; van Koten, G.; Spek, A. L.; Schoone, J. C. *J. Organomet. Chem.* **1982**, *225*, 365-376. (f) Edwards, P. G.; Gellert, R. W.; Marks, M. W.; Bau, R. *J. Am. Chem. Soc.* **1982**, *104*, 2072–2073. (g) Evans, D. G.; Hughes, G. R.; Mingos, D. M. P.; Bassett, J.-M.; Welch, A. J. *J. Chem. Soc., Chem. Comm.* **1980**, 1255–1257. (h) Thoennes, D.; Weiss, E. *Chem. Ber.* **1978**, *111*, 3157–3161. (i) Jonas, K.; Brauner, D. J.; Krüger, C.; Roberts, P. J.; Tsay Y.-H. *J. Am. Chem. Soc.* **1976**, *98*, 74–81. (j) Bradford, C. W.; Nyholm, R. S.; Gainsford, G. J.; Guss, J. M.; Ireland, P. R.; Mason, R. *J. Chem. Soc., Chem. Comm.* **1972**, 87–89. (k) Wehman, E.; van Koten, G.; Jastrzebski, J. T. B. H.; Rotteveel, M. A.; Stam, C. H. *Organometallics*, **1988**, *7*, 1477–1485. (l) ten Hoedt, R. W. M.; Notles, J. G.; van Koten, G.; Spek, A. L. *J. Chem. Soc. Dalton*, **1978**, 1800–1806. (m) Churchill, M. R.; Rotella, F.

J. *Inorg. Chem.* **1978**, *17*, 2614–2621. (n) Cotten, F. A.; Millar, M. *J. Am. Chem. Soc.* **1977**, *99*, 7886–7891. (o) van Koten, G.; Noltes, J. G. *J. Organomet. Chem.* **1975**, *84*, 129–138. (p) Guss, J. M.; Mason, R.; Søtofte, I.; van Koten, G.; Noltes, J. G. *J. Chem. Soc., Chem. Comm.* **1972**, 446–447.

(4) Ozawa, F.; Hidaka, T.; Yamamoto, T.; Yamamoto, A. *J. Organomet. Chem.* **1987**, *330*, 253–263.

(5) (a) Jordan, R. F.; Lapointe, R. E.; Bajgur, C. S.; Echols, S. F.; Willett, R. *J. Am. Chem. Soc.* **1987**, *109*, 4111–4113. (b) Mintz, E. A.; Molog, K. G.; Marks, T. J.; Day, V. W. *ibid.*,**1982**, *104*, 4692–4695. (c) Latesky, S. L.; McMullen, A. K.; Niccolai, G. P.; Rothwell, I. P.; Huffaman, J. C. *Organometallics*, **1985**, *4*, 902–908. (d) Bassi, I. W.; Scordamaglia, G. A. R.; Chioccola, G. *J. Am. Chem. Soc.* **1971**, *93*, 3787–3788. (e) Edwards, P. G.; Anderson, R. A.; Zalkin, A. *Organometallics* **1984**, *3*, 293–298. (f) Girolami, G. S.; Wilkinson, G.; Thornton-Pett, M.; Hursthouse, M. B. *J. Chem. Soc., Dalton Trans.* **1984**, 2789–2794. (g) Davies, G. R.; Kilbourn, J. A. J.; Pioli, A. J. P. *J. Chem. Soc., Chem. Comm.* **1971**, 677. (h) Davies, G. R.; Jarvis, J. A. J.; Kilbourn, J. A. J. *ibid.* **1971**, 1511–1512.

(6) (a) Effenberger, F.; Reisinger, F.; Schönwälder, K. H.; Bäuerle, P.; Stezowski, J. J.; Jogun, K. H.; Schöllkopf, K.; Stohrer, W.-D. *J. Am. Chem. Soc.* **1987**, *109*, 882–892. (b) Baenziger, N. C.; Nelson, A. D. *ibid.* **1968**, *90*, 6602–6607. (c) Olah, G. A.; Kuhn, S. J. *ibid.* **1985**, *80*, 6541–6545.

(7) (a) Mackenzie, P. B.; Ott, K. C.; Grubbs, R. H. *Pure Appl. Chem.* **1984**, *56*, 59–61. (b) Mackenzie, P. B.; Coots, R. J.; Grubbs, R. H. submitted for publication in *Organometallics*. A 1,5-COD represents a1,5-cyclooctadiene.

(8) Park, J. W.; Mackenzie, P. B.; Schaefer, W. P.; Grubbs, R. H. *J. Am. Chem. Soc.* **1986**, *108*, 6402–6404.

(9) Tauster, S. J. *Acc. Chem. Res.* **1987**, *20*, 389–394.

(10) Sakellson, S.; McMillan, M.; Haller, G. L. *J. Phys. Chem.* **1986**, *90*, 1733–1736.

(11) Ozawa, F.; Park, J. W.; Mackenzie, P. B.; Schaefer, W. P.; Henling, L. M.; Grubbs, R. H. *J. Am. Chem. Soc.* in press

(12) Upton, T. H.; Rappe, A. K. *J. Am. Chem. Soc.* **1985**, *107*, 1206–1218.

(13) (a) Lee, J. B.; Gajda, G. J.; Schaefer, W. P.; Howard, T. R.; Ikariya, T.; Straus, D. A.; Grubbs, R. H. *J. Am. Chem. Soc.* **1981**, *103*, 7358–7361. (b) Straus, D. A.; Grubbs, R. H. *Organometallics* **1982**, *1*, 1658–1661.

(14) The C-C bond length served as a better criterion than the planarity around the nitrogen atom.

(15) Vyas, M.; Sakore, T. D.; Biswas, A. B. *Acta Cryst.* **1987**, *B34*, 1366–1368.

(16) Rømming, C.; Talberg, H. J. *Acta Chem. Scand.* **1973**, *27*, 2246–2248.

(17) A symmetric molecular structure in the solution state can be an alternative explanation.

(18) Pasto, D. J.; Jhonson, C. R. *Laboratory Text for Organic Chemistry*: Prentice-Hall, New Jersey, 1979, pp 240.

(19) The poor availability of the proper data for the ^{13}C NMR hampered more accurate comparisons.

(20) (a) Tebbe, F. N.; Parshall, G. W.; Reddy, G. S. *J. Am. Chem. Soc.* **1987**,*100*, 3611–3613. (b) Lee, J. B.; Ott, K. C.; Grubbs, R. H. *Ibid.* **1982**, *104*, 7491–7496.

CHAPTER 3

Structure and Reactivity of Titanium–Platinum Heterobinuclear Complexes with μ-Methylene Ligand

ABSTRACT

Titanium–platinum heterobinuclear μ-methylene complexes $Cp_2\overline{TiCH_2PtX}(Me)(PMe_2Ph)$ have been prepared: X = Cl (**2b**), X = Me (**2c**). The μ-CH_2–μ-Cl complex **2b** crystallizes in the monoclinic system, in space group $P2_1/n$ (#14), with a = 13.249(3) Å, b = 11.646(3) Å, c = 14.542(5) Å, β = 114.45(2)°, V = 2042.6(10) $Å^3$; Z = 4 and density = 1.87 g cm^{-3}. The μ-CH_2–μ-CH_3 analogue *trans*-**2c** is isostructural to **2b** and also crystallizes in space group $P2_1/n$ (#14) with a = 13.333(4) Å, b = 11.686 Å, c = 14.351 Å, β = 115.03(2)°, V = 2026.0(8) $Å^3$; Z = 4 and density = 1.82 g cm^{-3}. Structural studies indicate the following: (1) the Ti–CH_2 bond possesses residual double bond character, (2) there is a dative Pt → Ti interaction which may be regarded as a π back donation from the platinum atom to the "Ti=CH_2" group, and (3) the μ-CH_3 group in *trans*-**2c** is bound to the titanium atom through a three-center, two-electron agostic bond. Isomerization of *trans*-**2c** to *cis*-**2c** was catalyzed by the addition of methyl magnesium iodide at room temperature. Complexes *trans*-**2c** and *cis*-**2c** react with tertiary phospines to give a equilibrium mixture of **2c**, $Cp_2Ti{=}CH_2(PR_3)$, and platinum complex at room temperature. Oxidative addition on platinum of **2b** with an excess amount of methyl iodide at room temperature produced a complex **4** which decomposed to give starting materials at 70 °C. The rate of the equilibration, which involves a C-H activation process, between the μ-CH_3 and the μ-CH_2 group was relatively slow in comparison with rhodium and iridium analogues.

INTRODUCTION

Recently much attention has been focused upon early transition-metal–late transition-metal heterobinuclear complexes[1] because of their potential applications in catalytic reactions. Also, these complexes have been studied in order to gain an understanding of the phenomenon of so-called "strong metal-support interactions (SMSI)" in heterogeneous catalysis.[2] It is well documented that late transition-metals, which are finely dispersed on early transition-metal oxide supports such as TIO_2 and ZrO_2, serve as highly active catalysts in the catalytic hydrogenation of carbon monoxide. SMSI have been observed in such systems. While the exact nature of the interaction is still unclear, SMSI are regarded as the prime reason for the enhanced catalytic activity.[3]

Key intermediates in heterogeneous CO-hydrogenation are μ-methylene species.[4] We recently developed a convenient synthetic route to titanium–late transition-metal μ-methylene complexes.[5] These complexes serve as possible models for surface methylene species on catalysts that exhibit the SMSI phenomenon. Reactions of the "$Cp_2Ti{=}CH_2$" species generated from bis(cyclopentadienyl)titanacyclobutanes or Tebbe's reagent with late transition-metal chlorides (L_nMCl) give a new class of μ-methylene complexes $Cp_2\overline{TiCH_2M(Cl)}L_n$ (**2**).[5b] Anion exchange of the μ-Cl ligand in **2** with MeMgX or MeLi forms μ-CH_2–μ-CH_3 complexes.[5c] These methods have enabled us to study a wide variety of early–late heterobinuclear complexes with μ-methylene ligands.

In this chapter the structure and reactivity of titanium–platinum μ-methylene complexes $Cp_2\overline{TiCH_2PtX}(Me)(PMe_2Ph)$ (X = Cl, Me) are described.

X-ray diffraction studies on the compounds have revealed that the Ti–CH_2 bond is intermediate in character between a single and a double bond, while the Pt–CH_2 bond exhibits both σ- and π-bonding properties.

RESULTS AND DISCUSSIONS

Synthesis of μ-Methylene Complexes. The μ-methylene complexes prepared in this study are listed in Table I. Reaction of bis(cyclopentadienyl)-titanacyclobutane (**1**) with $PtMeCl(SMe_2)_2$ in toluene affords a μ-methylene–μ-chloride complex with a SMe_2 ligand (**2a**) along with the evolution of a quantitative amount of isobutylene.[5b]

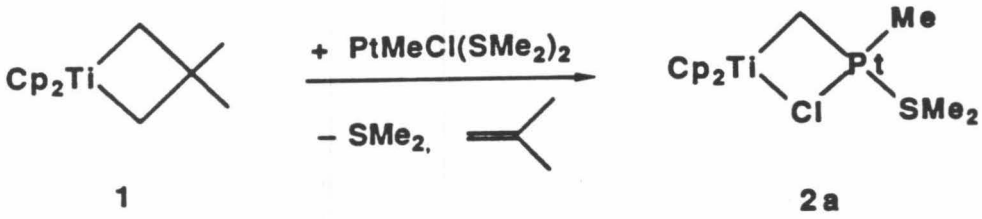

(1)

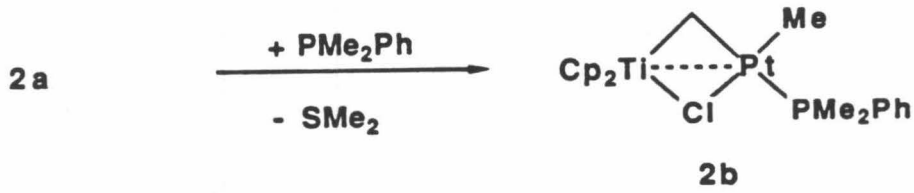

(2)

The bridging chloride ligand in **2b** is readily replaced by the methyl group of MeMgBr at room temperature to give the μ-CH_2–μ-CH_3 complex trans-**2c**, which has been isolated as red-orange crystals. This reaction proceeds with retention of the original configuration about the platinum center, while on prolonged reaction *trans*-**2c** is isomerized to its geometrical isomer *cis*-**2c**. The isomerization is a significantly slower process in the absence of MeMgBr, suggesting a MeMgBr-promoted isomerization reaction.[6] No isomerization

from *cis*-**2c** ,which is assumed to be a thermodynamic product, to *trans*-**2c** is observed even at elevated temperature, 70 °C. Reaction of **2b** with trimethylaluminum at room temperature gave a mixture of *trans*-**2c** (90%) and *cis*-**2c** (10%) in a low separation-yield (30%).

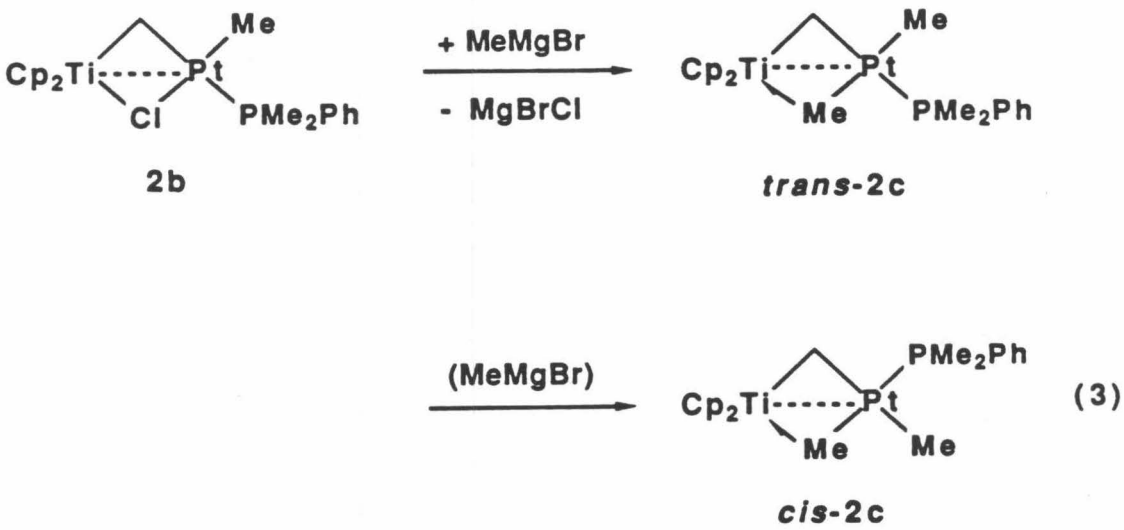

(3)

NMR. The ^{1}H and ^{13}C NMR resonances for the μ-CH_2 group appear in the typical regions reported for binuclear μ-methylene complexes (Table I).[4a] The $^1J_{CH}$ values are in the range of 135 ± 2 Hz; the values are intermediate between those for pure sp^2 and sp^3 carbons.[7] The geometries at platinum in the phosphine-coordinated complexes have been determined on the basis of coupling constants between phosphorus and carbons bound to metal.[8] The carbon which is *trans* to the phosphine ligand gives relatively large $^2J_{CP}$ values (51-88 Hz), whereas carbons in *cis* positions show a small coupling (< 10 Hz) with the phosphorus. In the ^{1}H NMR spectra of *trans*-**2c** and *cis*-**2c** at –82 °C, the protons in the bridging methyl group are observed as two sets of signals, doublet and triplet, in a 2 : 1 ratio with geminal coupling between the protons, which coalesce into a broad singlet at elevated temperatures. As seen from the

X-ray structure of *trans*-**2c** described below, the appearance of two sets of signals at low temperature is ascribed to the presence of an agostic interaction between the methyl group and the titanium atom. A similar bonding pattern has been observed for $Cp_2TiCH_2Rh(CH_3)(COD)$ (COD = 1,5-cyclooctadiene).[5c]

X-ray Strucrures. Complexes **2b** and *trans*-**2c** have been subjected to single-crystal X-ray diffraction studies. Selected bond lengths and angles are listed in Table II. Crystal and intensity collection data are shown in Table III, and IV. As seen from the ORTEP diagrams (Figures 1 and 2), both complexes have similar structures. The four central atoms – Ti, Pt, the μ-methylene carbon (C_1), and the other bridging atom (Cl in **2b** or μ-methyl C_{11} in *trans*-**2b**) – form a four-membered ring lying approximately in a plane with a methylene hydrogen and a Cp ring above and below the plane. The H–C–H angle of the μ-CH_2 group is normal for binuclear μ-methylene complexes. The plane composed of the methylene carbon and the two methylene hydrogens is tilted toward the platinum (Figure 3). The coordination geometry about titanium is pseudotetrahedral, whereas the platinum is basically in a square-planar environment.

Structure of *trans*-2c. The μ-methyl group forms a three-center, two-electron agostic bond with the titanium atom. The distance between titanium and agostic hydrogen HC_{11b} (1.935(5) Å) is shorter than that in $Cp_2TiRh(\mu\text{-}CH_2)(\mu\text{-}CH_3)(COD)$ (2.202(6) Å), whereas the Ti–CH_3 bond (2.395(8) Å) is longer than that in the Ti–Rh analogue (2.294(6) Å).[5b] The Ti–Pt distance is 2.776(1) Å, which is short enough to form a dative Pt → Ti bond.[1] The presence of the Pt–Ti bond is reflected in the narrow Ti–C1–Pt angle (82.9(3) Å); the magnitude of this angle is typical of binuclear μ-methylene complexes with a metal-metal bond. The Pt–CH_2 bond (2.078(7) Å) is slightly shorter than

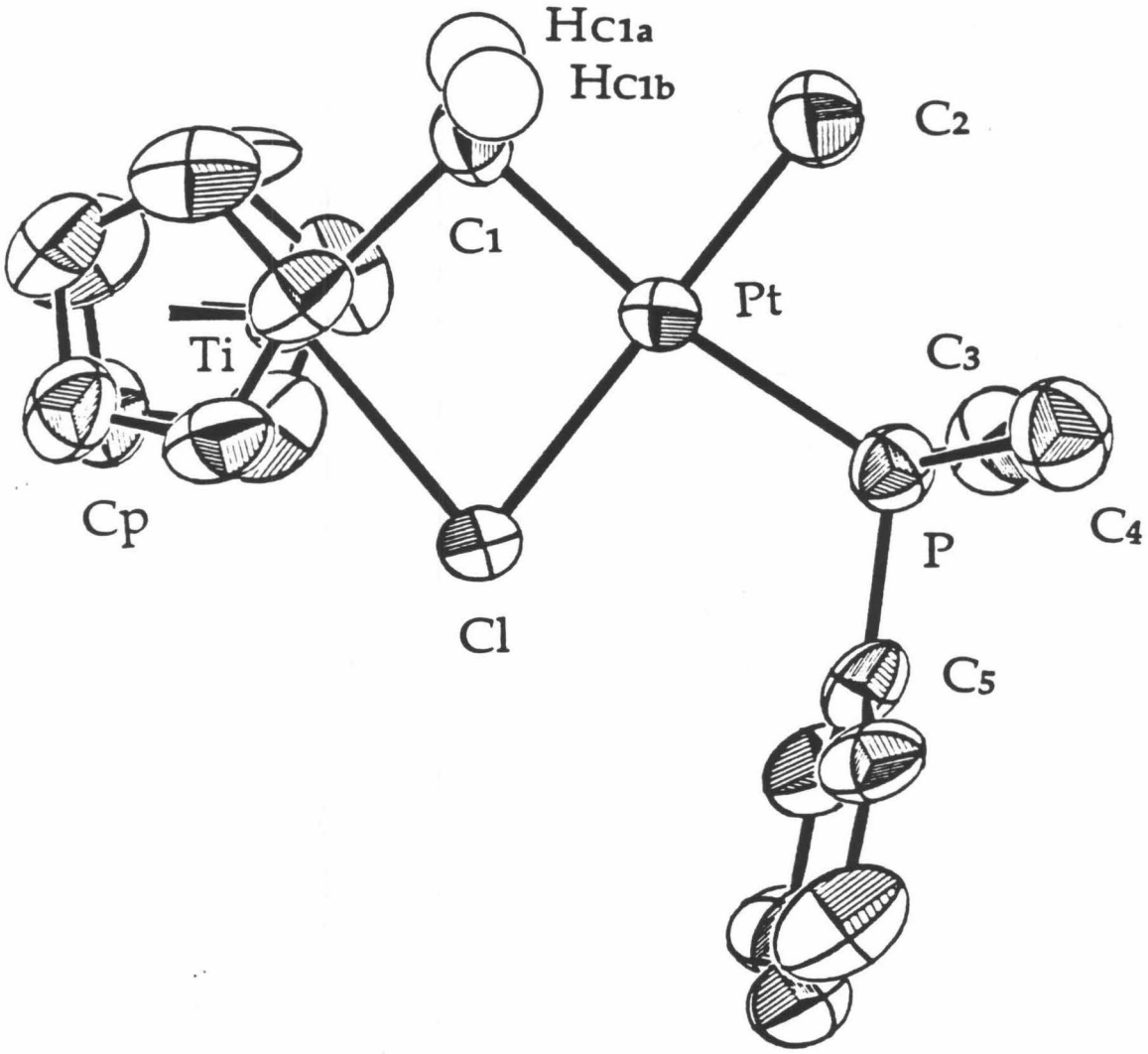

Figure 1. ORTEP diagram of complex **2b**. The ellipsoids are drawn at 50% probability level except for the hydrogen atoms. The hydrogen atoms of the cyclopentadienyl, terminal methyl, and PMe_2Ph ligands are omitted for clarity.

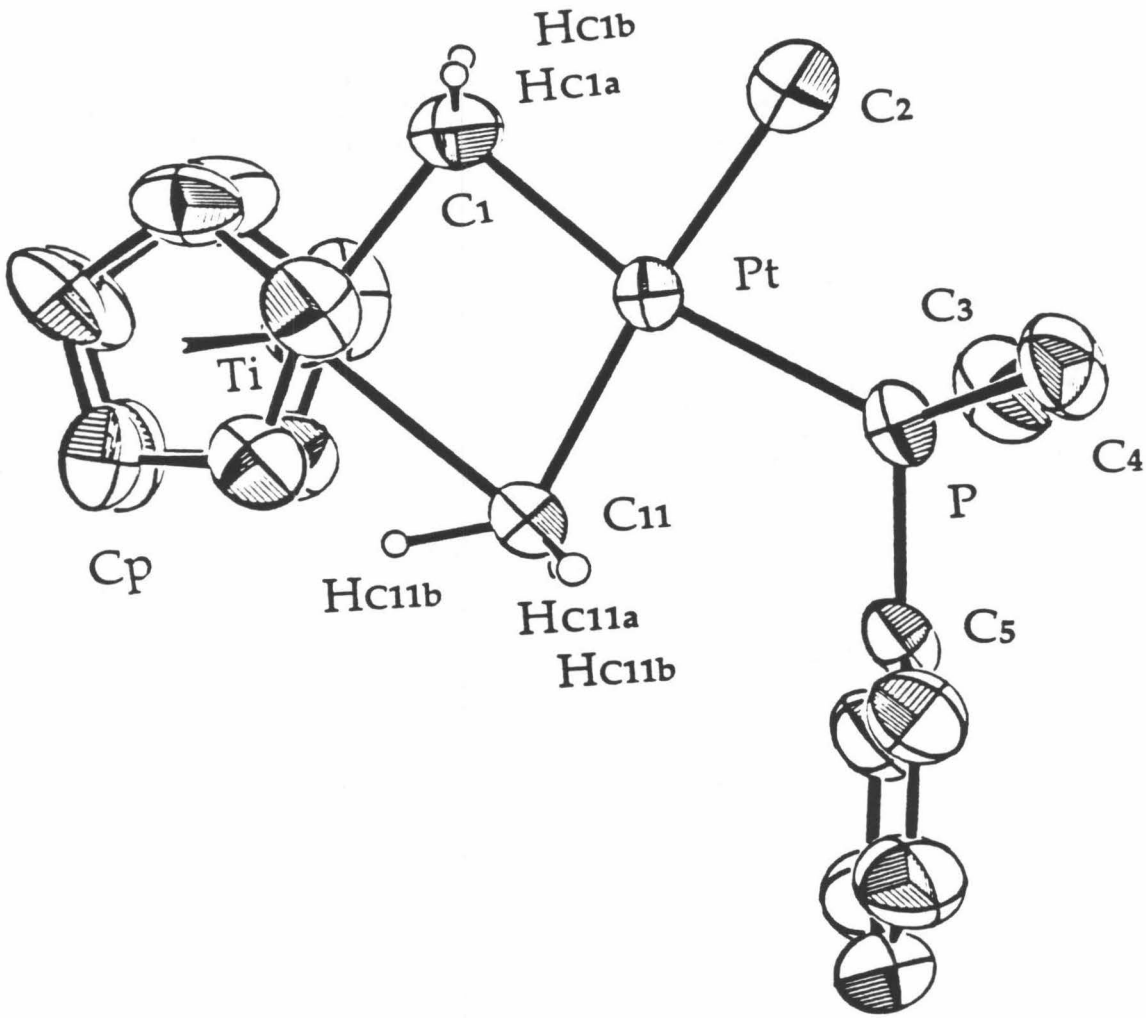

Figure 2. ORTEP diagram of complex ***trans*-2c**. The ellipsoids are drawn at the 50% probability level except for the hydrogen atoms. The hydrogen atoms of the cyclopentadienyl, terminal methyl, and PMe_2Ph ligands are omitted for clarity.

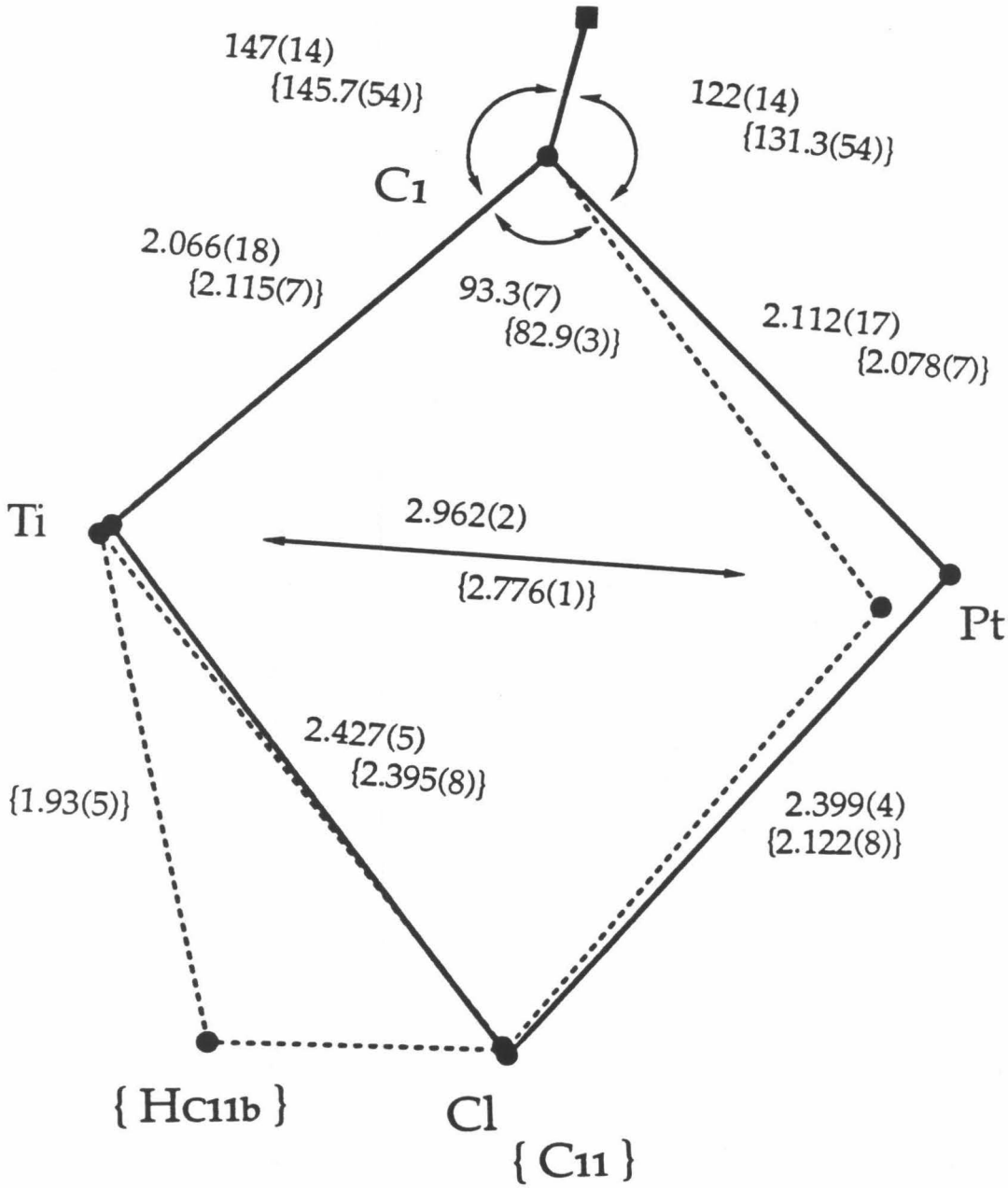

Figure 3. Comparison of the cores of complexes **2b** (–) and ***trans*-2c** (---). The square mark (■) shows the intermediate point of the two μ-CH_2 hydrogens. The distances are given in Å and the angles in deg. The information in brackets is for ***trans*-2c**.

those in bis(tertiary phospine)platinocyclobutanes (2.13–2.15 Å).[9] The Pt–Me bridging (2.122(8) Å) and terminal (2.108(6) Å) bond lengths are in the typical range of a Pt–Me bond having a *trans* ligand with a large *trans* influence.[10] The Ti–CH_2 distance (2.115(7) Å) is slightly shorter than that in $Cp_2Ti\overline{CH_2C(Me)_2C}H_2$ (2.16 Å),[11] but much longer than the calculated distance for the Ti=CH_2 double bond (1.85–1.88 Å).[12]

Structure of 2b. The Ti–Pt distance (2.962(2) Å) is significantly longer than that in *trans*-**2c**, but is still in the range where a weak Pt → Ti interaction is possible. The Pt–CH_2 distance (2.112(17) Å) is slightly longer than that in *trans*-**2c** and is a typical of a Pt–C single bond which is *trans* to a phosphine ligand. The Pt–Me bond length (2.081(6) Å) is comparable with that of *trans*-PtMeCl($PMePh_2$)$_2$ (2.081(6) Å).[13] The Pt–Cl and Ti–Cl distances are similar to those of the Cl-bridged compounds.[14]

Descriptions of bonding. The titanium/platinum μ-methylene complexes have two limiting descriptions of bonding, **I** and **II**.

I **II**

In structure **I**, the μ-methylene carbon is linked to the metal centers with σ-bonds. Structure **II**, on the other hands, consists of $Cp_2Ti{=}CH_2$ and PtMe(X)L moieties. The Ti=CH_2 group is bound to the platinum center in a π-bonding manner. The spectroscopic data and X-ray crystallographic results suggest that

the proper bonding description lies somewhere between **I** and **II**, and the relative contribution of both structures varies with the bridging ligand X.

The contribution of structure **II** is reflected in the short Ti–CH_2 distances in **2b** and *trans*-**2c**. The tilting of the CH_2 plane toward the platinum center, which indicates residual double bonding character between Ti and the CH_2 group, is also consistent with bonding description **II**. In this structure, the dative Pt – Ti interaction may be regarded as a π-back donation from an occupied d orbital on platinum to the π^* orbital of the "titanaolefin" group, which is localized on the electropositive titanium atom. Similar to the bonding of general transition-metal olefin complexes, the π-back donation will shorten the Ti–Pt and Pt–CH_2 bonds and elongate the Ti–CH_2 distance. That is, the longer Ti–CH_2 bond and shorter Ti–Pt and Pt–CH_2 distances in *trans*-**2c** than in **2b** can be considered to reflect the higher contribution of **II** to *trans*-**2c**. In complex *trans*-**2c**, the μ-Me group is ligated to titanium with its C–H σ-bonding electrons and to platinum by a normal covalent bond. The greater π-acidic nature of titanium compared to platinum may responsible for this bonding pattern and facilitates the contribution of **II** to *trans*-**2c**.

Reaction with $^{13}CH_3MgI$. Reaction of **2b** with $^{13}CH_3MgI$ gave a mixture of *trans*-**2c** and *cis*-**2c** which have ^{13}C labelled methyl group at the bridging methyl and/or terminal methyl position. Reaction of *trans*-**2c** with one equivalent of $^{13}CH_3MeI$ gave a *cis*-**2c** whose bridging and/or terminal methyl group were enriched by ^{13}C. A mechanism for the substitution reaction is shown in Scheme I. A mechanism for the isomerization in Scheme II involves peudorotation,[15] and another mechanism in Scheme III involves consecutive displacement.[15] Further studies on the mechanism for the isomerizarion were not pursued.

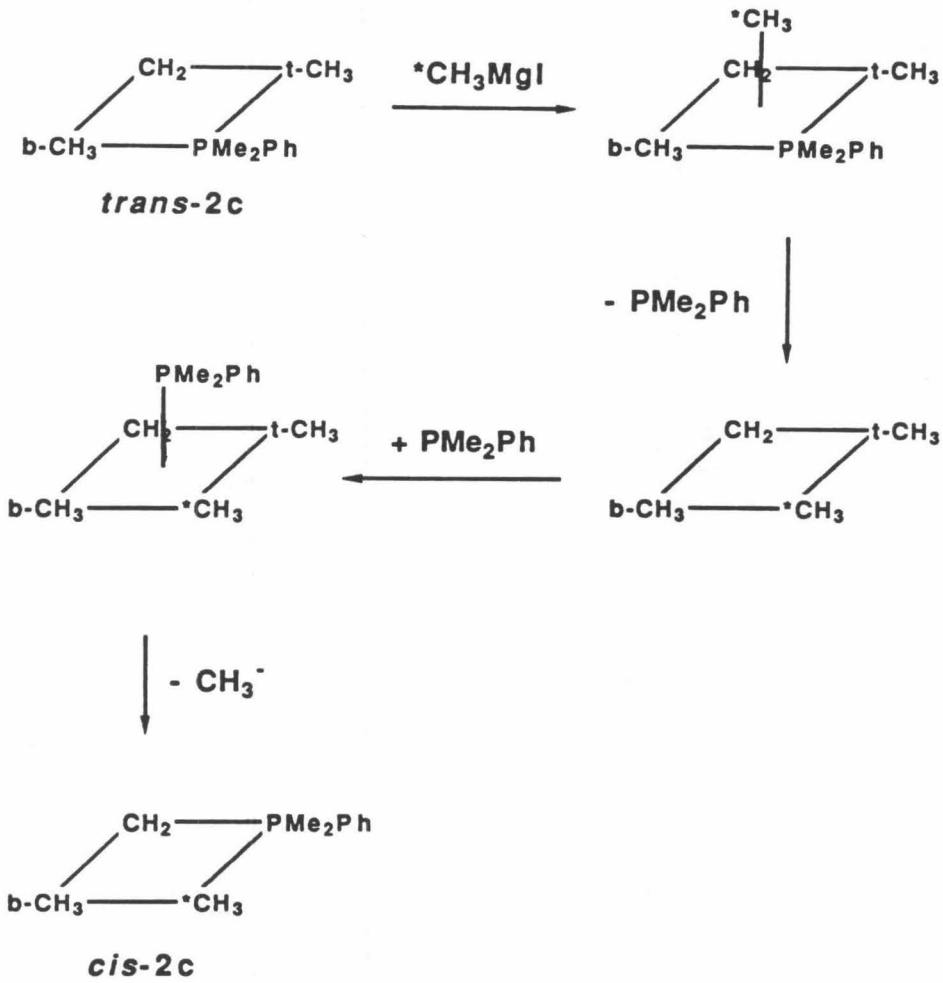

Scheme I. A mechanism for the reaction of **2b** with $^{*}CH_3MgI$ ($^{*}C = {}^{13}C$) to generate ***trans*-2c** which have ^{13}C labelled methyl group at the bridging methyl or terminal methyl position. Negative charge for the intermediate was omitted for simplicity. Symbols b and t designate bridging and terminal, respectively.

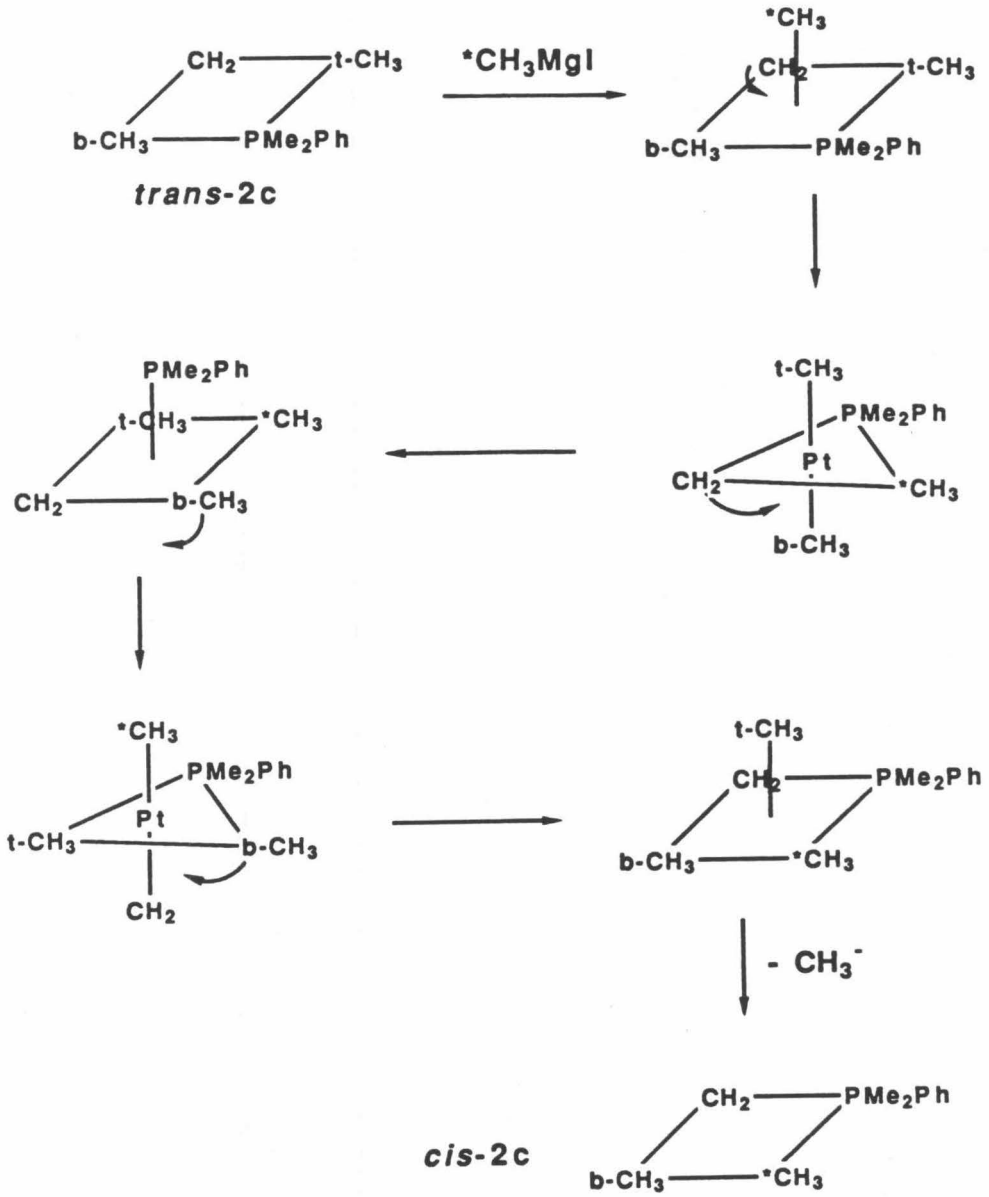

Scheme II. A mechanism involving a pesudorotation for the isomerization of ***trans*-2c** to ***cis*-2c** with CH_3MgI as a catalyst. $^{13}CH_3MgI$ was used to show isotope exchange together with the isomerization. Isotope exchange can be happened through the substitution reaction to give ***trans*-2c** whose bridging methyl group is enriched by ^{13}C.

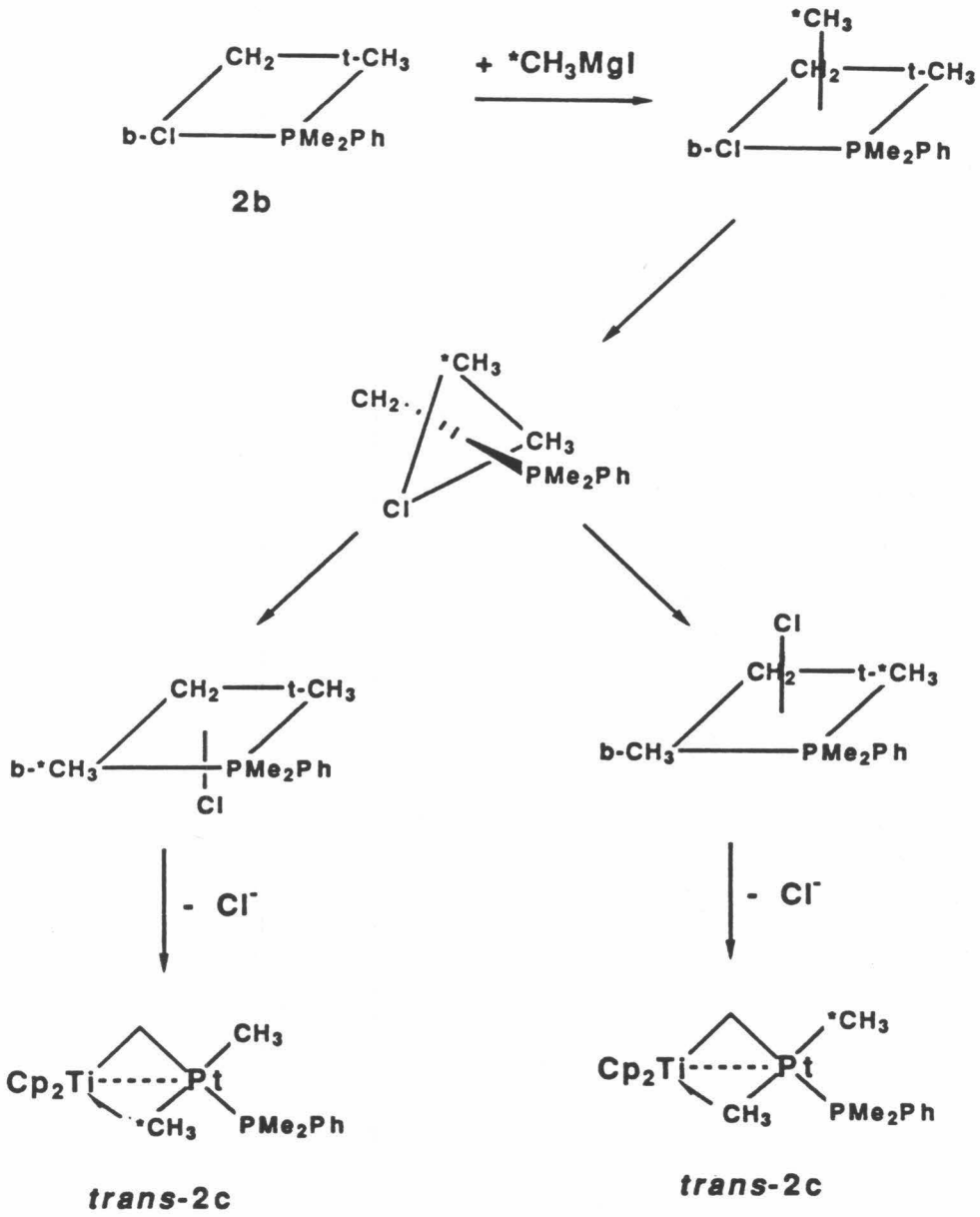

Scheme III. Another mechanism involving consecutive displacements for the isomerization of ***trans*-2c** to ***cis*-2c** with CH_3MgI as a catalyst.

Reaction with Tertiary Phosphines. An equimolar mixture of *trans*-**2c** and PMe_2Ph gave a mixture of *trans*-**2c**, $Cp_2Ti{=}CH_2(PMe_2Ph)$,[16] and a platinum complex after several hours at room temperature. No isomerization of *trans*-**2c** to *cis*-**2c** was observed. Reaction of *trans*-**2c** with PMe_3 gave a mixture of $Cp_2Ti{=}CH_2(PMe_2Ph)$, $Cp_2Ti{=}CH_2(PMe_3)$, *trans*-**2c**, *trans*-**2c'**, and a platinum complex, which were identified by ^1H, $^{31}P\{^1H\}$ NMR. $Cp_2Ti{=}CH_2(PMe_2Ph)$, $Cp_2Ti{=}CH_2(PMe_3)$ did not react with excess CO at –50 °C. No expected intermediate **3**[16] was observed upon warming slowly to room temperature, where only the decomposition happened.

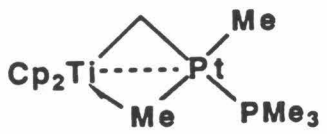

trans-**2c'**

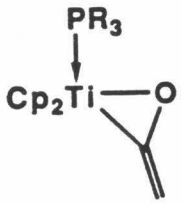

$PR_3 = PMe_2Ph, PMe_3$

3

Oxidative Addition of Methyl Iodide and Acetyl Chloride. Ten equivalents of methyl iodide were added oxidatively on platinum center of **2b** at room temperature to yield complex **4**, which has unsymmetrical Cp groups and bridging methylene protons as identified in ^1H NMR. (A resonance with platinum satellites (J_{PtP} = 1620 Hz) in $^{31}P\{^1H\}$ NMR confirmed a single product.) The product was fairly stable regardless of the absence of excessive methyl iodide at room temperature. Upon heating at 70 °C for 2 hours, the complex **4** was converted to starting materials. Longer thermolysis of **4** at 70 °C gave only paramagnetic species without evolution of ethane. Two equivalents of acetyl chloride reacted with **2b** at room temperature to produce several

resonances in ^1H NMR for Cp groups with low conversion (approximately 30%). No change was observed for the reaction of *trans*-**2c** with excess of methyl iodide below 0 ^oC. At room temperature products formed with low conversion decomposed nonselectively.

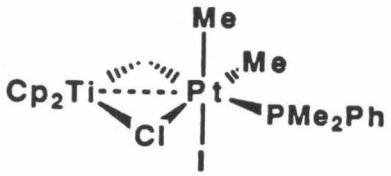

4

CH Activation. A mixture of *trans*-**2c** and *cis*-**2c** which have ^{13}C labelled methyl group at the bridging methyl and/or terminal methyl position was prepared to measure the rate of equilibration between the μ-CH_3 and the μ-CH_2. The measured rate of equilibration which involves CH activation process was relatively slow ($k = 6.7 \times 10^{-7} sec^{-1}$) in comparison with the rhodium and the iridium analogues ($k = 2.0 \times 10^{-5}$, $1.1 \times 10^{-5} sec^{-1}$). The further studies were inhibited by the decomposition to unidentified compounds and generation of unknown peaks in the region of μ-CH_2 group in the ^{13}C NMR.

Table I. NMR Data for the μ-Methylene Complexes:[a]

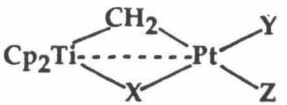

Complexes			^{1}H NMR			^{13}C{^{1}H} NMR					^{31}P{^{1}H} NMR	
				J(Hz)			J(Hz)			Assign-		$^1J_{PtP}$
X	Y	Z	δ	PH	PtH	δ	PC	PtC	[$^1J_{CH}$]	ments	δ[b]	(Hz)
Cl	Me	PMe_2Ph	8.09(d)	5.1	39.3	179.2(d)	58	409	136	μ-CH_2	-8.1	2788
	(2b)		5.57(s)	0.0	0.0	108.1(s)	0	0	174	Cp		
			1.51(d)	9.0	26.9	14.9(d)	31	34	129	PMe		
			1.01(d)	8.5	93.8	-14.4(d)	5	822	130	PtMe		
Me	Me	PMe_2Ph	7.92(d)	4.4	33.5	178.5(d)	66	472	137	μ-CH_2	-2.8	2450
	(*trans*-2c)		5.28(s)	0.0	0.0	105.1(s)	0	0	173	Cp		
			1.44(d)	8.3	23.7	13.8(d)	30	30	129	PMe		
			0.72(d)	8.8	64.7	-10.1(d)	8	565	125	PtMe		
			~-3(br)	c	c	47.6(s)	0	381	115[d]	μ-Me (at r.t.)		
			1.20(d)	(non-agostic μ-CH_3)		$^2J_{HH}$ = 12.5 Hz					μ-Me (at -82°C)	
			-12.4(t)	(agostic μ-CH_3)								
Me	PMe_2Ph	Me	7.42(d)	6.0	22.5	180.0(d)	5	324	133	μ-CH_2	-3.5	2690
	(*cis*-2c)		5.22(s)	0.0	0.0	105.0(s)	0	0	173	Cp		
			1.45(d)	8.8	25.9	14.2(d)	34	34	129	PMe		
			0.82	7.8	59.6	-10.6(d)	9	540	125	PtMe		
			~-3(br)	c	c	46.9(d)	88	553	120[d]	μ-Me (at r.t.)		
			1.61(d)	(non-agostic μ-CH_3)		$^2J_{HH}$ = 12.8 Hz				μ-Me (at -82°C)		
			-11.3(t)	(agostic μ-CH_3)								

a) All data are recorded at room temperature in benzene-d_6 unless otherwise noted. b) Chemical shift is referred to an external 85% H_3PO_4 standard (downfield positive). c) Coupling constant is obscure due to broadening. d) See ref. 5c.

Table II. Selected Distances and Angles.

Complex 2a

Distances (Å)		Angles (°)	
Pt–Ti	2.962(2)	C1–Pt–C2	83.1(6)
Cl–C1	3.374(18)	C1–Pt–P	170.4(5)
Pt–Cl	2.399(4)	C1–Pt–Cl	96.6(5)
Pt–C1	2.112(17)	C2–Pt–P	87.7(5)
Pt–C2	2.071(15)	Pt–Cl–Ti	75.7(1)
Pt–P	2.261(4)	Cl–Ti–C1	97.0(5)
Ti–Cl	2.427(5)	Ti–C1–Pt	90.3(7)
Ti–C1	2.066(18)	Pt–P–C3	113.0(5)
C1–HC1a	1.03(11)	Pt–P–C4	116.3(5)
C1–HC1b	0.82(14)	Pt–P–C5	117.2(5)
P–C3	1.842(16)	HC1a–C1–HC1b	110.1(113)
P–C4	1.809(16)		
P–C5	1.833(15)		
Pt–HC1a	2.66(11)		
Pt–HC1b	2.44(13)		
Ti–HC1a	2.71(11)		
Ti–HC1b	2.57(13)		

Complex *trans*-2c

Distances (Å)		Angles (°)	
Pt–C1	2.078(7)	C1–Pt–C11	105.7(3)
Pt–C11	2.122(8)	C11–Pt–P	87.6(2)
Pt–C2	2.108(6)	P–Pt–C2	86.3(2)

Pt–P	2.279(2)	C2–Pt–C1	80.3(3)
Pt–Ti	2.776(1)	C1–Ti–C11	95.7(3)
Pt–HC1a	2.58(5)	Pt–C1–Ti	82.9(3)
Pt–HC1b	2.61(5)	Pt–C1–HC1a	112.1(32)
Pt–HC11a	2.48(6)	Pt–C1–HC1b	113.3(31)
Pt–HC11c	2.53(7)	Ti–C1–HC1a	116.3(32)
Pt–HC11b	2.89(5)	Ti–C1–HC1b	121.1(31)
Ti–C1	2.115(7)	HC1a–C1–HC1b	109.0(45)
Ti–C11	2.395(8)	Pt–C11–Ti	75.6(2)
Ti–HC1a	2.67(5)	Pt–C11–HC11a	105.1(42)
Ti–HC1b	2.74(5)	Pt–C11–HC11c	103.7(40)
Ti–HC11b	1.93(5)	Pt–C11–HC11b	127.1(28)
Ti–HC11a	2.94(6)	Ti–C11–HC11b	51.7(27)
Ti–HC11c	3.07(7)	Ti–C11–HC11a	122.3(42)
C1–C11	3.348(11)	Ti–C11–HC11c	126.3(40)
P–C3	1.828(9)	HC11a–C11–HC11b	101.2(50)
P–C4	1.829(9)	HC11b–C11–HC11c	109.3(48)
P–C5	1.829(6)	HC11c–C11–HC11a	109.9(58)
C1–HC1a	0.94(5)	Pt–P–C3	112.4(3)
C1–HC1b	0.96(5)	Pt–P–C4	115.9(3)
C11–HC11a	0.85(6)	Pt–P–C5	119.0(2)
C11–HC11c	0.97(7)		
C11–HC11b	1.06(5)		

Table III. Crystal and Intensity Collection Data for Complex **2b**.

Formula: $C_{20}H_{26}ClPPtTi$	Formula Weight: 575.84
Crystal Color: orange-red	Habit: irregular plates
a = 13.249(3) Å	
b = 11.646(3) Å	β = 114.45(2)°
c = 14.542 Å	
V = 2042.6(10) Å^3	Z = 4
λ = 0.71073 Å	T: 23 °C
Graphite monochromator	
Space group: $P2_1/n$	Absences: 0k0, k odd; h0l, h + l odd
Crystal Size: 0.24 x 0.13 x 0.04 mm	μ = 77.98 cm^{-1} (μr_{max} = 1.08)
CAD-4 Diffractometer	θ-2θ scan
2θ range: 2° – 40°	Octants collected; ±h, ±k, l
Number reflections measured: 3837	
Number of independent reflections: 1900	
Number with $F_o^2 > 0$: 1717	
Number with $F_o^2 > 3\sigma(F_o^2)$: 1233	
Goodness of fit for merging data: 1.07	
Final R-index: 0.0621 (0.035 for $F_o^2 > 3\sigma(F_o^2)$)	
Final goodness of fit: 1.15	

Table IV. Crystal and Intensity Collection Data for Complex *trans*-**2c**.

Formula: $C_{21}H_{29}PPtTi$	Formula Weight: 555.42
Crystal Color: orange-red	Habit: prismatic
a = 13.333(4) Å	
b = 11.686(2) Å	β = 115.03(2)°
c = 14.351(3) Å	
V = 2026.0(8) Å^3	Z = 4
λ = 0.7107 Å	T: 23 °C
Graphite monochromator	
Space group: $P2_1/n$	Absences: 0k0, k odd; h0l, h + l odd
Crystal Size: 0.42 x 0.14 x 0.15 mm	μ = 77.42 cm^{-1} (μr_{max} = 1.81)
CAD-4 Diffractometer	θ-2θ scan
2θ range: 2° – 50°	Octants collected; ±h, k, ±l
Number reflections measured: 8745	
Number of independent reflections: 3540	
Number with $F_o^2 > 0$: 3308	
Number with $F_o^2 > 3\sigma(F_o^2)$: 2614	
Goodness of fit for merging data: 0.99	
Final R-index: 0.0394 (0.0242 for $F_o^2 > 3\sigma(F_o^2)$)	
Final goodness of fit: 1.12	

EXPERIMENT

General. ^1H and $^{13}C\{^1H\}$ NMR spectra were recorded on JEOL GX-400 (^1H, 399.8 MHz; ^{13}C, 100.4 MHz) and FX-90Q (^1H, 89.6 MHz) spectrometers by using ^1H (of residual protons) and ^{13}C NMR signals of deuterated solvents as internal references [benzene-d_6(^1H, δ 7.15; ^{13}C, δ 128.0), toluene-d_8(^1H, δ 2.09; ^{13}C, δ 20.4), THF-d_8(^1H, δ 3.58; ^{13}C, δ 67.4), $CDCl_3$ (^1H, δ 7.24)]. $^1J_{CH}$ values were determined by ^{13}C NMR spectroscopy in an INEPT sequence. $^{31}P\{^1H\}$ NMR signals were obtained on a JEOL FX-90Q spectrometer (36.2 MHz) and their chemical shifts referred to an external 85% H_3PO_4 standard (downfield positive). Infrared spectra were measured on a Perkin-Elmer 1720 (FT) spectrometer. Elemental analyses were performed by the California Institute of Technology Analytical Facility.

All manipulations were carried out under argon or vacuum with standard Schlenk techniques or in a nitrogen-filled glove box. Argon was purified by passage through columns of Chemalog R3-11 catalyst and Linde 4 Å molecular sieves. Toluene, benzene, diethyl ether, pentane, and THF, including NMR solvents, were dried over sodium benzophenon ketyl, and vacuum transferred and stored in flasks equipped with Teflon screw valves. Tertiary phosphines (Strem) , methyl iodide (Aldrich), and acetyl chloride (Aldrich) were degassed by freeze-pump-thaw processes and stored in flasks equipped with Teflon screw valves. An etheral solution of $^{13}CH_3MgI$ was prepared from $^{13}CH_3I$, and titrated by *sec*-butanol with 1,10-phenanthroline as an indicator. Carbon monoxide (Matheson), and a etheral solution of MeMgBr (Aldrich) were used as purchased.

Preparation of 2b. To a toluene solution of **2a** prepared from

$Cp_2\overline{TiCH_2C(Me)CH_2}$ (**1**, 0.20g, 0.82 mmol), $PtMeCl(SMe_2)_2$[18] (0.30 g, 0.82 mmol), and toluene (3ml) was added 116 μL of PMe_2Ph at –20 °C. After the solution was stirred for 2 h at room temperature, volatiles were removed under vacuum. The resulting red solid was dissolved in toluene (2 mL), diluted with pentane (4 mL), and then filtered through a filter paper-tipped cannula. The filtrate was slowly cooled to –50 °C to yield red crystals of **2c**, which were collected by filtration, washed with cold pentane (2 mL x 2), and dried under vacuum (0.43 g, 92%). Anal. Calcld for $C_{20}H_{26}ClPPtTi$: C, 41.72; H, 4.55. Found: C, 41.56; H, 4.59.

Preparation of *trans*-2c. A Et_2O solution of MeMgBr (2.2 ml, 4.1 mmol) was added dropwise to a homogeneous solution of **2b** (0.70 g, 1.2 mmol) in toluene (11 mL) and Et_2O (11 mL) mixture at room temperature. After stirring for 3 h, the mixture was concentrated to dryness under vacuum and extracted with toluene (22 mL). The extract was again concentrated to dryness to give a reddish orange solid, which was dissolved in Et_2O (30 ml) and cooled to –50 °C to yield crystals of *trans*-**2c** (0.29 g, 42%). ^1H NMR analysis showed that the product contains 4% of geometrical isomer *cis*-**2b**, which could not be removed by repeated recrystallizations. Anal. Calcd for $C_{21}H_{29}PPtTi$: C, 45.41; H, 5.26. Found: C, 45.37; H, 5.07. IR(KBr): 3050, 2931, 2887, 2808, 2516 (ν_{CH} of the agostic hydrogen), 1443, 1432, 1420, 1283, 1105, 1028, 1014, 950, 925, 805, 748, 710, 700, 679 cm^{-1}.

Preparation of *cis*-2c. A solution of *trans*-**2b** (0.20 g, 0.36 mmol) in toluene (3 mL) and Et_2O (3 mL) was combined with a Et_2O solution of MeMgBr (200 μL, 0.37 mmol) at room temperature. After the solution was stirred for 19 h, volatiles were removed under vacuum, and the resulting solid was extracted with toluene (4 mL). The extract was again concentrated to dryness to form a

precipitate of *cis*-**2c**. The crude product was recrystallized from Et_2O (5 mL) at –50 °C to yield reddish orange crystals (0.13 g, 65%). ^1H NMR spectrum of the product revealed contamination with *trans*-**2c** (4%) and an unidentified compound (6%), which could not be removed by repeated recrystallizations. Anal. Calcld for $C_{21}H_{29}PPtTi$: C, 45.41; H, 5.26. Found: C, 44.59; H, 5.05. IR(KBr): 2934, 2894, 2872, 2518 (ν_{CH} of the agostic hydrogen), 1434, 1420, 1281, 1103, 1021, 1013, 948, 922, 836, 808, 798, 748, 708, 698, 681, 517, 499, 432 cm^{-1}.

X-ray Diffraction Study. (2b) An irregular pate obtained by slow cooling of a Et_2O solution of **2b** was mounted in a capillary and placed on a CAD-4 diffractometer. Unit cell dimension plus an orientation matrix were obtained from the setting angles of 25 reflections with $15^o < 2\theta < 21^o$. The cell dimensions suggested a monoclinic cell and systematic absences in the diffractometer data indicated the space group $P2_1/n$, an unconventional setting of $P2_1/c$. Data were collected at a scan rate of 2° per minute, with three reflections monitored every 10,000 seconds of X-ray exposure. These indicated a small linear crystal decay; the data were corrected for this and for absorption, Lorentz and polarization factors were applied, and the data were placed on a approximately absolute scale by Wilson's method. The platinum position was easily found from a Patterson map and subsequent structure factor-Fourier cycles showed the remaining non-hydrogen atoms. After 6 cycles of least squares, hydrogen atoms were introduced at calculated positions on the benzene and cyclopentadienyl rings and at positions determined from difference maps for the methyl and methylene hydrogen atoms. Further refinement of the positional and anisotropic parameters of the bridging methylene group hydrogen atoms (the remaining hydrogen atoms being repositioned once) converged, with no shift greater than 0.03σ. The R-index for

reflections with $F_o^2 > 3\sigma(F_o^2)$ was 0.035.

(***trans*-2c**). A single crystal prepared by slow cooling of a Et_2O solution of *trans*-**2c** was mounted in a greased capillary and centered on the diffractometer. Unit cell parameters and an orientation matrix were obtained by a least squares calculation from the setting angles of 23 reflections with $42^o < 2\theta < 46^o$. Two equivalent data sets out to a 2θ of 50° were collected and corrected for absorption and a slight decay. Lorentz and polarization factors were applied and the two data sets were then merged to yield the final data set. Several cracks parallel to the (100) planes did not noticeably affect the scan profiles. Systematic absences in the diffractometer data led to the choice of space group $P2_1/n$. Starting non-hydrogen atom positions were assumed from the results of **2b**. Hydrogen atom positions were determined by calculation (for benzene and cyclopentadienyl rings) or from difference maps (for the methyl and methylene groups). The three hydrogen atoms of the terminal methyl group bonded to the platinum atom were modelled by six evenly-spaced half-population hydrogen atoms at calculated positions with isotropic B values 10% greater than that of the attached carbon; these were not refined. The complete least squares full matrix, consisting of spatial and isotropic thermal parameters for the remaining hydrogen atoms, a scale factor, and a secondary extinction coefficient, contained 322 parameters. The hydrogen results were quite acceptable. A final difference map showed deviations of less than 1 $eÅ^{-3}$, mostly attributable to absorption ripple near the two heavy atoms. The final R-index was 0.0394 (0.0242 for $F_o^2 > 3\sigma(F_o^2)$) with a goodness of fit of 1.12.

Calculations were performed with programs of the CRYM Crystallographic Computing System and ORTEP. Scattering factors and corrections for anomalous scattering were taken from a standard reference.[19]

$R = \Sigma | F_o - | F_c | | / \Sigma F_o$, for only $F_o^2 > 0$, and goodness of fit = $[\Sigma w(F_o^2 - F_c^2)^2/(n-p)]^{1/2}$ where n is the number of data and p the number of parameters refined. The function minimized in least squares was $\Sigma w(F_o^2 - F_c^2)^2$, where $w = 1/\sigma^2(F_o^2)$. Variances of the individual reflections were assigned based on counting statistics plus an additional term, $0.014I^2$. Variances of the merged reflections were determined by standard propagation of error plus another additional term, $0.014\langle I\rangle^2$. The absorption correction was done by Gaussian integration over an 8 x 8 x 8 grid. The transmission factors varied from 0.438 to 0.716 for **2b** and from 0.317 to 0.409 for *trans*-**2c**, respectively. The secondary extinction parameters[20] were refined to $0.039(10) \times 10^{-6}$ (for **2b**) and $0.0477(1) \times 10^{-6}$ (for *trans*-**2c**).

REFERENCES AND NOTES

(1) (a) Jacobsen, E. N.; Goldberg, K. I.; Bergman, R. G. *J. Am. Chem. Soc.* **1988**, *110*, 3706-3707. (b) White, G. S.; Stephan, D. W. *Organometallics* **1988**, *7*, 903-910. (c) Gelmini, L.; Stephan, D. W. *Ibid.* **1988**, *7*, 849-855. (d) White, G. S.; Stephan, D. W. *Ibid.* **1987**, *6*, 2169-2175 and references cited therein. (e) Sartain, W. J.; Selegue, J. P. *Organometallics* **1987**, *6*, 1812-1815; *J. Am. Chem. Soc.* **1985**, *107*, 5818-5820. (f) Casey, C. P.; Jordan, R. F.; Rheingold, A. L. *J. Am. Chem. Soc.* **1983**, *105*, 665-667 and references cited therein. (g) Casey, C. P.; Palermo, R. E.; Rheingold, A. L. *Ibid.* **1986**, *108*, 549-550. (h) Casey, C. P.; Palermo, R. E.; Jordan, R. F.; Rheingold, A. L. *Ibid.* **1985**, *107*, 4597-4599. (i) Casey, C. P.; Jordan, R. F.; Rheingold, A. L. *Organometallics* **1984**, *3*, 504-506. (j) Casey, C. P.; Nief, F. *Ibid.* **1985**, *4*, 1218-1220. (k) Barger, P. T.; Bercaw, J. E. *Ibid.* **1984**, *3*, 278-284. (l) Choukroun, R.; Gervais, D.; Jaud, J.; Kalck, P.; Senocq, F. *Ibid.* **1986**, *5*, 67-71. (m) Ferguson, G. S.; Wolczanski, P. T. *Ibid.* **1985**, *4*, 1601-1605. (n) Tso, C. T.; Cutler, A. R. *J. Am. Chem. Soc.* **1986**, *108*, 6069-6071. (o) Oritz, J. V. *Ibid.* **1986**, *108*, 550-551. (p) Sternal, R. S.; Sabat, M.; Marks, T. J. *Ibid.* **1987**, *109*, 7920-7921. (q) Sternal, R. S.; Marks, T. J. *Organometallics* **1987**, *6*, 2621-2623. (r) Bullock, R. M.; Casey, C. P. *Acc. Chem. Res.* **1987**, *20*, 167-173.

(2) (a) Baker, R. T. K.; Tauser, S. J.; Dumestic, J. A., Eds. *Strong Metal-Support Interaction*; American Chemical Society: Washington, D. C., 1986. (b) Imelik, B.; Naccache, C.; Coudurier, G.; Praliaud, H.; Meriaudeau, P.; Gallezot, P.; Martin, G. A.; Verdrine, J. C. Eds. *Metal-Support and Metal-Additive Effects in Catalysis;* Elsevier: New York, 1982.

(3) For recent examples see: (a) Mori, T.; Masuda, H.; Imai, H.; Taniguchi, S.;

Miyamoto, A.; Hattori, T.; Murakami, Y. *J. Chem. Soc. Chem. Commun.* **1986**, 1244-1245. (b) Iwasawa, Y.; Sato, H. *Chem. Lett.* **1985**, 507-510. (c) Doi, Y.; Miyake, H.; Soga, K. *J. Chem. Soc. Chem, Commun.* **1987**, 347-349. (d) Rieck, J. C.; Bell, A. T. *J. Catal.* **1986**, *99*, 262-277. (e) Vannice, M. A.; Twu, C. C. *Ibid.* **1983**, *82*, 213-222. (f)Vannice, M. A.; Sudhakar, C. *J. Phys. Chem.* **1984**, *88*, 2429-2432.

(4) (a) Herrmann, W. A. *Adv. Organomet. Chem.* **1982**, *20*, 159-263. (b) Masters, C. *Ibid.* **1979**, *17*, 61-103. (c) Herrmann, W. A. *Angew. Chem., Int. Ed. Engl.*, **1982**, *21*, 117-130. (d) Holton, J.; Lappert, M. F.; Pearce, R.; Yarrow, P. I. W. *Chem. Rev.* **1983**, *83*, 135-201. (e) Casey, C. P.; Audett, J. D. *Ibid.* **1986**, *86*, 339-352.

(5) (a) Mackenzie, P. B.; Ott, K. C.; Grubbs, R. H. *Pure and Appl. Chem.* **1984**, *56*, 59-61. (b) Mackenzie, P. B.; Coots, R. J.; Grubbs, R. H. submitted for publication in *Organometallics*. (c) Park, J. W.; Mackenzie, P. B.; Schaefer, W. P.; Grubbs, R. H. *J. Am. Chem. Soc.* **1986**, *108*, 6402-6404.

(6) (a) Ozawa, F.; Kurihara, K.; Yamamoto, T.; Yamamoto, A. *J. Organomet. Chem.* **1985**, *279*, 233-243. (b) Ozawa, F.; Kurihara, K.; Fujimori, M.; Hidaka, T.; Toyashima, T.; Yamamoto, A. *Organometallics*, in press.

(7) Silverstein, R. M.; Bassler, G. C.; Morrill, T. C. *Spectrometric Identification of Organic Compounds*, 4th ed.; Wiley: New York, 1981.

(8) Pregosin, P. S.; Kunz, R. W. *^{31}P and ^{13}C NMR of Transition Metal Phosphine Complexes*; Springer-Verlag: Berlin, 1979.

(9) (a) Yarrow, D. J.; Ibers, J. A.; Lenarda, M.; Graziani, M. *J. Organomet. Chem.* **1974**, *70*, 133-145. (b) Rajaram, J.; Ibers, J. A. *J. Am. Chem. Soc.* **1978**, *100*, 829-838. (c) Lenarda, M.; Pahor, N. B.; Calligaris, M.; Graziani, M.; Randaccio, L. *J. Chem. Soc., Dalton Trans.* **1978**, 279-282.

(10) Wisner, J. M.; Bartczak, T. J.; Ibers, J. A.; Low, J. J.; Goddard III, W. A. *J. Am. Chem. Soc.* **1986**, *108*, 347-348.

(11) (a) Straus, D. A.; Grubbs, R. H. *Organometallics* **1982**, *1*, 1658-1661. (b) Straus, D. A. Ph. D. Thesis, California Institute of Technology, Pasadena, CA, 1983.

(12) Upton, T. H.; Rappe, A. K. *J. Am. Chem. Soc.* **1985**, *107*, 1206-1218.

(13) Benett, M. A.; Chee, H.-K.; Robertson, G. B. *Inorg. Chem.* **1979**, *18*, 1061-1070.

(14) (a) Parsons, E. J.; Larsen, R. D.; Jennings, P. W. *J. Am. Chem. Soc.* **1985**, *107*, 1793-1794. (b) Whitla, W. A.; Powell, H. M.; Venanzi, L. M. *J. Chem. Soc., Chem. Commun.* **1966**, 310-311. (c) De Renzi, A.; Di Blassio, B.; Paiaro, G.; Panunzi, A.; Pedone, C. *Gazz. Chim. Ital.* **1976**, *106*, 765. (d) Struchkov, Y. T.; Aleksandrov, G. G.; Pukhnarevich, V. B.; Sushchinskaya, S. P.; Voronkov, M. G. *J. Organomet. Chem.* **1979**, *172*, 269-272. (e) Goel, A. B.; Goel, S.; Vanderveer, D. *Inorg. Chim. Acta* **1981**, *54*, L267-269. (f) Olthof, G. J. *J. Organomet. Chem.* **1977**, *128*, 367-373. (g) Jungst, R.; Sekutowski, D.; Davis, J.; Luly, M.; Stucky, G. *Inorg. Chem.* **1977**, *16*, 1645-1655. (h) van der Wal, H. R.; Overzet, F.; van Oven, H. O.; de Boer, J. L.; de Liefde Meijer, H. J.; Jellinek, F. *J. Organomet. Chem.* **1975**, *92*, 329-340. (i) Sekutowski, D.; Jungst, R.; Stucky, G. D. *Inorg. Chem.* **1987**, *17*, 1848-1855.

(15) (a) Andersen, G. K.; Cross, R. J. *Chem. Soc. Rev.* **1980**, *9*, 185-215. (b) Peloso, A. *Coordination Chem. Rev.* **1973**, *10*, 123-181. (c) Petrosyan, V. S.; Permin, A. B.; Bodgdashkina, V. I.; Krut'ko, D. P. *J. Organomet. Chem.* **1985**, *292*, 303-309. (d) Wood, J. S. *Prog. Inorg. Chem.* **1972**, *16*, 227-486.

(16) (a) Meinhart, J. D.; Ansyln, E. V.; Park, J. W.; Grubbs, R, H. unpublished results. (b) Meinhart, J. D. Ph. D. thesis, California Institute of

Technology, Pasadena, California, 1987.

(17) (a) Scott, J. D.; Puddephatt, R. J. *Organometallics* **1986**, *5*, 7522-2529. (b) Scott, J. D.; Puddephatt, R. J. *Organometallics* **1985**, *4*, 1221-1223. (c) Scott, J. D.; Puddephatt, R. J. *Organometallics* **1986**, *5*, 1253-1257.

(18) (a) Scott, J. D.; Puddephatt, R. J. *Organometallics* **1983**, *2*, 1643-1648. (b) Cox, E. G.; Saenger, H.; Wardlaw, W. *J. Chem. Soc.* **1934**, 182-186. (c) Roulet, R.; Barbey, C. *Helv. Chim. Acta* **1973**, *56*, 2179-2186.

(19) Cromer, D. T.; Waber, J. T. *International Tables for X-ray Crystallography;* Kynoch: Birmingham, UK, 1974; Vol. IV, p. 71 and p. 149.

(20) Equation (3) in Larson, E. C. *Acta Cryst.* **1967**, *23*, 664-665.

CHAPTER 4

Structure and Reactivity of Titanocene (η^2-thioformaldehyde) Trimethylphosphine Complex

ABSTRACT

Titanocene (η^2-thioformaldehyde) was prepared from titanocene methylidene phosphine complex and sulfur-containing organic compounds (e.g. alkene sulfide, triphenylphosphine sulfide) including elemental sulfur. The product **3** crystallized in the orthorhombic system, in space group *Pnma* (#62), with a = 13.719(3) Å, b = 12.384(1) Å, c = 8.671(1) Å, V = 1473.2(6) $Å^3$; Z = 4. Mechanistic studies utilizing *trans*-styrene sulfide-d_1 suggested the stepwise reaction to explain equimolar mixture of *trans*- and *cis*-styrene-d_1 as by-products. The complex **3** reacted with methyl iodide to produce cationic titanocene (η^2-thiomethoxymethyl) complex (**6a**), which crystallized with acetonitrile in the orthorhombic system, space group *Pbca* (#61) with a = 14.839(2) Å, b = 15.184(14) Å, c = 18.461(3) Å, V = 4159.5(14)$Å^3$, Z = 8. Complexes having less coordinating anion like BF_4 or BPh_4 could be obtained through metathesis. Together with structural analyses, the further reactivities of the complex **3** and **6** were examined.

INTRODUCTION

Titanocene metallacycles[1] show a wide variety of reactivities with organic and inorganic reagents. Methylene transfer to organic carbonyls, including enolizable carbonyls, is one of the well-established reactions.[2,3] The reactions include ring opening polymerization,[4] complexation with metal halides,[5] and olefin metathesis.[6] All these reactions occur through a reactive intermediate which exhibits behavior consistent with that of a transition metal carbene.[7] Titanocene methylidene trimethylphosphine complex, which is derived from titanocene metallacyclobutanes, is known to have similar reactivities.[8]

In this chapter, the preparation of titanocene (η^2-thioformaldehyde) from titanocene methylidene phosphine complex and sulfur-containing organic compounds is described. Unstable thioaldehyde is known to be stabilized through the coordination to transition metals.[9] Also, the interest in the preparation and properties of thioformaldehyde complexes was stimulated by the fact that formaldehyde complexes were postulated as intermediates in the hydrogenation of carbon monoxide. Several thioaldehyde complexes of late transition-metals have been reported. However, only one example has been published for the early transition-metals.[9a,b]

The reaction of metal carbenes with organic sulfides or elemental sulfur to make thioformaldehyde complexes will serve as a model for the heterogeneous hydrodesulfurization (HDS)[10] and poisoning of catalysts during the Fischer-Tropsch reaction.[11]

RESULTS AND DISCUSSION

The complex $Cp_2Ti(\eta^2\text{-}CH_2S)\cdot PMe_3$ (**3**) was prepared from the compound $Cp_2Ti{=}CH_2\cdot PMe_3$ (**2a**), one of the well-characterized titanocene methylidene compounds, and various sulfur-containing compounds including elemental sulfur (eq 1–2). Reaction of **2a** with propene sulfide gave **3** in the highest yield (83% based on the amount of **2a**), while separation yield was 70%. Easily polymerized styrene sulfide and impure cyclohexene sulfide (P = 85%) gave **3** in low yields (42 and 65%, respectively). Elemental sulfur and triphenylphosphine sulfide gave the same product in a similar yield (41, 35% respectively) with the formation paramagnetic species. In all the above reactions, the complex **3** was the only observable product in ^1H NMR. Alkene sulfides and triphenylphosphine sulfide were used to make the thioaldehyde ligand for the late transition-metal methylidenes.[9] Utilization of elemental sulfur for this type of transformation has a precedent only in the case of rhodium vinylidene complex.[12] Recently a different type of route to make an early transition-metal (η^2-thioaldehyde) complex from dimethyl zirconocene and thiols has been reported.[9a,b]

(1)

1a R = CH_3, R' = CH_3
b R = CH_3, R' = n-Pr

2a $PR''_3 = PMe_3$
b $PR''_3 = PMe_2Ph$
c $PR''_3 = PEt_3$

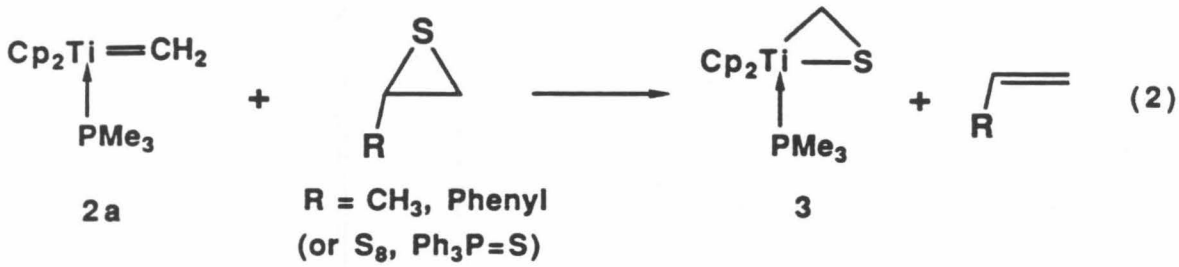

Trimethylene sulfide, which has less ring strain than alkene sulfide, reacted with **3** to make a different type of product (**4**) (eq 3). However, tetrahydrothiophene and thiophene were inert toward **3**.

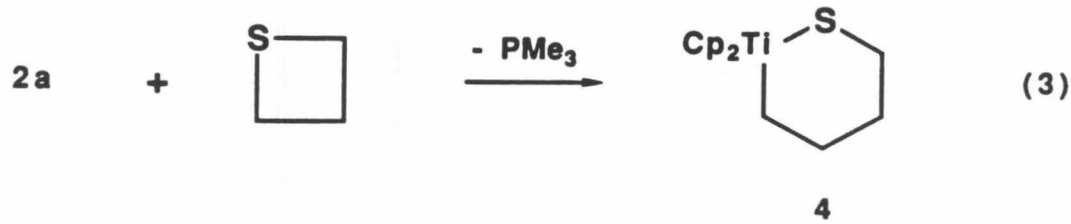

Crystal Structure of 3. Complex **3** were subjected to single crystal X-ray diffraction studies. Selected bond lengths and angles are listed in Table I. The crystal and intensity collection data are shown in Table III. An ORTEP diagram is shown in Figure 1. The molecule lies in a mirror plane, with the Ti, S, P, C1, and C2 atoms in this plane. The mirror relates the two Cp rings and two of the phosphine methyl groups plus the hydrogen atoms on C1. The Cp ring is coordinated normaly to the titanium atom, with T–C distances averaging 2.393(12) Å. The CH_2S group is bonded to titanium at both S and C. The H1a–C1–H1a' plane nearly bisects the Ti–C1–S angle; in particular, the hydrogen atoms are not in the plane through C1 and S perpendicular to the

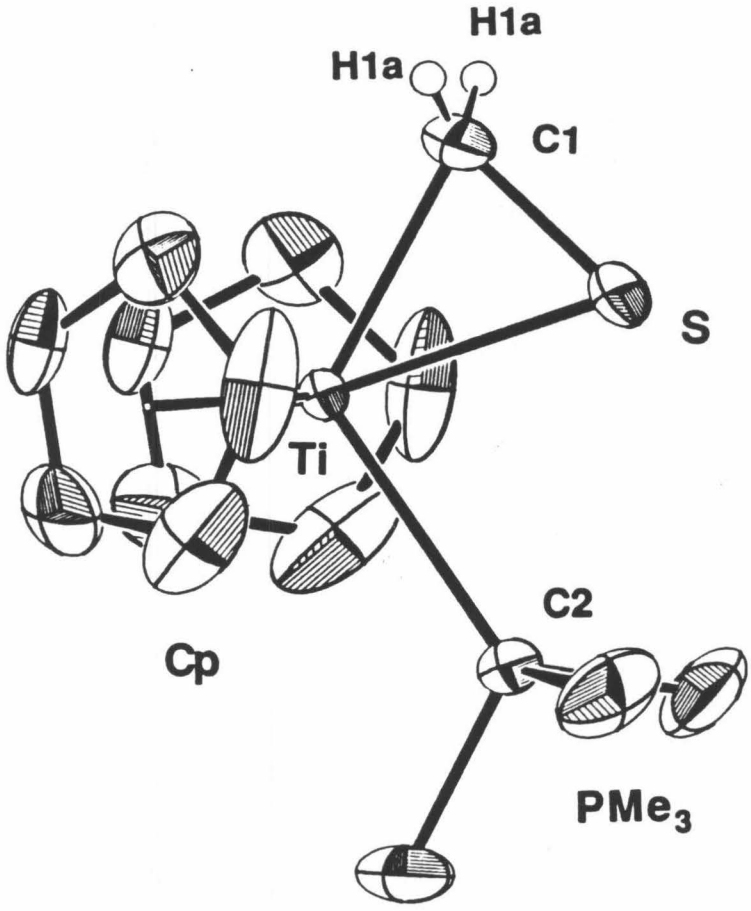

Figure 1. ORTEP diagram of complex **3**. The ellipsoids are drawn at 50% probability level except for the hydrogen atoms. The hydrogen atoms of the cyclopentadienyl and PMe_3 ligands are omitted for clarity.

mirror plane. The trimethylphosphine ligand has normal distances and angles. The C1–S bond distance of 1.744(3) Å reflects the intermediate bonding character between single and double bond.[13] This carbon–sulfur distance more resembles that of rhenium thioformaldehyde (1.742(9) Å)[9c] than those of zirconium thioacetaldehyde (1.785(11)Å)[9b] and thioformaldehyde on osmium clusters (1.77(2), 1.82(3) Å),[9d] implying stronger tendency of Ti(II) formation. This reasonable amount of back-donation explains the long Ti–S distance (2.452(1) Å).[14] Also, the high ^{1}H-^{13}C coupling constant of thioformaldehyde group (157 Hz) agrees with the above conclusion. However, the chemical shift did not serve as a good criterion of bonding character due to anisotropic effects of cyclopentadienyl groups and metal.

Mechanism for the Formation of 3. Because of convenient synthesis, *trans*-styrene sulfide-d_1 was used to study the mechanism. Stereospecific conversion of *trans*-styrene oxide-d_1 to *trans*-styrene sulfide-d_1 was achieved through the use of triphenylphosphine sulfide.[15] When the complex **2** was allowed to react with excess *trans*-styrene sulfide-d_1 at room temperature, a mixture of **3**, polystyrene sulfide, *trans*-styrene-d_1, and *cis*-styrene-d_1 was observed in ^{1}H NMR (eq 4).

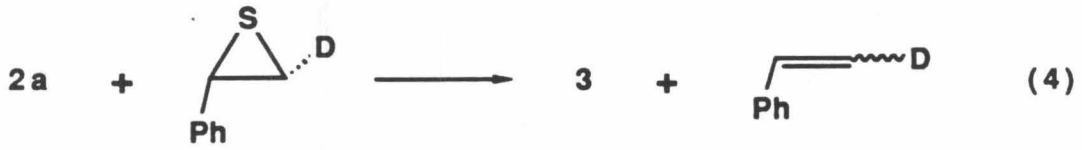

(4)

The ratio of *trans*-styrene-d_1 and *cis*-styrene-d_1 was 0.48 : 0.52 as analyzed by ^{2}H NMR. No styrene sulfide-d_1 was observed after the reaction, because the polymerization of styrene sulfide was fast with the above reaction conditions.

The equimolar mixture of *trans*- and *cis*- styrene-d_1 required a stepwise reaction mechanism. A 6-membered ring was formed from the reaction between complex **2a** and trimethylene sulfide. This type of reactivity supports the above mechanism, because the ring closure is favored over the formation of a cyclopropane and complex **2a**. (Scheme I, II).

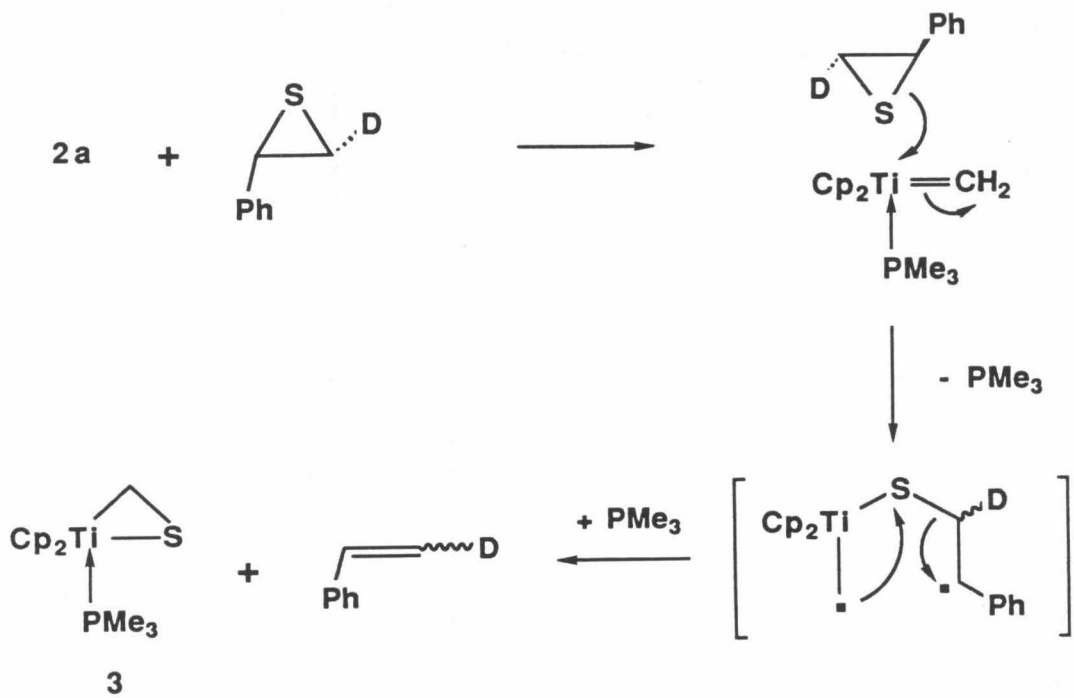

Scheme I. A stepwise mechanism for the reaction of **2a** with styrene sulfide was required to explain the equimolar mixture of *trans*- and *cis*-styrene-d_1 as by-products. A radical mechanism is preferred in view of the analogous reaction.

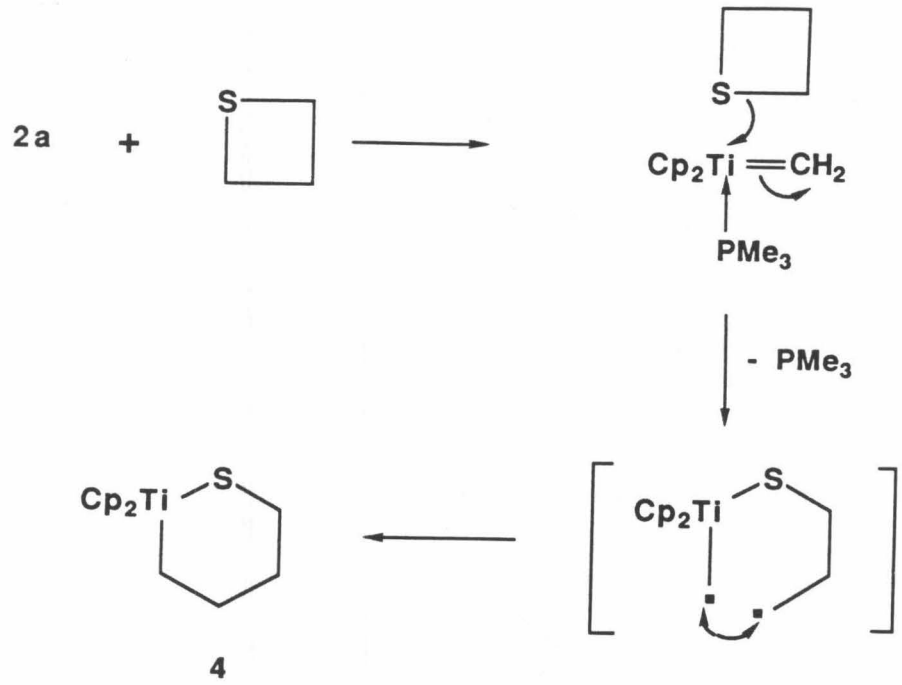

Scheme II. A biradical mechanism for the reaction of **2a** with trimethylene sulfide. The formation of a three membered cyclopropane ring is unfavorable.

This stepwise mechanism can be thought of as the general mechanism for the reaction of **2a** with alkene sulfide. An attempt to quench the reaction was unsuccessful since polymerization of styrene sulfide was the major pathway at low temperature. Analogous reaction with styrene oxide is known to proceed with a similar stepwise mechanism.[16] (However, the product is different due to thermodynamically high energy pathway leading to titanocene formaldehyde complex.) The small substituent effect on the rates of the reaction implied the radical mechanism in the styrene oxide case. Also, a mechanism involving initial electron transfer was proposed for the reaction of **2a** with benzyl chloride.[17] A radical mechanism for the reaction of **2a** with alkene sulfide is preferred in view of the similarity of the these reactions.

Reactivity of 3. The complex **3** did not show clean insertion products with various triple (C≡C, C≡N) and double (C=C, C=O, C=S) bonds. Among many proton sources (e.g. HCl, CF_3CO_2H, H_2O, CH_3OH), trifluoroacetic acid manifested the cleanest protonolysis giving a mixture of $Cp_2Ti(O_2CCF_3)_2$, PMe_3, and CH_3SH (eq 5). The reaction of complex **3** with dihydrogen yielded $Cp_2Ti(SMe)_2$ (For ORTEP diagram, see Figure 2) and an air-sensitive unidentified compound, presumably through disproportionation after hydrogenolysis (eq 6). Two resonances of $Cp_2Ti(SMe)_2$ in ^1H NMR broadened at high temperature (65–105 °C) and restored at lower temperature. The possibility of exchanges between Cp groups and thiomethoxy groups was conceived. To check the possibility, $Cp_2Ti(SCH_2D)_2$ was prepared with the use of D_2. However, no incorporation of deuterium into Cp ring was observed after prolonged heating at 100 °C. Reaction of **3** with acetyl chloride gave a new product together with Cp_2TiCl_2 as minor product (eq 7). The new product (5) was characterized only by ^1H NMR. The tentative structure was based on the structure of the product **6a** (*vide infra*). Reaction with methyl iodide resulted in a cationic titanocene (η^2-thiomethoxymethyl) complex with iodide anion as a counterion (eq 8). This type of reaction was manifested by several early and late transition-metal thioaldehydes.[18] In contrast to the formation of ionic species, zirconocene thioaldehyde complex gave a covalent complex with a loss of trimethylphosphine.[9b]

$$\mathbf{3} + 2CF_3CO_2H \xrightarrow{-\,PMe_3} Cp_2Ti(O_2CCF_3)_2 + CH_3SH \qquad (5)$$

$$\mathbf{3} + H_2 \longrightarrow Cp_2Ti(SCH_3)_2 \qquad (6)$$

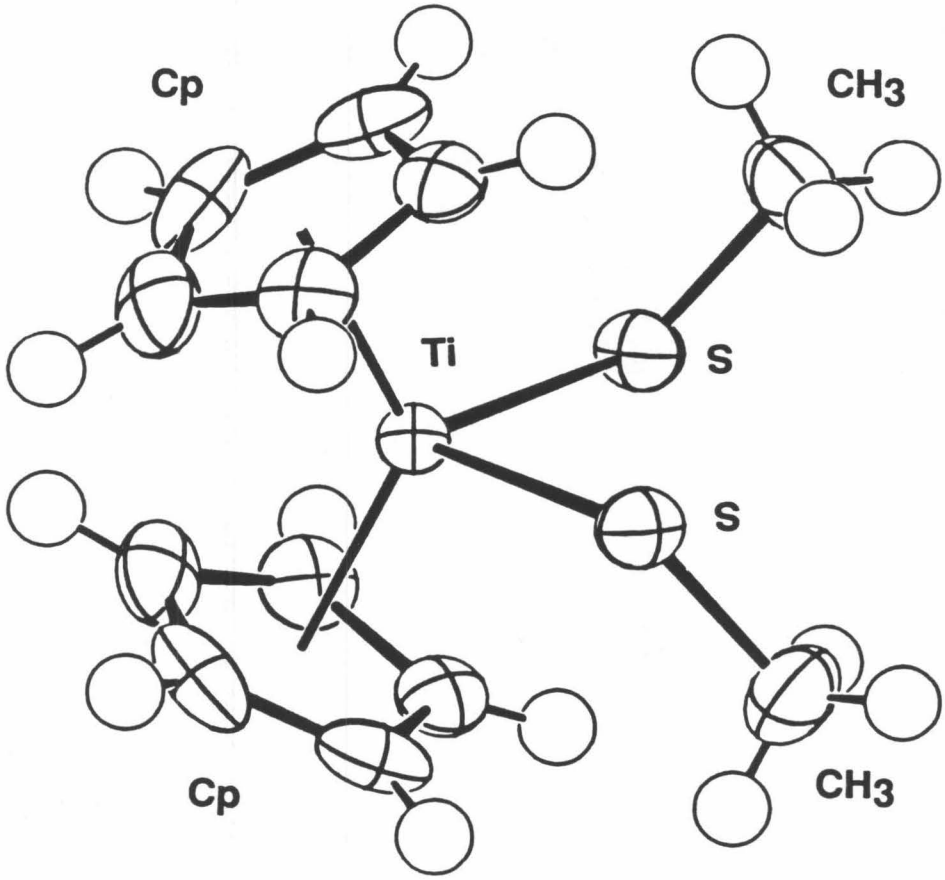

Figure 2. ORTEP diagram of $Cp_2Ti(SMe)_2$. The ellipsoids are drawn at 50% level except for the hydrogen atoms.

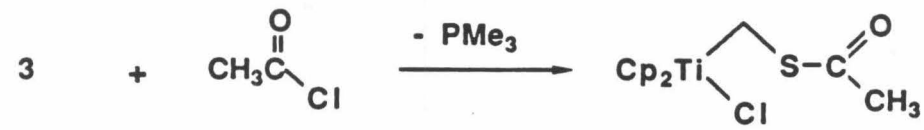

(7)

5

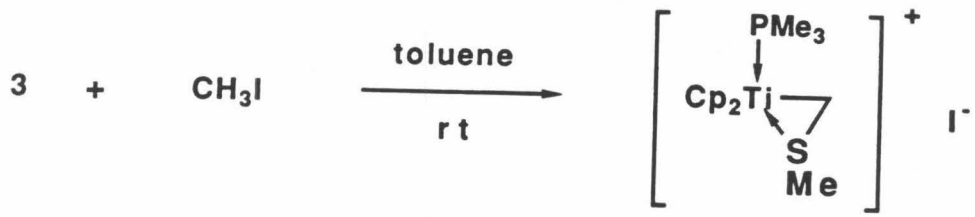

(8)

6a

Crystal Structure of 6a. Complex **6a** was subjected to single crystal X-ray diffraction studies. Selected bond lengths and angles are listed in Table II. Crystal and intensity collection data are shown in Table IV. An ORTEP diagram is shown in Figure 3. The titanium atom is bonded normally to the two Cp rings, with a ring centroid–Ti–ring centroid angle of 130.4° and Ti–C distances averaging 2.381 Å. Coordinated to the titanium in the wedge between the ring are a CH_2SCH_3 group and a trimethylphosphine. The CH_2SCH_3 group is coordinated to the metal atom through both the methylene carbon, at 2.215(5) Å, and the sulfur at 2.555(1) Å. The CS1–S bond distance of 1.751(5) Å is slightly longer than that of parent molecule, **3** (1.744(3) Å). Also, the titanium–sulfur distance, 2.555(1)Å, is longer than that of the complex **3** (2.452(1) Å) and typical Ti–S single bond distance (2.40 Å) but short enough to interact each other. The trimethyl phosphine ligand is adjacent to the methylene carbon of the CH_2SCH_3 group and has normal distances and angles.

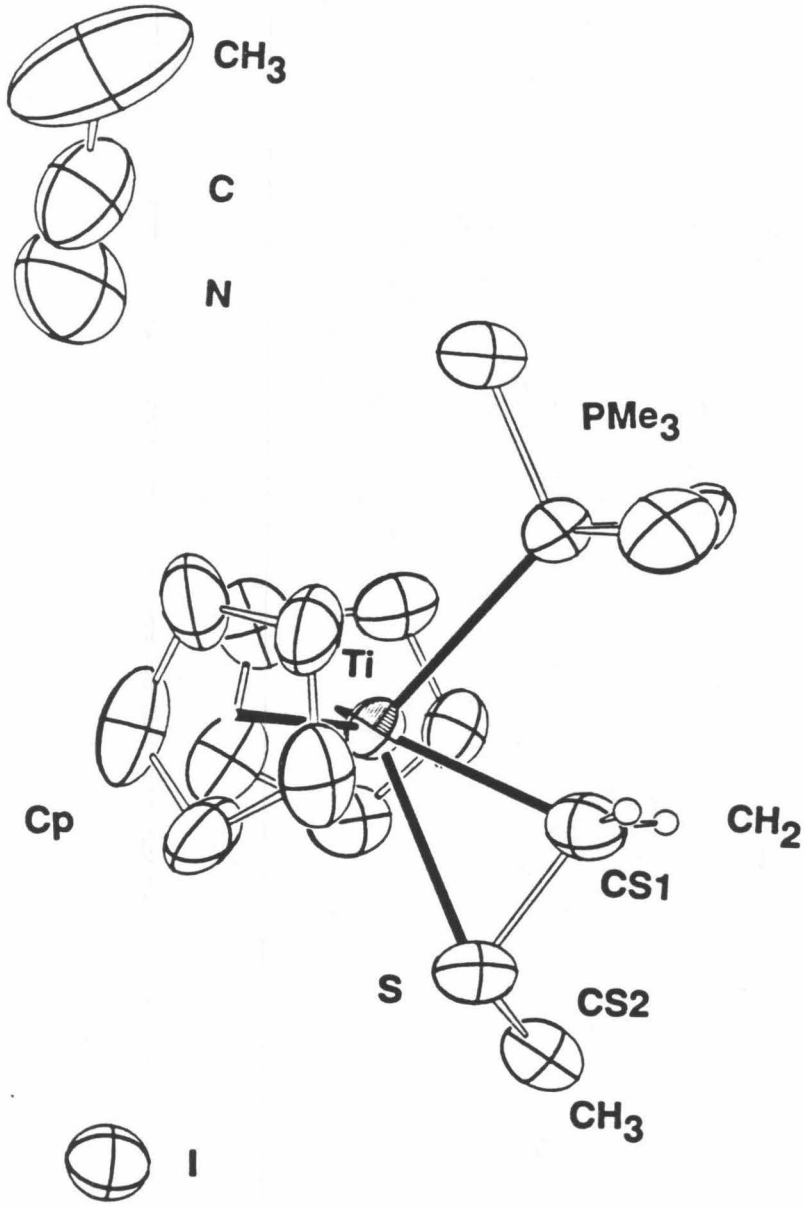

Figure 3. ORTEP diagram of complex **6a**. The ellipsoids are drawn at 50% level except for the hydrogen atoms. The hydrogen atoms of the cyclopentadienyl, terminal methyl, PMe_3 ligands, and acetonitrile are omitted for clarity.

The position of sulfur was changed from the "inside" to "outside" as in the compound **3**. This type of conformational changes is well-known among the $Cp_2M(X)(\eta^2\text{-A–B})$ type of the structure (both A and B group interact with metal atom).[19] The titanium and these three coordinated atoms lie in the same plane within ±.04 Å. The methyl carbon of the CH_2SCH_3 group is 1.52 Å from this plane. The charge balancing iodide ion interacts with neither the titanium nor the sulfur atom. The Ti–I and S–I distances (5.027(1) Å and 4.075(1) Å) are greater than the sums of the van der Waals' radii. Likewise, the acetonitrile, solvent of recrystallization, is isolated from any significant interaction with other atoms.

Preparation of 6b, c. Silver salts have been applied to the complex **6a** in order to metathesize iodide anion by less coordinating BF_4 and BPh_4 anions (eq 9). After isolation of the complex **6c**, copper(I) chloride[20] was added to make phosphine-free complex(**7c**) in the dichloromethane (eq 10). Free $CuCl(PMe_3)_x$ was observed in ^1H, $^{31}P\{^1H\}$ NMR, and phosphine-free product was confirmed by the loss of ^{31}P coupling in ^1H NMR. This cationic titanium complex with vacant ligand-site did not polymerize ethylene and methyl vinyl ether but decomposed above room temperature. This behavior can be explained by two reasons: (1) the different reactivities of titanocene methyl cation[21] relative to that of zirconium methyl cation,[22] which catalyzed the polymerization of ethylene in noncoordinating solvent, (2) the presence of intramolecular sulfur ligand which is expected to bind more strongly to more electron-deficient titanium.

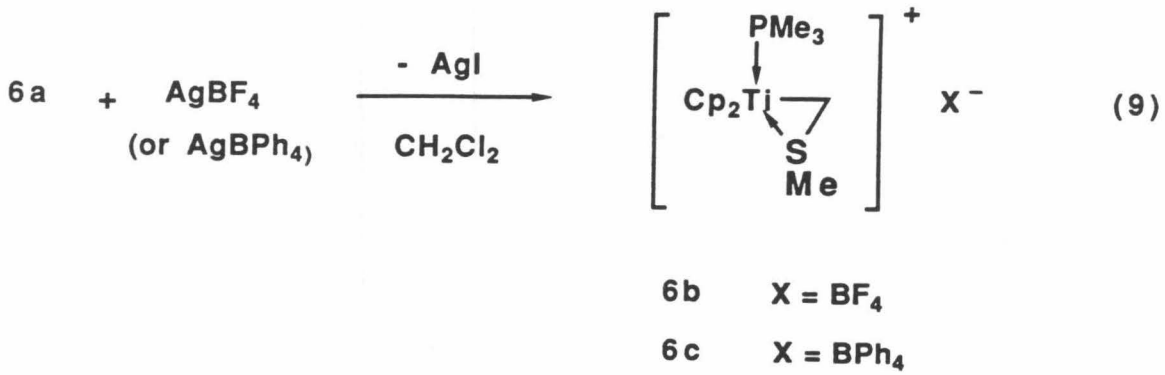
6a
+
AgBF4
(or AgBPh4)
- AgI
CH2Cl2
PMe3
Cp2Ti
S
Me
+
X-
(9)
6b X = BF4
6c X = BPh4

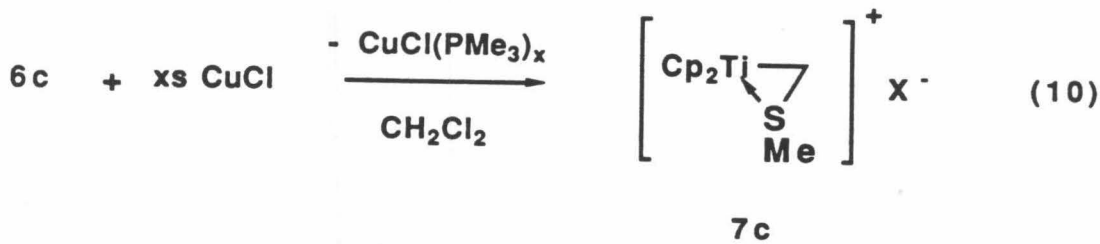
6c
+
xs CuCl
- CuCl(PMe3)x
CH2Cl2
Cp2Ti
S
Me
+
X-
(10)
7c

Table I. Selected Bond Distances and Angles for Complex **3**.

Distance (Å)		Angle (°)	
Ti–S	2.452(1)	CPa–Ti–S	115.6(0)
Ti–P	2.601(1)	CPa–Ti–P	102.3(0)
Ti–C1	2.245(3)	CPa–Ti–C1	104.2(1)
Ti–CPa	2.097(0)	CPb–Ti–CPa	127.4(0)
S–C1	1.744(3)	S–Ti–P	74.1(0)
P–C2	1.824(5)	C1–Ti–S	43.3(1)
P–C3	1.813(4)	C1–S–Ti	62.0(1)
C1–H1a	0.90(3)	S–C1–Ti	74.7(1)
		H1a–C1–Ti	118.2(19)
		H1a–C1–S	115.2(19)
		H1a–C1–H1a	111.1(27)

Table II. Selected Bond Distances and Angles for Complex **6a**.

Distance (Å)		Angle (°)	
Ti–S	2.555(1)	CpA–Ti–CpB	130.7
Ti–CS1	2.215(5)	CpA–Ti–P	102.3
Ti–P	2.581(1)	CpB–Ti–P	102.4
Ti–CpA	2.065	CpA–Ti–S	107.3
Ti–CpB	2.078	CpB–Ti–S	99.6
S–CS1	1.751(5)	CpA–Ti–CS1	115.8(1)
S–CS2	1.803(7)	CpB–Ti–CS1	112.1(1)
I–Ti	5.027(1)	P–Ti–CS1	73.0(1)
I–S	4.075(1)	S–Ti–CS1	42.3(1)
N–Ti	5.132(7)	S–Ti–P	115.2(4)
N–S	5.372(7)	Ti–CS1–S	79.3(2)
		Ti–S–CS1	58.4(2)
		CS1–S–CS2	105.4(3)
		Ti–S–CS2	119.0(2)
		HCS1–CS1–HCS2	104.9(35)
		S–CS1–HCS1	115.7(23)
		S–CS1–HCS2	116.0(26)
		Ti–CS1–HCS1	122.9(23)
		Ti–CS1–HCS2	117.0(26)
		C5–C4–N	177.0(8)

Table III. Crystal and Intensity Collection Data for Complex **3**.

Formula: $C_{14}H_{21}SPTi$	Formula Weight: 300.25
Crystal Color: red	
a = 13.719(3) Å	
b = 12.384(1) Å	
c = 8.671(1) Å	
V = 1473.2(6) $Å^3$	Z = 4
λ = 0.71073 Å	T: 21 °C
Graphite monochromator	
Space group: *Pnma*	Absences: hk0, h odd; 0kl, k + l odd
Crystal Size: 0.48 x 0.41 x 0.56 mm	$\mu = 8.22\ cm^{-1}$ ($\mu r_{max} = 0.35$)
CAD-4 Diffractometer	θ-2θ scan
2θ range: 2° – 50°	Octants collected; h, k, ±l

Number of reflections measured: 2969

Number of independent reflections: 1354

Number with $F_o^2 > 0$: 1319

Number with $F_o^2 > 3\sigma(F_o^2)$: 1200

Goodness of fit for merging data: 0.991

Final R-index: 0.0311 (R factor for 1153 reflections with 2 observations = 0.020)

Final goodness of fit: 2.75

Table IV. Crystal and Intensity Collection Data for Complex **6a**.

Formula: $C_{15}H_{24}SPTiI{\cdot}CH_3CN$	Formula Weight: 483.25
Crystal Color: yellow	
a = 14.839(2) Å	
b = 15.184(14) Å	
c = 18.461(3) Å	
V = 4159.5(14) $Å^3$	Z = 8
λ = 0.7107 Å	T: 21 °C
Graphite monochromator	
Space group: *Pbca*	Absences: 0kl, k odd; h0l, l odd; hk0, h odd
Crystal Size: 0.15 x 0.43 x 0.61 mm	μ = 20.98 cm^{-1} (μr_{max} = 0.80)
CAD-4 Diffractometer	ω scan
2θ range: 2° – 50°	Octants collected; h, k, ±l
Number of reflections measured: 8065	
Number of independent reflections: 3650	
Number with $F_o^2 > 0$: 3294	
Number with $F_o^2 > 3\sigma(F_o^2)$: 2195	
Goodness of fit for merging data: 0.947	
Final R-index: 0.0598 (0.0326 for $F_o^2 > 3\sigma(F_o^2)$)	
Final goodness of fit: 1.33	

Table V. Crystal and Intensity Collection Data for $Cp_2Ti(SMe)_2$.

Formula: $C_{12}H_{16}TiS_2$	Formula Weight: 272.29
Crystal Color: red	Habit: needles
a = 9.300(1) Å	
c = 14.500(2) Å	
V = 1254(1) $Å^3$	Z = 4
λ = 0.71073 Å	T: 21 °C
Graphite monochromator	
Space group: $P4_12_12$	Absences: 00l, $l \neq 4n$; h00, $h \neq 2n$
Crystal Size: 0.18 x 0.13 x 0.34 mm	μ = 9.89 cm^{-1} (μr_{max} = 0.20)
CAD-4 Diffractometer	θ - 2θ scan
2θ range: 2° – 50°	Octants collected; h, k, ±l

Number of reflections measured: 2656

Number of independent reflections: 1139

Number with $F_o^2 > 0$: 1109

Number with $F_o^2 > 3\sigma(F_o^2)$: 920

Goodness of fit for merging data: 1.01 (R for merging = 0.065)

Final R-index: 0.0403 (0.0288 for $F_o^2 > 3\sigma(F_o^2)$)

Final goodness of fit: 1.22

EXPERIMENT

General. All manipulation of air and/or moisture sensitive compounds was carried out with use of standard Schlenk or vacuum line techniques. Argon was purified by passage through columns of BASF RS-11 catalyst (Chemalog) and Linde 4 Å molecular sieves. Solids were transferred and stored in a N_2-filled Vacuum Atmosphere glove box equipped with a MO-40-1 purification train and a DK-3E Dri-Kool conditioner, and Dri-Cold Freezer.

Toluene, benzene, and diethyl ether were stirred over CaH_2 and then transferred to purple sodium-benzophenone ketyl. Pentane was stirred over concentrated H_2SO_4, washed with H_2O, dried over CaH_2, and then transferred to purple sodium-benzophenone ketyl. Dichloromethane and acetonitrile were dried over P_2O_5 or CaH_2 and degassed by evacuation using freeze-pump-thaw cycles. Dried degassed solvents were vacuum-transferred into dry glass vessels equipped with Teflon valve closures and stored under argon. Benzene-d_6 and toluene-d_8 (Cambridge Isotope) were dried and vacuum-transferred from purple sodium-benzophenone ketyl. Dichloromethane-d_2 and acetonitrile-d_3 (Cambridge Isotope) were dried over CaH_2 and degassed by several freeze-pump-thaw cycles. Propene sulfide, cyclohexene sulfide (85%), trimethylene sulfide, methyl iodide, triphenylphosphine sulfide, trifluoroacetic acid, silver tetrafluoroborate, copper(I) chloride (Aldrich), hydrogen (H_2), and deuterium (D_2) (Matheson) were used as purchased. β,β-Dimethyltitanacyclobutane **1**, $Cp_2Ti{=}CH_2{\cdot}PR''_3$ **2**,[8] $AgBPh_4$,[23] and styrene sulfide[15] were prepared using the known method.

NMR spectra were recorded on Varian EM-390 (90 MHz, ^1H), JEOL

FX-90Q (89.60 MHz, ^1H; 22.53 MHz, ^{13}C; 36.27 MHz, ^{31}P; 84.29 MHz, ^{19}F), and JEOL GX-400 (399.65 MHz, ^1H; 61.35 MHz, ^2H; 100.4 MHz, ^{13}C) spectrometers. Chemical shifts are reported in δ, referenced to residual solvent signals. $^{31}P\{^1H\}$ NMR data are referenced externally to 85% H_3PO_4 (downfield positive). $^{19}F\{^1H\}$ NMR data are referenced externally to C_6F_6 (downfield positive). Elemental analyses (C, H, N, S) were performed by either California Institute of Technology Analytical Services or SPANG Microanalytical Laboratory.

Preparation of 3. Propene sulfide (248 μL, 3.16 mmol) was added to the compound **2a** (825 mg, 3.08 mmol) in toluene (27 mL) at 0 °C. The solution was evaporated to dryness after it was allowed to react for 5 minutes at room temperature. (^1H NMR analysis with the internal standard showed that the yield was 83 % based on the amount of **2a**.) Diethyl ether (13 mL) was added to wash the resultant residue. The precipitate was filtered and washed with diethyl ether (5 mL) at –78 °C. Drying *in vacuo* produced yellow powder (678 mg, 2.26 mmol, 74 %). For recrystallization, pentane (28 mL) was layered on top of the solution after the powder was dissolved in dichloromethane (7 mL). At –50 °C, the solution produced huge needle-type crystals (550 mg, 71 %) suitable for single crystal X-ray crystallography and elemental analysis. ^1H NMR (C_6D_6) δ 4.93 (s, 10H, Cp), 2.72 (s, 2H, CH_2), 1.01 (d, 9H, J_{CH} = 6.3 Hz, PMe_3); ^{13}C NMR (C_6D_6) δ 102.9 (dm, J_{CH} = 172 Hz, Cp), 43.3 (t, J_{CH} = 157 Hz, CH_2), 17.3 (dq, J_{CH} = 129 Hz, J_{PC} = 16 Hz, PMe_3); $^{31}P\{^1H\}$ NMR (C_6D_6) δ 10.8 (s). Anal. Calcd for $C_{14}H_{21}PSTi$: C, 56.00; H, 7.05; S, 10.68. Found: C, 55.87; H, 7.17; S, 10.58.

Reaction of the compound **2a** with cyclohexene sulfide, styrene sulfide, elemental sulfur, and triphenylphosphine sulfide gave the same product **3**

with poor yields (Y = 65, 42, 41, 35%, respectively). The reaction with triphenylphosphine sulfide produced a green solution indicating the presence of Ti(III) species.

Preparation of 4. A mixture of trimethylene sulfide (270 μL, 3.54 mmol) and the compound **2a** (500 mg, 1.86 mmol) in toluene (10 mL) was stirred for two hours at room temperature. (^{1}H NMR analysis with the internal standard showed that the yield was 75% based on the amount of **2a**.) Diethyl ether (30 mL) was used to extract the product and evaporated to give concentrated solution (10 mL). Pentane (40 mL) was added to make a double layered solution. The pentane/ether layer produced the red precipitates (188 mg, 0.706 mmol, 38%) at –50 °C. ^{1}H NMR (C_6D_6) δ 5.71 (s, 10H, Cp), 3.31 (s, 2H, CH_2), 2.06 (s, 2H, CH_2), 1.35 (br, 2H, CH_2), 0.91 (br, 2H, CH_2); ^{13}C NMR (C_6D_6) δ 112.0 (dm, J_{CH} = 174 Hz, Cp), 64.7 (t, J_{CH} = 129 Hz, CH_2), 41.3 (t, J_{CH} = 136 Hz, CH_2), 34.9 (t, J_{CH} = 125 Hz, CH_2), 34.1 (t, J_{CH} = 125 Hz, CH_2). Anal. Cacld for $C_{14}H_{18}STi$: C, 63.16; H, 6.81. Found: C, 62.84; H, 6.82.

Crystal Structure Determination of 3. The compound **3** formed large prismatic crystals; a small chunk was cut from one with a razor blade and mounted in a capillary. Data collection details are given in Table 1. The titanium atom was located from a Patterson map, and the remaining atoms were found by successive structure factor-Fourier calculations. The centrosymmetric space group *Pnma* (rather than $Pna2_1$) was chosen based on statistics and confirmed by the successful refinement. The refinement converged quickly. Hydrogen atoms were placed by calculation or difference maps and subsequently included in the single full matrix refinement. The carbon-hydrogen distances range from 0.7(0) Å to 1.00(4) Å, but all are in acceptable locations.

Calculations were done with programs of the CRYM Crystallographic Computing System and ORTEP. Scattering factors and corrections for anomalous scattering were taken from a standard reference (International Tables for X-ray Crystallography, Vol. IV, p. 71, p. 149; Birmingham, Kynoch, 1974). $R = \Sigma | F_o - | | F_c | | / \Sigma F_o$, for only $F_o^2 > 0$, and goodness of fit = $[\Sigma w(F_o^2 - F_c^2)^2/(n - p)]^{1/2}$ where n is the number of data and p is the number of parameters refined. The function minimized in least squares was $\Sigma w(F_o^2 - F_c^2)^2$, where $w = 1/\sigma^2(F_o^2)$. Variances of the individual reflections were assigned based on counting statistics plus an additional term, $0.014I^2$. Variances of the merged reflections were determined by standard propagation of error plus another additional term, $0.014\langle I\rangle^2$. The absorption correction was done by Gaussian integration over an 8 x 8 x 8 grid. Transmission factors varied from 0.677 to 0.735. The secondary extinction parameter (Larson, E. C. *Acta Cryst.* **1967**, *23*, 664, eq 3) refined to 1.8×10^{-6}.

Preparation of *trans* -Styrene Sulfide-d_1. *trans*- Styrene oxide-d_1 was synthesized from phenyl acetylene *via* hydrozirconation,[24] hydrolysis with D_2O, and epoxidation of double bond with *m*-chloroperbenzoic acid.[25] Stereospecific conversion of styrene oxide to styrene sulfide could be achieved through the use of triphenylphosphine sulfide. Trifluoroacetic acid (0.64 mL, 8.3 mmol) was added to a mixture of *trans*-styrene oxide-d_1 (1.00 g, 8.25 mmol) and triphenylphosphine sulfide (2.45 g, 8.32 mmol) in dry benzene (35 mL) at room temperature. The solution was stirred overnight with excess sodium bicarbonate, after the solution was allowed to react for 2.5 hours. After filtration, the solvent was evaporated to dryness. Triphenylphosphine oxide was filtered after benzene (5 mL) was introduced again. The chemically pure product, *trans*-styrene sulfide-d_1 was separated by the flash column

chromatography (eluent, benzene; R_f value, 0.8; separation yield ≥ 30%). ^1H NMR (C_6D_6) δ 7.02 (m, 5H, Ph), 3.42 (d, 1H, J_{HH} = 5.4 Hz, α-CH), 2.28 (m, 0.14 H, β-CH), 2.16 (d, 1H, J_{HH} = 5.4 Hz, β-CH). (The product contained 14% of hydrogen at the *trans*- α-position of styrene sulfide.) The product was polymerized when it was stored in neat at room temperature overnight. Polymerization can be avoided through dilution with benzene and freezing at low temperature(–50 °C).

Reaction of 2a with *trans*-Styrene Sulfide-d_1. *trans*-Styrene sulfide-d_1 (10 μL, 0.082 mmol) was injected into a NMR tube which holds the solution of complex **2a** (10 mg, 0,037 mmol) in C_6D_6 (0.4 mL) at room temperature. A mixture of **3**, polystyrene sulfide, *trans*-styrene-d_1, and *cis*-styrene-d_1 was observed in ^1H NMR. (^1H NMR (C_6D_6, r. t.) of independently prepared polystyrene sulfide-d_1; δ 7.08 (br, 5H, Ph), 3.64-3.55 (br, 1H), 2.66 (br, 1H).) The ratio of *trans*-styrene-d_1 and *cis*-styrene-d_1 was easily analyzed by ^2H NMR. (^2H NMR (toluene-d_8, r.t.); δ 5.63 (*cis* isomer, 52%), 5.10(*trans* isomer, 48%).) After the reaction mixture was prepared, NMR spectra were taken at various temperatures (–78 °C–r.t.). A trial to quench the reaction was unsuccessful because polymerization of *trans*-styrene sulfide-d_1 and decomposition of **2a** was the major pathway of the reaction at low temperature.

Reaction of 3a with Trifluoroacetic Acid. The red color of the C_6D_6 solution changed to orange when the complex **3** (10 mg, 0.033 mmol) and trifluoroacetic acid (6 μL, 0.078 mmol) were allowed to react for 30 minutes at room temperature. ^1H NMR (C_6D_6, r.t.) δ 5.76 (br, $Cp_2Ti(O_2CCF_3)_2$), 1.51 (d, J_{HH} = 7.2 Hz, $C\underline{H}_3SH$), 0.85 (br, PMe_3 and $CH_3S\underline{H}$).

Reaction of 3 with H_2. An intense purple colored solution was obtained when **3** in C_6D_6 was allowed to react with hydrogen at room temperature. The

color of the solution changed to red immediately after the solution was exposed to air. One of the products decomposed very fast with the presence of moist air, while another product was stable. The air-stable compound was identified as $Cp_2Ti(SMe)_2$[26] by ^1H NMR. ^1H NMR (C_6D_6) δ 5.70 (s, 10H, Cp), 2.70 (s, 6H, SMe). Also, single crystal X-ray crystallographic study confirmed the structure. Line-broadening of two resonances in ^1H NMR observed at high temperature (65–105 °C) required a check of the possibility of exchanges between Cp groups and thiomethoxy groups. To check the exchange process, $Cp_2Ti(SCH_2D)_2$ was prepared with the use of D_2. ^1H NMR (C_6D_6) δ 5.70 (s, 10H, Cp), 2.68 (t, J_{HD} = 2.3 Hz, 4H, CH_2D); ^2H NMR (C_6H_6) δ 2.57 (br). No incorporation of deuterium into Cp rings was observed after heating overnight at 100 °C.

Reaction of 3 with Acetyl Chloride. Distilled acetyl chloride[27] (23.5 μL, 0.33 mmol) was dropped into the compound **3** (50 mg, 0.167 mmol) in toluene (3 mL) at room temperature. The solution was filtered and concentrated to 1 mL after a stirring for an hour at room temperature. Pentane (4 mL) was layered on the top of the toluene solution. Storing the solution at –50 °C produced orange powder and red crystals. The red crystals were identified as Cp_2TiCl_2 with ^1H NMR. The orange powder was assumed to be **5** based on the ^1H NMR data. ^1H NMR (C_6D_6) δ 5.75 (s, 10H, Cp), 2.80 (s, 2H, CH_2), 2.03 (s, 3H, CH_3).

Preparation of 6a. Finely ground compound **3** (680 mg, 2.27 mmol) was stirred in toluene (35 mL) for 30 minutes to dissolve. The solution was allowed to react with excess methyl iodide (286 μL, 4.59 mmol) at room temperature. Additional methyl iodide (143 μL, 2.30 mmol) was dropped after 3 hours. A yellow powder (825 mg, 1.87 mmol, 82%) was filtered after the solution was allowed to react for another 3 hours. Diethyl ether was layered on the top of

solution after the powder was dissolved in acetonitrile at -20 °C. Crystals suitable for single crystal X-ray crystallography and elemental analysis were obtained after storing the solution at –25 °C for several days. ^{1}H NMR (CD_3CN, –20 °C) δ 5.59 (br, 10H, Cp), 2.28(s, 2H, CH_2), 1.95 (s, 3H, CH_3), 1.47 (d, 9H, J_{PH} = 8 Hz, PMe_3); ^{13}C NMR (CD_3CN, –20 °C) δ 106.1 (dm, J_{CH} = 178 Hz, Cp), 41.7 (td, J_{CH} = 155 Hz, J_{PC} = 36 Hz, CH_2), 21.9 (q, J_{CH} = 140 Hz, CH_3), 17.3 (dq, J_{CH} = 130 Hz, J_{PC} = 23 Hz, PMe_3); ^{31}P{^{1}H} NMR (CD_3CN, r.t.) δ 18.85. Anal. Calcd for $C_{15}H_{24}IPSTi{\cdot}CH_3CN$: C, 42.25; H, 5.63; N, 2.90. Found: C, 42.40; H, 5.53; N, 3.04.

Crystal Structure Determination of 6a. A pale yellow crystal was mounted in a greased capillary and centered on a CAD-4 diffractometer. Unit cell parameters and an orientation matrix were obtained by a least squares calculation from the setting angles of 25 reflections with 39° < 2θ < 46°. Two equivalent data sets out to a 2θ of 50° were collected and corrected for absorption and decay. Lorentz and polarization factors were applied and the two data sets were then merged to yield the final data set. Systematic absences in the diffraction data revealed the space group to be *Pbca*.

The iodide ion was located from a Patterson map and positions of the other non-hydrogen atoms were obtained from successive structure factor-Fourier calculations. The three acetonitrile hydrogen atoms, represented by six half-weight hydrogen atoms at calculated positions with isotropic B values 20% greater than that of the attached carbon, were not refined. The remaining 24 hydrogen atoms, located by calculation or from difference maps, were included in the least-squares calculations. The final full matrix contained 295 parameters: a scale factor, spatial and anisotropic thermal parameters for non-hydrogen atoms, and spatial and anisotropic thermal parameters for the refined hydrogen atoms. The hydrogen results were reasonable. A final

difference Fourier showed maximum excursions of –.75 and +.90 eÅ^{-3} in the neighborhood of the iodide ion, with deviations of less than ±. 64 eÅ^{-3} elsewhere. The R-index refined to 0.0598 (0.0326 $F_o^2 > 3\sigma(F_o^2)$) with a goodness of fit of 1.33.

Calculations were done with programs of the CRYM Crystallographic Computing System and ORTEP. Scattering factors and corrections for anomalous scattering were taken from a standard reference (International Tables for X-ray Crystallography, Vol. IV, p. 71, p. 149; Birmingham, Kynoch, 1947). $R = \Sigma | F_o - |F_c| | / \Sigma F_o$, for only $F_o^2 > 0$, and goodness of fit = $[\Sigma w(F_o^2 - F_c^2)^2 / (n - p)]^{1/2}$ where n is the number of data and p is the number of parameters refined. The function minimized in least squares was $\Sigma w(F_o^2 - F_c^2)^2$, where $w = 1/\sigma^2(F_o^2)$. Variances of the individual reflections were assigned based on couting statistics plus an additional term, $0.014I^2$. Variances of the merged reflections were determined by standard propagation of error plus another additional term, $0.014\langle I\rangle^2$. The absorption correction was done by Gaussian integration over an 8 x 8 x 8 grid. Transmission factors varied from 0.431 to 0.732.

Preparation of 6b. A mixture of **6a** (200 mg, 0.45 mmol) and $AgBF_4$ (88 mg, 0.45 mmol) in dichloromethane (25 mL) was allowed to react for 3 hours at –20 °C. The resultant solution was filtered and evaporated to give yellow powder (130 mg, 0.32 mmol, 72%). ^1H NMR (CD_2Cl_2, –10 °C) δ 5.57(s, 5H, Cp), 5.54 (s, 5H, Cp), 2.20 (d, J_{CH} = 10 Hz, 1H, CH_2), 2.03 (d, J_{CH} = 10 Hz, 1H, CH_2), 1.99 (s, 3H, CH_3), 1.51 (d, J_{PH} = 7.2 Hz, 9H, PMe_3); $^{31}P\{^1H\}$ NMR (CD_2Cl_2, –10 °C) δ 18.58; $^{19}F\{^1H\}$ NMR (CD_2Cl_2, –10 °C) δ 13.3.

Preparation of 6c. A mixture of **6a** (200mg, 0.45 mmol) and $AgBPh_4$ (200 mg, 0.46 mmol) in dichloromethane (35 mL) was stirred for 5 hours at –20 °C.

The solution was stirred for additional one hour at room temperature to facilitate the dissolution. After the solution was filtered and evaporated to dryness, the yellow residue was dissolved in dichloromethane (15 mL). Slow addition of pentane (30 - 40 mL) precipitated yellow powder. The product (160 mg, 0.25 mmol, 56%) was recovered by filtration at –78 °C. ^{1}H NMR (CD_3CN, r.t.) δ 7.25–6.9 (m, 20 H, Ph), 5.59 (s, 5H, Cp), 5.56 (s, 5H, Cp), 2.23 uncertain, 1.90 (s, 3H, CH_3), 1.47 (d, J_{PH} = 9 Hz, 9H, PMe_3); $^{31}P\{^1H\}$ NMR (CD_3CN, r.t.) δ 17.23.

Reaction of 6c with CuCl. A mixture of **6c** (20 mg, 0.03 mmol) and CuCl (6 mg, 0.06 mmol) in dichloromethane-d_2 was allowed to react at –20 °C. The yellow-red solution obtained after an hour showed a new product together with $CuCl(PMe_3)_x$ in ^{1}H NMR. ^{1}H NMR (CD_2Cl_2, –20 °C) δ 7.36 - 7.14 (m, 20H, Ph), 6.37 (s, 10H, Cp), 2.25 (s, 3H, CH_3), 2.15 (s, 2H, CH_2), 0.95 (d, J_{PH} = 7.2 Hz, free $CuCl(PMe_3)_x$); $^{31}P\{^1H\}$ NMR δ –42.87 (br, free $CuCl(PMe_3)_x$). This new phosphine-free compound did not polymerize ethylene, methyl vinyl ether at room temperature.

REFERENCES AND NOTES

(1) Lee, J. B.; Gajda, G. J.; Schaefer, W. P.; Howard, T. R.; Ikariga, T.; Straus, D. A.; Grubbs, R. H. *J. Am. Chem. Soc.* **1981**, *103*, 7358-7361.

(2) (a) Clawson, L. E.; Buchwald, S. L.; Grubbs, R. H. *Tetrahedron Lett.* **1984**, *50*, 5733. (b) Brown-Wensley, K. A. Ph. D. Thesis, California Institute of Technology, Pasadena, California, 1981. (c) Pine, S. H.; Zahler, R.; Evans, D. A.; Grubbs, R. H. *J. Am. Chem. Soc.* **1980**, *102*, 3270-3272. (d) Cannizzo, L. F.; Grubbs, R. H. *J. Org. Chem.* **1985**, *50*, 2316-2323. (e) Stille, J. R.; Grubbs, R. H. *J. Am. Chem. Soc.* **1986**, *108*, 855-856. (f) For review, see Brown-Wensley, K. A.; Buchwald, S. L.; Cannizzo, L. F.; Clawson, L. E.; Ho, S.; Meinhart, J. D.; Stille, J. R.; Straus, D. A.; Grubbs, R. H. *Pure Appl. Chem.* **1983**, *55*, 1733-1744.

(3) Stille, J. R.; Grubbs, R. H. *J. Am. Chem. Soc.* **1983**, *105*, 1664-1665.

(4) (a) Gilliom, L. R.; Grubbs, R. H. *J. Am. Chem. Soc.* **1986**, *108*, 733-742. For reviews, see (b) Calderon, N. *J. Macromol. Sci.–Revs. Macromol Chem.* **1972**, *C7(1)*, 105-159. (c) Katz, J. J.; Lee, S. J.; Shippey, M. A. *J. Mol. Catal.* **1980**, *8*, 219-226.

(5) (a) Mackenzie, P. B.; Ott, K. C.; Grubbs, R. H. *Pure Appl. Chem.* **1984**, *56*, 59-61. (b) Park, J. W.; Mackenzie, P. B.; Schaefer, W. P.; Grubbs, R. H. *J. Am. Chem. Soc.* **1986**, *108*, 6402-6404. (c) Ozawa, F.; Park, J. W.; Mackenzie, P. B.; Schaefer, W. P.; Henling, L. M.; Grubbs, R. H. *J. Am. Chem. Soc.* in press. (d) Mackenzie, P. B.; Coots, R. J.; Grubbs, R. H. *Organometallics* in press.

(6) (a) Tebbe, F. N.; Parshall, G. W.; Ovenall, D. W. *J. Am. Chem. Soc.* **1979**,

101, 5074-5075. (b) Klabunde, U.; Tebbe, F. N.; Parshall, G. W.; Harlow, R. L. *J. Mol. Catal.* **1980**, *8*, 37-51. (c) Howard, T. R.; Lee, J. B.; Grubbs, R. H. *J. Am. Chem. Soc.* **1980**, *102*, 6876-6878. (d) Lee, J. B.; Ott, K. C.; Grubbs, R. H. *J. Am. Chem. Soc.* **1982**, *104*, 7491-7496. (e) Straus, D. A.; Grubbs, R. H. *J. Mol. Catal.* **1985**, *28*, 9-25.

(7) Ansyln, E. V.; Grubbs, R. H. *J. Am. Chem. Soc.* **1987**, *109*, 4880-4890.

(8) Meinhart, J. D. Ph. D. Thesis, California Institute of Technology, Pasadena, California, 1987.

(9) (a) Buchwald, S. L.; Nielson, R. B. *J. Am. Chem. Soc.* **1988**, *110*, 3171-3175. (b) Buchwald, S. L.; Nielson, R. B.; Dewan, J. C. *J. Am. Chem. Soc.* **1987**, *109*, 1590-1591. (c) Buhro, W. E.; Etter, M. C.; Georgiou, S.; Gladysz, J. A.; McCormick, F. B. *Organometallics* **1987**, *6*, 1150-1156. (d) Adams, R. D.; Babin, J. E.; Tasi, M. *Organometallics* **1987**, *6*, 1717-1727. (e) Mayr, A.; McDermott, G. A.; Dorries, A. M.; Holder, A. K.; Fultz, W. C.; Rheingold, A. L. *J. Am. Chem. Soc.* **1986**, *108*, 310-311. (f) Hofman, L.; Werner, H. *Chem. Ber.* **1985**, *118*, 4229. (f) Hill, A. F.; Roper, W. R.; Waters, J. M.; Wright, A. H. *J. Am. Chem. Soc.* **1983**, *105*, 5939-5940.

(10) For homogeneous model of HDS, see (a) Spies, G. H.; Angelici, R. J. *Organometallics* **1987**, *6*, 1897-1903. (b) Sanchez-Delgado, R. A.; Tiripicchio, A.; Tiripicchio, C. M. *J. Organomet. Chem.* **1986**, *316*, C35-38.

(11) Collman, J. P.; Hegedus, L. S.; Norton, J. R.; Finke, R. G. *Principles and Applications of Organotransition Metal Chemistry*, Unversity Science: Mill Valley, California, 1987, pp 653-659.

(12) Werner, H.; Wolf, J.; Zolk, R.; Schubert, U. *Angew. Chem. Int. Ed. Engl.* **1983**, *22*, 981-982.

(13) Typical C=S and C–S bond distances are 1.70 Å and 1.82 Å, respectively.

Sutton, L. E. Ed. *Tables of Interatomic Distances and Configuration in Molecules and Ions*; Chemical Society: London, Supplement 1956-1959, 1965.

(14) Typical Ti–S bond distance is 2.40 Å, see (a) Carrondo, Maria A. A. F. de C. T.; Jeffrey, G. A. *Acta Crystallogr., Sect. C*, **1983**, *C39*, 42-44. (b) Kutoglu, V. A. *Z. Anorg. Allg. Chem.* **1972**, *390*, 195-209.

(15) Chan, T. H.; Finkenbine, J. R. *J. Am. Chem. Soc.* **1972**, *94*, 2880-2882.

(16) Park, J. W. Ph. D. Thesis, California Institute of Technology, Pasadena, California, 1989.

(17) Buchwald, S. L.; Anslyn, E. V.; Grubbs, R. H. *J. Am. Chem. Soc.* **1985**, *107*, 1766-1768.

(18) (a) Werner, H.; Kolb, O.; Schubert, U.; Ackermann, K. *Chem. Ber.* **1985**, *118*, 873-879. (b) Werner, H.; Paul, W. *Angew. Chem. Int. Ed. Engl.* **1983**, *22*, 316-317.

(19) (a) Rodulfo de Gil, E.; Dahl, L. F. *J. Am. Chem. Soc.* **1969**, *91*, 3751-3756. (b) Sepelak, D. J.; Pierpont, C. G.; Barefield, E. K.; Budz, J. T.; Poffenberger, C. A. *J. Am. Chem. Soc.* **1976**, *98*, 6178-6185. (c) Karsch, H. H.; Deubelly, B.; Hofmann. J.; Pieper, U.; Müller, G. *J. Am. Chem. Soc.* **1988**, *110*, 3654-3656. (d) Erker, G.; Dorf, U.; Atwood, J. L.; Hunter, W. E. *J. Am. Chem. Soc.* **1986**, *108*, 2251-2257. (e) Tatsumi, K.; Nakamura, A.; Hofmann, P.; Stauffert, P.; Hoffmann, R. *J. Am. Chem. Soc.* **1985**, *107*, 4440-4451. (f) Hofmann, P.; Stauffert, P.; Shore, N. E. *Chem. Ber.* **1982**, *115*, 2153-2174. (g) Fagan, P. J.; Manriquez, J. M.; Vollmer, S. H.; Day, C. S.; Day, V. W., Marks, T. J. *J. Am. Chem. Soc.* **1981**, *103*, 2206-2220.

(20) Pedersen, S. F.; Schrock, R. R. *J. Am. Chem. Soc.* **1982**, *104*, 7483-7491.

(21) The nitrile and phosphine ligands of titanocene methyl cation are too

tightly bonded to be displaced by alkenes or alkynes. (a) Bochmann, M.; Wilson, L. M.; Hursthouse, M. B.; Motevalli, M. *Organometallics* **1988**, *7*, 1148-1154. (b) Bochmann, M.; Wilson, L. M.; Hursthouse, M. B.; Short, R. L. *Organometallics* **1987**, *6*, 2556-2563.

(22) (a) Jordan, R. F.; Bajgur, C. S.; Willett, R.; Scott, B. *J. Am. Chem. Soc.* **1986**, *108*, 7410-7411. (b) Jordan, R. F.; LaPointe, R. E.; Bajgur, C. S.; Echols, S. F.; Willett, R. *J. Am. Chem. Soc.* **1987**, *109*, 4111-4113.

(23) Wittig, V. G.; Raff, P. *Ann. Chem.* **1951**, *573*, 195-209.

(24) Collman, J. P.; Hegedus, L. S.; Norton, J. R.; Finke, R. G. *Principles and Applications of Organotransition Metal Chemistry*; University Science: Mill Valley, California, 1987, pp 698-704.

(25) Fieser, L. F.; Fieser, M. *Reagents for Organic Synthesis*; Wiley: New York, 1967, Vol. 1, pp 135-139.

(26) (a) Köpf, H.; Block, B.; Schmidt, M. *Chem. Ber.* **1968**, *101*, 272-276. (b) Giddings, S. A. *Inorg. Chem.* **1967**, *6*, 849-850. (c) Chaudhari, M. A.; Stone, F. G. A. *J. Chem. Soc. (A)* **1966**, 838-841.

(27) Perrin D. D.; Armarego, W. L. F.; Perrin, D. D. *Purification of Laboratory Chemicals*; Pergamon: Oxford, 1966, p 59.

CHAPTER 5

Reaction of Titanocene Methylidene Trimethylphosphine Complex with Styrene Oxide; Mechanistic Study and Synthetic Application

ABSTRACT

The complex $Cp_2\overline{TiOCH_2CH(Ph)CH_2}$ (**2**) was prepared from the compound $Cp_2Ti{=}CH_2{\cdot}PMe_3$ (**1**) and styrene oxide. The product was characterized with ^1H-^1H correlated 2-dimensional NMR, selective decoupling of ^1H NMR, and differential NOE. Stereospecificity of deuterium in the product was lost when *trans*-styrene oxide-d_1 was allowed to react. Relative rates of the reaction were measured with varying substituents on the phenyl ring. Better linearity ($r = -0.98$, $\rho^+ = -0.79$) was observed with $\sigma_p{}^+$ than σ ($r = -0.87$, $\rho = -1.26$). The small magnitude of ρ^+ value and stereospecificity loss during the formation of product were best explained by the generation of biradicals, but partial generation of charge cannot be excluded. Carbonylation of complex **2** followed by exposure to iodine yields the corresponding β-phenyl γ-lactone.

INTRODUCTION

Stoichiometric and catalytic oxidation of carbon–carbon double bonds with metal oxides have been studied for synthetic applications and understanding of biological oxidation processes.[1] The hemin-catalyzed epoxidation of alkenes is usually stereospecific, but rearranged products and alkenes were obtained in many cases. Based on these observations, both an electron transfer (radical) mechanism and a concerted mechanism leading to a metallacycle have been suggested.[2] The reverse reaction, oxidation of a metal center with epoxides, has been investigated.[3] Information concerning the mechanism of the reverse reaction assists in the understanding of the forward oxidation processes. For example, *cis-trans* isomerization of β-methylstyrene oxide catalyzed by ruthenium(II) phorphyrins supported a stepwise mechanism for the oxidation processes.[3a]

Titanocene metallacycles[4] show a wide variety of reactivities with organic and inorganic reagents. Methylene transfer to organic carbonyls, including enolizable carbonyls, is one of the well-established reactions.[5,6] The reactions include ring opening polymerization,[7] complexation with metal halides,[8] and olefin metathesis.[9] All these reactions occur through a reactive intermediate which exhibits behavior consistent with that of transition metal carbene.[10] Titanocene methylidene trimethylphosphine complex, which is derived from titanocene metallacyclobutanes, is known to have similar reactivities.[11] The formation of $Cp_2\overline{TiOCH_2CH(Ph)CH_2}$ from titanocene methylidene trimethylphosphine complex and styrene oxide provides an opportunity to study the mechanism of adduct formation which resembles the oxidation of metal with alkene oxide. Also, synthetic applications can be

achieved through ring expansion of a heterocyclic 3-membered ring.

RESULTS AND DISCUSSION

The reaction of complex $Cp_2Ti{=}CH_2{\cdot}PMe_3$ (**1**), one of the well-characterized titanocene methylidene, with styrene oxide at room temperature yields complex $Cp_2TiOCH_2CH(Ph)CH_2$ (**2**) (eq 1). This type of reactivity is quite different from that of pentamethyltitanocene methylidene generated at high temperature.[13] In addition, the formation of $Cp_2Ti(\eta^2$-formaldehyde) was not observed. This differs from the reaction of complex **1** with styrene sulfide which yields $Cp_2Ti(\eta^2$-thioformaldehyde) complex.[12] Also, this difference implies that the formation of $Cp_2Ti(\eta^2\text{-}CH_2O)$[14] is thermodynamically less favorable than that of $Cp_2Ti(\eta^2\text{-}CH_2S)$. The complex **1** reacted slowly with cyclohexene oxide, butadiene monoxide, and propene oxide to give a similar type of product in a low yield. This behavior can be explained with the electronic effect of phenyl group (*vide infra*). A similar type of adduct could not be prepared with *N*-methylphenyl aziridine and phenyl aziridine, probably because of the weaker Ti–N bond.

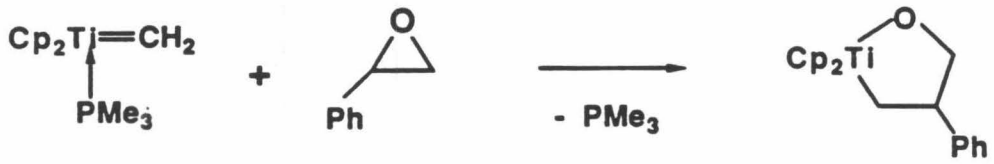

(1)

1 **2**

Characterization of Complex 2. Complex coupling patterns prevented straightforward interpretation of the ^1H NMR spectra for complex **2**. ^1H-^1H correlated 2-dimensional NMR spectrum showed the long range coupling between H_3 and H_5, and confirmed the structure of the complex

$Cp_2TiOCH_2CH(Ph)CH_2$. (Another candidate, $Cp_2TiOCH(Ph)CH_2CH_2$, was excluded based on the information in the two-dimensional NMR spectrum.) Selective decoupling of ^1H NMR agreed with the structure based on the two-dimensional NMR. In differential NOE, irradiation of the phenyl protons enhanced the intensities of H_1, H_2, and H_4. This result designated the position of H_2 and H_4 which are *cis* in relation to phenyl group. Irradiation of the cyclopentadienyl protons enhanced the intensities of H_1, H_2, H_4, and H_5. No enhancement of the H_3 proton implied the nonplanarity of the 5-membered ring[15] and confirmed the β-position (based on the titanium) of H_2, H_3 protons (Figure 1).

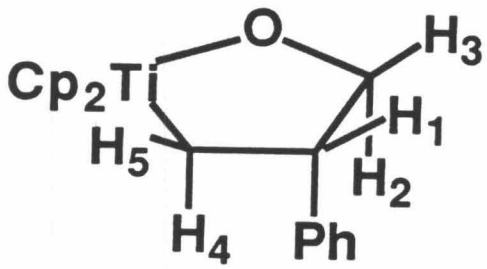

Figure 1. Numbering scheme for the hydrogens of complex **2**.

Mechanistic Studies. 1. Reaction with *trans*-Styrene Oxide-d_1. The deuterium was incorporated into the position of H_2 and H_3 when *trans*-styrene oxide-d_1 was allowed to react with the complex **1** (Scheme I). This observation exclude the possibility of another route where *trans*-styrene-d_1 was inserted quickly after the formation of $Cp_2Ti(\eta^2\text{-}CH_2O)$ complex.[13a] Also, the

stepwise mechanism was required to explain the equimolar content of deuterium in the position of H_2 and H_3 as analyzed by ^1H, ^2H NMR.

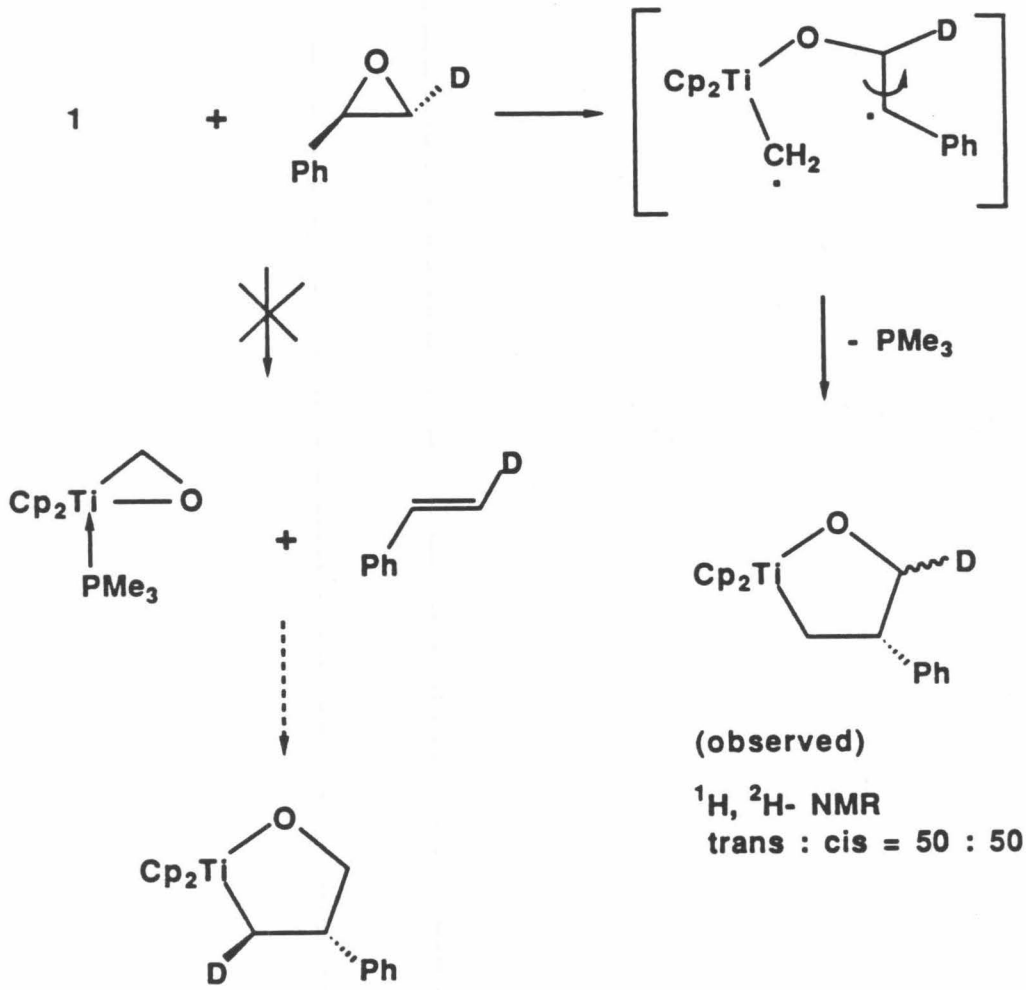

Scheme I. Mechanistic scheme for the reaction of complex **1** with *trans*-styrene oxide-d_1.

2. Substituent Effect. Several styrene oxides with different substituent (X = H, Cl, F, Me, OMe) were allowed to react with the complex **1** (eq 2). Analysis of individual products showed that the substituent had a large effect on the chemical shifts of H_4, H_5, and the cyclopentadienyl protons. The relative rates were calculated through the integration of these protons in the ^1H NMR spectra after two types of styrene oxide were reacted simultaneously with the complex **1**. A linear Hammett plot could be obtained with the relative rates (Table I) and σ_p^+ substituent parameters (Figure 2). Better linearity ($r = -0.98$, $\rho^+ = -0.79$) was observed with σ_p^+ than σ ($r = -0.87$, $\rho = -1.26$). This behaviour has precedent in the hemin-catalyzed epoxidation[2a] and photocatalyzed oxidative cleavage of olefins.[16] In both systems, the small magnitude of ρ^+ values (–0.84, –0.56) was explained by either the radical mechanism or a different delocalization effect.[2a] Also, a similar magnitude of variation was observed for the reaction of the complex **1** with benzyl chloride where electron transfer between two compounds initiated the formation of $Cp_2TiCl(CH_2CH_2Ph)$.[17] In conclusion, the reaction with styrene oxide is best explained by the formation of biradicals, but partial formation of charge cannot be excluded.

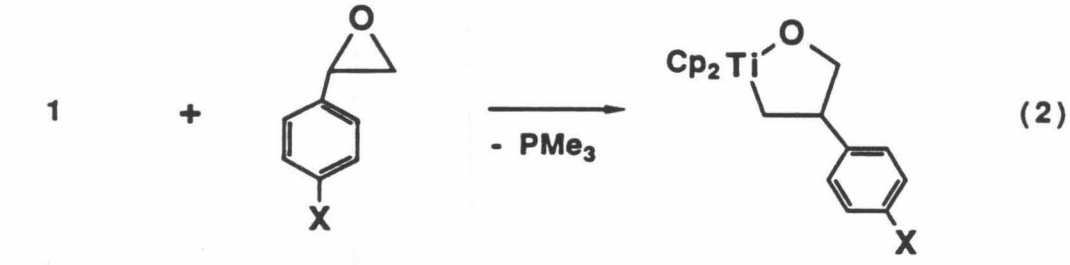

(X = H, Cl, F, Me, and OMe)

Table I. Relative rates for the reaction of complex **1** with various styrene oxides and substituent parameters (σ_p^+).

substituent	Cl	H	F	Me	OMe
k_{rel}	0.91	1.00	0.91	1.65	4.14
log k_{rel}	–0.04	0.00	–0.04	0.22	0.62
σ_p^+	0.11	0.00	–0.07	–0.31	–0.78

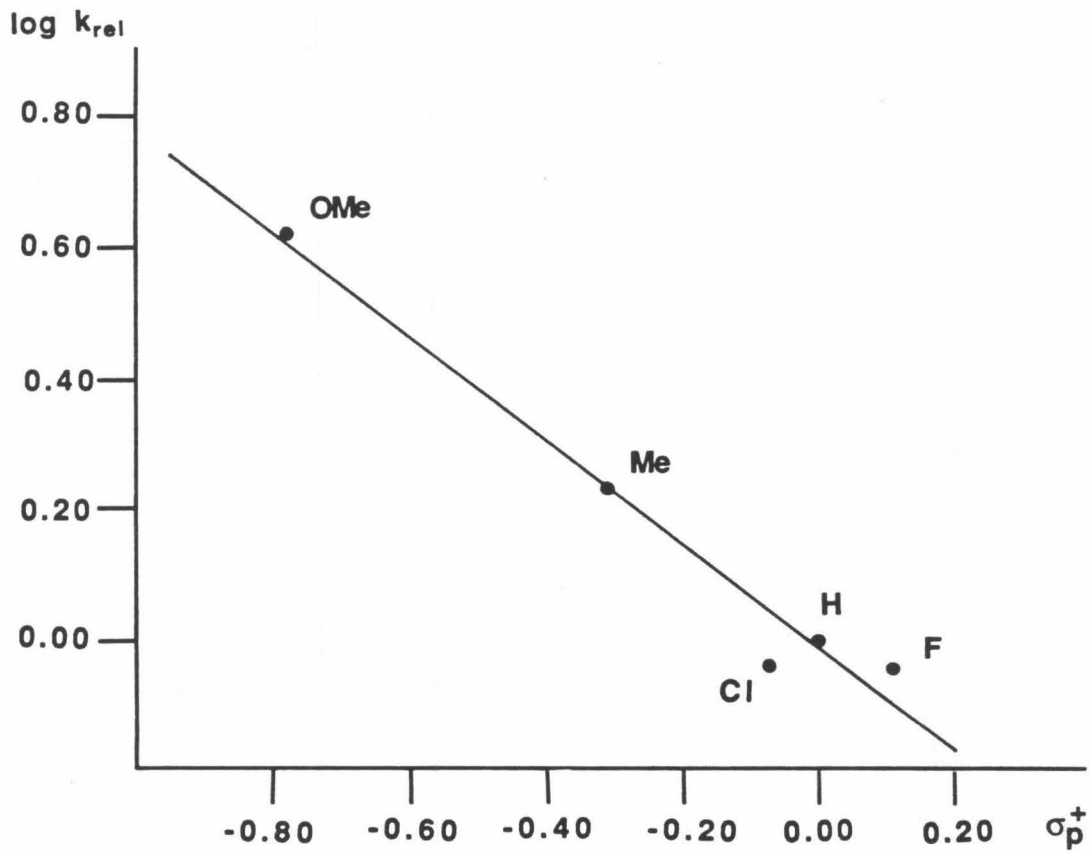

Figure 2. Correlation of log k_{rel} for the reaction in eq 2 with σ_p^+.

Preparation of γ-Lactone from Complex 2. Reaction of the complex **2** with excess carbon monoxide overnight gave the CO-inserted product with the expansion of the ring (eq 3). The slow nature of the reaction can be rationalized by the strong π-donation of the alkoxide ligand.[18] The insertion product gave the β-phenylγ-lactone (**4**) with iodine (eq 4). This process is reminiscent of the formation of cyclopropanes from the reaction of titanocene cyclobutanes with iodine.[19] Also, this mild route can be utilized to make γ-lactones from alkenes after epoxidation.[20]

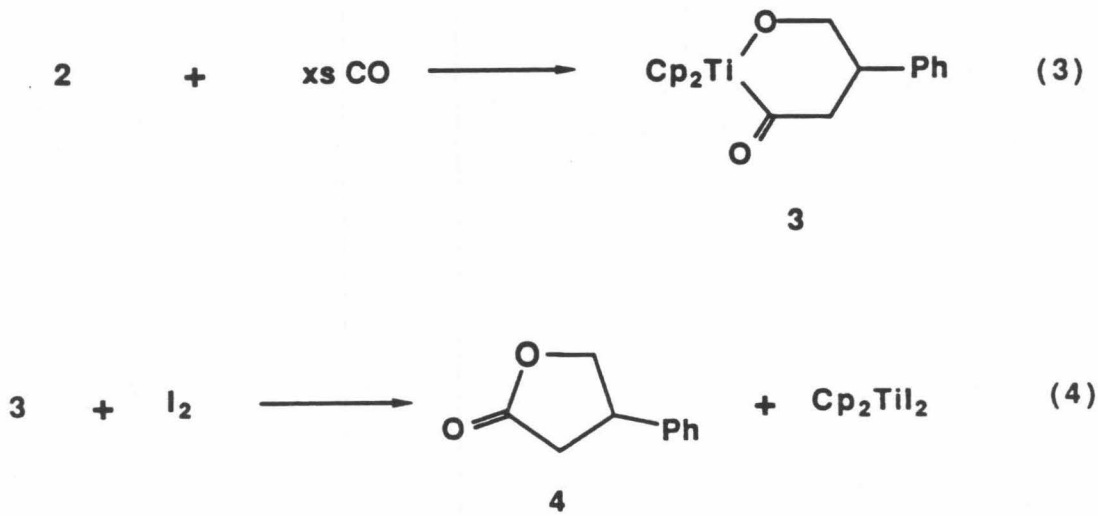

EXPERIMENT

General. All manipulation of air and/or moisture sensitive compounds were carried out with use of standard Schlenk or vacuum line techniques. Argon was purified by passage through columns of BASF RS-11 catalyst (Chemalog) and Linde 4 Å molecular sieves. Solids were transferred and stored in a N_2-filled Vacuum Atmosphere glove box equipped with a MO-40-1 purification train and a DK-3E Dri-Kool conditioner, and Dri-Cold Freezer.

Toluene and benzene were stirred over CaH_2 and then transferred to purple sodium-benzophenone ketyl. Pentane was stirred over concentrated H_2SO_4, washed with H_2O, dried over CaH_2, and then transferred to purple sodium-benzophenone ketyl. Dried degassed solvents were vacuum-transferred into dry glass vessels equipped with Teflon valve closures and stored under argon. Benzene-d_6 and toluene-d_8 (Cambridge Isotope) were dried and vacuum-transferred from purple sodium-benzophenone ketyl. Styrene oxide, trimethylene oxide, cyclohexene oxide, butadiene monoxide, *m*-chloroperbenzoic acid, *p*-methylstyrene, *p*-chlorostyrene, *p*-fluorostyrene, anisaldehyde, trimethylsulfonium iodide, iodine (Aldrich), and carbon monoxide(Matheson) were used as received. β-β-Dimethyltitanacyclobutane, $Cp_2Ti{=}CH_2{\cdot}PR''_3$ **1**,[11] *N*-methyl phenyl aziridine,[21] and phenyl aziridine[22] were prepared using the known method.

NMR spectra were recorded on Varian EM-390 (90 MHz, ^1H), JEOL FX-90Q (89.60 MHz, ^1H; 22.53 MHz, ^{13}C), and JEOL GX-400 (399.65 MHz, ^1H; 61.35 MHz, ^2H; 100.4 MHz, ^{13}C) spectrometers. Chemical shifts are reported in δ referenced to residual solvent signals. Elemental analysis (C, H, N) was

performed by California Institute of Technology Analytical Services.

Preparation of 2. Styrene oxide (86 μL, 0.75 mmol) was added to the compound **1** (200 mg, 0.75 mmol) dissolved in toluene (6.6 mL) at 0 °C. The mixture was warmed to room temperature and stirred for 30 minutes. (^{1}H NMR analysis with internal standard showed that the yield was 80%.) Pentane (20 mL) was dropped during stirring to precipitate the product at –78 °C. The reddish precipitate (135 mg, 58%) was filtered, at –78 °C, and dried *in vacuo* at room temperature. For further purification, pentane (10 mL) was layered on the top of the solution after powder was dissolved in toluene (2.6 mL). At –50 °C, the solution gave red droplets (100 mg, 43%) suitable for elemental analysis. ^{1}H NMR (C_6D_6) δ7.25–7.09 (m, 5H, Ph), 5.89 (s, 5H, Cp), 5.87 (s, 5H, Cp), 4.66 (m, 1H, H_1), 4.45 (dd, J_{H2H3} = 9.0 Hz, J_{H2H1} = 11.0 Hz, H_2), 4.23 (ddd, J_{H3H1} = 6.6 Hz, J_{H3H2} = 9.0 Hz, J_{H3H5} = 2.2 Hz, 1H, H_3), 3.10 (dd, J_{H4H5} = 10.5 Hz, J_{H4H1} = 12.5 Hz, 1H, H_4), 1.30 (ddd, J_{H5H1} = 5.3 Hz, 1H, H_5); ^{13}C NMR (C_6D_6) δ 147.8 (s, C_{ipso}, Ph), 128.4 (d, J_{CH} = 158 Hz, Ph), 127.0 (d, J_{CH} = 161 Hz, Ph), 126.0 (d, J_{CH} = 159 Hz, Ph), 114.5 (dm, J_{CH} = 172 Hz, Cp), 114.2 (dm, J_{CH} = 172 Hz, Cp), 81.1 (br t, J_{CH} = 141 Hz), 66.2 (d, J_{CH} = 126 Hz), 57.2 (t, J_{CH} = 134 Hz). Anal. Calcd for $C_{19}H_{20}OTi$: C, 73.08; H, 6.46. Found: C, 72.84; H, 6.41.

Reaction of 1 with *trans*-styrene oxide-d$_1$. *trans*-Styrene oxide-d$_1$ was synthesized from phenylacetylene *via* hydrozirconation,[23] hydrolysis with D_2O, and epoxidation of double bond with *m*-chloroperbenzoic acid.[24] (^{1}H, ^{2}H NMR analysis showed that the product contained 83% of *trans*-styrene oxide-d$_1$, 13% of styrene oxide, and 4% of α-styrene oxide-d$_1$.) Styrene oxide-d$_1$ (43.4 μL, 0.38 mmol) was added to the compound **1** (100 mg, 0.37 mmol) dissolved in toluene (3.3 mL) at 0 °C. The mixture was warmed to room temperature and stirred for 30 minutes. The same method as above was used

to separate the product. The product was analyzed with ^1H, ^2H, and ^{13}C NMR. The ratio of the integration for H_2 and H_3 was 50.4 : 49.6 in ^1H NMR. ^2H NMR (C_6D_6) δ 4.40 (0.47D, H_2), 4.18 (0.53D, H_3); ^{13}C NMR (C_6D_6) δ 80.7 (t, J_{CD} = 22.0 Hz).

The stereochemistry of *trans*-styrene oxide-d_1 was followed during the reaction. *trans*-Styrene oxide-d_1 (8.7 μL, 0.076 mmol) was mixed with the compound **1** (20 mg, 0,075 mmol) dissolved in toluene-d_8 at –78 °C. The NMR tube was warmed to –10 °C for 1–2 minutes and then cooled to –50 °C for the analysis. (The reaction was quenched three times before the completion.) No increase of the integration for the *trans*-β-^1H was observed during the reaction.

Measurement of Relative Rates with Varying Substituents. Several styrene oxides with different substituent were prepared. *p*-Chloro, *p*-methyl, and *p*-fluoro styrene oxide were derived from corresponding styrene, and *m*-chlorobenzoic acid,[24] while *p*-mehtoxy styrene oxide was prepared from *p*-anisaldehyde and trimethylsulfonium iodide.[21a,25] Analysis of individual adducts showed that the substituent had a large effect on the chemical shift of cyclopentadienyl, H_4, and H_5 protons. The relative rates were calculated through the integration of ^1H NMR spectra, after two types of styrene oxide were coinjected together into the complex **1** in C_6D_6. For example, an equimolar mixture of *p*-methoxy (5.5 μL, 0.037 mmol) and *p*-chloro styrene oxide (5.1 μL, 0.037 mmol) was reacted with the compound **1** (10 mg, 0.037 mmol) in C_6D_6 (0.4 mL). The average relative ratio based on the integration of H_4, H_5, and the cyclopentadienyl protons was 1.00 : 0.22. The same type of comparison was repeated for all possible combinations.

Carbon Monoxide Insertion of Complex 2. When complex **2** was allowed to react with excess carbon monoxide overnight, color of the

solution changed to purple. The insertion product (**3**) is not susceptible to decarbonylation under vacuum. ^{1}H NMR (C_6D_6) δ 7.24–7.08 (m, 5H, Ph), 5.83 (s, 5H, Cp), 5.73 (s, 5H, Cp), 4.57 (dd, 1H), 4.28 (t, 1H), 2.97 (m, 1H), 2.7–2.5 (m, 2H). When iodine was added to the solution, the black Cp_2TiI_2 (^{1}H NMR δ 6.11)[26] was observed together with γ-lactone (**4**). ^{1}H NMR δ 7.13–6.53 (m, 5H, Ph), 3.78 (t, 1H, J_{HH} = 9 Hz, J_{HH} = 9 Hz), 3.51 (t, 1H, J_{HH} = 9 Hz, J_{HH} = 9 Hz), 2.72 (m, 1H), 2.14 (dd, J_{HH} = 9 Hz, J_{HH} = 17 Hz), 1.99 (dd, J_{HH} = 9 Hz, J_{HH} = 17 Hz).

REFERENCES AND NOTES

(1) Sheldon, R. A.; Kochi, J. K. *Metal-catalyzed Oxidation of Organic Compounds*; Academic: New York, 1981, pp 152-188.

(2) (a) Traylor, T. G.; Xu, F. *J. Am. Chem. Soc.* **1988**, *110*, 1953-1958. (b) Groves, J. T.; Kruper, W. J.; Haushalter, R. C. *J. Am. Chem. Soc.* **1980**, *102*, 6377-6380. (c) Guengerich, F. P.; MacDonald, T. L. *Acc. Chem. Res.* **1984**, *17*, 9-16.

(3) (a) Groves, J. T.; Ahn, K.-H.; Quinn, R. *J. Am. Chem. Soc.* **1988**, *110*, 4217-4220. (b) Lenarda, M.; Pahor, N. B.; Calligaris, M.; Graziani, M.; Randaccio, L. *J. Chem. Soc., Dalton* **1978**, 279-282. (c) Schlodder, R.; Ibers, J. A.; Lenarda, M.; Graziani, M. *J. Am. Chem. Soc.* **1974**, *96*, 6893-6900.

(4) Lee, J. B.; Gajda, G. J.; Schaefer, W. P.; Howard, T. R.; Ikariga, T.; Straus, D. A.; Grubbs, R. H. *J. Am. Chem. Soc.* **1981**, *103*, 7358-7361.

(5) (a) Clawson, L. E.; Buchwald, S. L.; Grubbs, R. H. *Tetrahedron Lett.* **1984**, *50*, 5733. (b) Brown-Wensley, K. A. Ph. D. Thesis, California Institute of Technology, Pasadena, California, 1981. (c) Pine, S. H.; Zahler, R.; Evans, D. A.; Grubbs, R. H. *J. Am. Chem. Soc.* **1980**, *102*, 3270-3272. (d) Cannizzo, L. F.; Grubbs, R. H. *J. Org. Chem.* **1985**, *50*, 2316-2323. (e) Stille, J. R.; Grubbs, R. H. *J. Am. Chem. Soc.* **1986**, *108*, 855-856. (f) For review, see Brown-Wensley, K. A.; Buchwald, S. L.; Cannizzo, L. F.; Clawson, L. E.; Ho, S.; Meinhart, J. D.; Stille, J. R.; Straus, D. A.; Grubbs, R. H. *Pure Appl. Chem.* **1983**, *55*, 1733-1744.

(6) Stille, J. R.; Grubbs, R. H. *J. Am. Chem. Soc.* **1983**, *105*, 1664-1665.

(7) (a) Gilliom, L. R.; Grubbs, R. H. *J. Am. Chem. Soc.* **1986**, *108*, 733-742. For reviews, see (b) Calderon, N. *J. Macromol. Sci.–Revs. Macromol Chem.*

1972, *C7(1)*, 105-159. (c) Katz, J. J.; Lee, S. J.; Shippey, M. A. *J. Mol. Catal.* **1980**, *8*, 219-226.

(8) (a) Mackenzie, P. B.; Ott, K. C.; Grubbs, R. H. *Pure Appl. Chem.* **1984**, *56*, 59-61. (b) Park, J. W.; Mackenzie, P. B.; Schaefer, W. P.; Grubbs, R. H. *J. Am. Chem. Soc.* **1986**, *108*, 6402-6404. (c) Ozawa, F.; Park, J. W.; Mackenzie, P. B.; Schaefer, W. P.; Henling, L. M.; Grubbs, R. H. *J. Am. Chem. Soc.* in press. (d) Mackenzie, P. B.; Coots, R. J.; Grubbs, R. H. *Organometallics* in press.

(9) (a) Tebbe, F. N.; Parshall, G. W.; Ovenall, D. W. *J. Am. Chem. Soc.* **1979**, *101*, 5074-5075. (b) Klabunde, U.; Tebbe, F. N.; Parshall, G. W.; Harlow, R. L. *J. Mol. Catal.* **1980**, *8*, 37-51. (c) Howard, T. R.; Lee, J. B.; Grubbs, R. H. *J. Am. Chem. Soc.* **1980**, *102*, 6876-6878. (d) Lee, J. B.; Ott, K. C.; Grubbs, R. H. *J. Am. Chem. Soc.* **1982**, *104*, 7491-7496. (e) Straus, D. A.; Grubbs, R. H. *J. Mol. Catal.* **1985**, *28*, 9-25.

(10) Ansyln, E. V.; Grubbs, R. H. *J. Am. Chem. Soc.* **1987**, *109*, 4880-4890.

(11) Meinhart, J. D. Ph. D. Thesis, California Institute of Technology, Pasadena, California, 1987.

(12) Park, J. W. Ph. D. Thesis, California Institute of Technology, Pasadena, California, 1989.

(13) Gibson, C. P.; Dabbagh, G.; Bertz, S. H. *J. Chem. Soc., Chem. Commun.* **1988**, 603-605.

(14) For examples of early transition-metal formaldehyde complex, see (a) Green, M. L. H.; Parkin, G. *J. Chem. Soc., Chem. Commun.* **1986**, 90-91. (b) Gambarotta, S.; Floriani, C.; Chiesi-Villa, A.; Guastini, C. *J. Am. Chem. Soc.* **1982**, *104*, 2019-2020. (c) Threlkel, R. S.; Bercaw, J. E. *J. Am. Chem. Soc.* **1981**, *103*, 2650-2659.

(15) The β-methylene oxatitanacyclobutane ring was puckered, see Ho, S. C.; Hentges, S.; Grubbs, R. H. *Organometallics*, **1988**, *7*, 780-782.

(16) Fox, M. A.; Chen, C.-C. *Tetrahedron Lett.* **1983**, *24*, 547-550.

(17) Buchwald, S. L.; Ansyln, E. V. ; Grubbs, R. H. *J. Am. Chem. Soc.* **1985**, *107*, 1766-1768.

(18) Marsella, J. A.; Moloy, K. G.; Caulton, K. G. *J. Organomet. Chem.* **1980**, *201*, 389-398.

(19) Ho, S. C.; Strauss, D. A.; Grubbs, R. H. *J. Am. Chem. Soc.* **1984**, *106*, 1533-1534.

(20) For conventional methods for the preparation of γ-lactones from alkenes, see (a) Heiba, E. I.; Dessau, R. M., Godewald, P. G. *J. Am. Chem. Soc.* **1974**, *96*, 1977-1981. (b) Das Gupta, T. K.; Felix, D.; Kempe, U. M.; Eschenmoser, A. *Helv. Chim. Acta* **1972**, *55*, 2198-2205. (c) Boldt, P.; Thielecke, W.; Etzemüler, J. *Chem. Ber.* **1969**, *102*, 4157-4163.

(21) (a) Borsetti, A. P.; Crist, D. R. *J. Heterocycl. Chem.* **1975**, *12*, 1287-1289. (b) Chapman, N. B.; Triggle, D. J. *J. Chem. Soc.* **1963**, 1385-1400.

(22) (a) Ittah, Y.; Sasson, Y.; Shahak, I.; Tsaroom, S.; Blum, J. *J. Org. Chem.* **1978**, *43*, 4271-4273. (b) McEwen, W. E.; Conrad, W. E.; VanderWerf, C. A. *J. Am, Chem. Soc.* **1952**, *74*, 1168-1171.

(23) Collma, J. P.; Hegedus, L. S.; Norton, J. R.; Finke, R. G. *Principles and Applications of Organotransition Metal Chemistry*; University Science: Mill Valley, California, 1987, pp 698-704.

(24) Fieser, L. F.; Fieser, M. *Reagents for Organic Synthesis*; Wiley: New York, 1967, Vol. 1, pp 135-139.

(25) (a) Franzen, V.; Driesen, H.-E. *Chem. Ber.* **1963**, *87*, 1881-1890. (b) Corey, E. J.; Chaykovsky, M. *J. Am. Chem. Soc.* **1965**, *87*, 1353-1364.

(26) Wailes, P. C.; Coutts, R. S. P.; Weigold, H. *Organometallic Chemistry of Titanium, Zirconium, and Hafnium*; Academic: New York, 1974, p 55.

Appendix I.

Crystal Structure Data of $Cp_2Ti(\mu\text{-}CH_2)(\mu\text{-}CH_3)Rh(COD)$

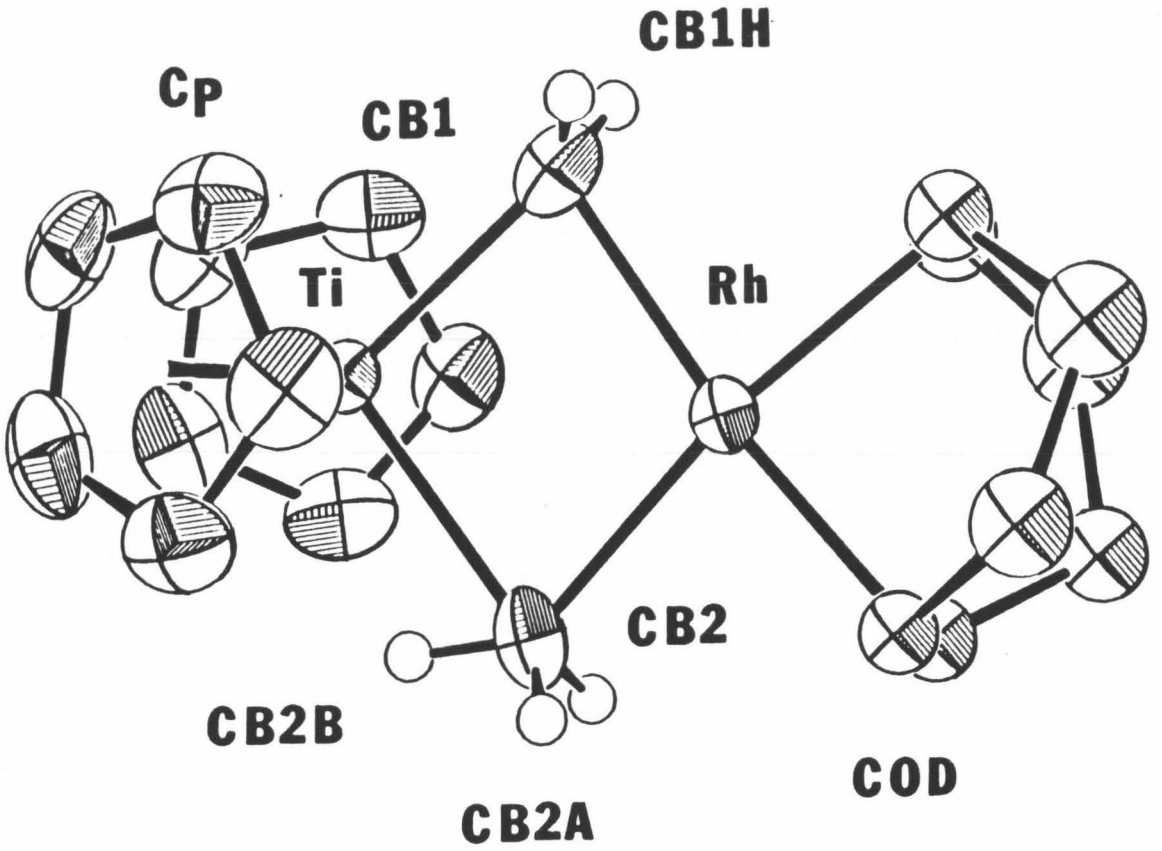

Figure 1. ORTEP diagram.

Table I. Complete Bond Distances and Angles.

ATOM	ATOM	DISTANCE	SIGMA		SYM
RH	TI	2.8348	0.001	*	0
RH	CB 1	2.0940	0.005	*	0
RH	CB 2	2.1101	0.006	*	0
RH	CD1A	2.1938	0.008	*	0
RH	CD1B	2.1919	0.006	*	0
RH	CD1	2.0826	0.006	*	0
RH	CD4A	2.2038	0.008	*	0
RH	CD4B	2.1836	0.008	*	0
RH	CD4	2.0867	0.008	*	0
TI	CB 1	2.1469	0.005	*	0
TI	CB 2	2.2937	0.006	*	0
TI	CB2B	2.0162	0.054	*	0
TI	CP	2.0760	0.004	*	0
C 1	C 2	1.3698	0.006		0
C 1	C 5	1.3886	0.006		0
C 1	CPH1	0.8348	0.035		0
C 2	C 3	1.3982	0.006		0
C 2	CPH2	0.9597	0.033		0
C 3	C 4	1.3800	0.006		0
C 3	CPH3	0.8684	0.036		0
C 4	C 5	1.3814	0.006		0
C 4	CPH4	0.9685	0.036		0
C 5	CPH5	0.8904	0.037		0
CB 1	CB1H	0.9058	0.034	*	0
CB 2	CB2A	0.9756	0.044	*	0
CB 2	CB2B	0.9244	0.054	*	0
CD1A	CD2A	1.4935	0.012		0
CD1A	H 1A	0.9510	0.008	*	0
CD1A	CD1B	1.3729	0.010		18
CD1B	CD2B	1.5129	0.010		0
CD1B	H 1B	0.9506	0.006	*	0
CD2A	CD3A	1.5394	0.012		0
CD2A	H2AA	0.9526	0.009	*	0
CD2A	H2AB	0.9478	0.009	*	0
CD2B	CD3B	1.4886	0.012		0
CD2B	H2BA	0.9506	0.008	*	0
CD2B	H2BB	0.9516	0.008	*	0
CD3A	CD4A	1.5233	0.011		0
CD3A	H3AA	0.9475	0.008	*	0
CD3A	H3AB	0.9516	0.008	*	0
CD3B	CD4B	1.5219	0.012		0
CD3B	H3BA	0.9530	0.009	*	0
CD3B	H3BB	0.9467	0.009	*	0
CD4A	H 4A	0.9522	0.008	*	0
CD4A	CD4B	1.3528	0.011		18
CD4B	H 4B	0.9486	0.008	*	0

Table I. (Cont.)

ATOM	ATOM	ATOM	ANGLE	SIGMA			SY1	SY3
RH	CB 1	TI	83.89	0.196	*		0	0
RH	CB 2	TI	80.02	0.196	*		0	0
CB 1	RH	CB 2	101.68	0.216	*		0	0
CB 1	TI	CB 2	94.41	0.206	*		0	0
RH	CB 1	CB1H	104.84	2.158	*		0	0
RH	CB 2	CB2B	141.10	3.365	*		0	0
RH	CB 2	CB2A	100.38	2.609	*		0	0
TI	CB 1	CB1H	123.49	2.164	*		0	0
TI	CB 2	CB2B	61.08	3.343	*		0	0
TI	CB 2	CB2A	124.41	2.615	*		0	0
CD1	RH	CB 1	86.74	0.230	*		0	0
CD1	RH	CB 2	168.33	0.237	*		0	0
CD1	RH	CD4	85.95	0.282	*		0	0
CD4	RH	CB 1	170.30	0.265	*		0	0
CD4	RH	CB 2	86.49	0.271	*		0	0
CP	TI	CB 1	105.71	0.187	*		0	0
CP	TI	CB 2	106.00	0.188	*		0	0
C 5	C 1	C 2	108.98	0.358			0	0
CPH1	C 1	C 2	127.14	2.400			0	0
CPH1	C 1	C 5	123.88	2.400			0	0
C 3	C 2	C 1	107.25	0.347			0	0
CPH2	C 2	C 1	130.35	1.985			0	0
CPH2	C 2	C 3	122.31	1.982			0	0
C 4	C 3	C 2	108.10	0.356			0	0
CPH3	C 3	C 2	119.70	2.372			0	0
CPH3	C 3	C 4	131.49	2.376			0	0
C 5	C 4	C 3	108.17	0.363			0	0
CPH4	C 4	C 3	126.73	2.155			0	0
CPH4	C 4	C 5	125.01	2.155			0	0
C 4	C 5	C 1	107.47	0.365			0	0
CPH5	C 5	C 1	126.62	2.413			0	0
CPH5	C 5	C 4	125.79	2.413			0	0
CB1H	CB 1	CB1H	108.19	3.047	*	#	-18	0
CB2B	CB 2	CB2A	101.54	4.245	*		0	0
CB2A	CB 2	CB2A	110.32	3.689	*	#	-18	0
H 1A	CD1A	CD2A	117.06	0.743	*		0	0
CD1B	CD1A	CD2A	125.97	0.706			-18	0
CD1B	CD1A	H 1A	116.97	0.725	*		-18	0
CD2B	CD1B	CD1A	123.92	0.634			0	18
H 1B	CD1B	CD1A	118.18	0.649	*		0	18
H 1B	CD1B	CD2B	117.90	0.626	*		0	0
CD3A	CD2A	CD1A	113.46	0.720			0	0
H2AA	CD2A	CD1A	108.03	0.799	*		0	0
H2AB	CD2A	CD1A	108.38	0.803	*		0	0
H2AA	CD2A	CD3A	108.49	0.798	*		0	0
H2AB	CD2A	CD3A	108.99	0.802	*		0	0
H2AB	CD2A	H2AA	109.44	0.906	*		0	0
CD3B	CD2B	CD1B	114.26	0.669			0	0
H2BA	CD2B	CD1B	107.94	0.703	*		0	0
H2BB	CD2B	CD1B	107.97	0.703	*		0	0
H2BA	CD2B	CD3B	108.81	0.746	*		0	0
H2BB	CD2B	CD3B	108.49	0.745	*		0	0
H2BB	CD2B	H2BA	109.28	0.806	*		0	0
CD4A	CD3A	CD2A	113.90	0.681			0	0
H3AA	CD3A	CD2A	108.74	0.744	*		0	0
H3AB	CD3A	CD2A	108.26	0.741	*		0	0
H3AA	CD3A	CD4A	108.24	0.720	*		0	0
H3AB	CD3A	CD4A	108.09	0.718	*		0	0
H3AB	CD3A	H3AA	109.55	0.808	*		0	0
CD4B	CD3B	CD2B	112.89	0.704			0	0
H3BA	CD3B	CD2B	108.51	0.772	*		0	0
H3BB	CD3B	CD2B	108.98	0.777	*		0	0
H3BA	CD3B	CD4B	108.33	0.761	*		0	0
H3BB	CD3B	CD4B	108.59	0.765	*		0	0
H3BB	CD3B	H3BA	109.49	0.857	*		0	0
H 4A	CD4A	CD3A	117.84	0.713	*		0	0
CD4B	CD4A	CD3A	124.62	0.707			-18	0
CD4B	CD4A	H 4A	117.54	0.751	*		-18	0
CD4A	CD4B	CD3B	126.64	0.734			18	0
H 4B	CD4B	CD3B	116.79	0.750	*		0	0
H 4B	CD4B	CD4A	116.57	0.774	*		0	18

Table II. Final Parameters.

Atom	x	y	z	U_{eq} or B
Rh	0.16349(4)	0.24413(2)	1/4	305(1)
Ti	0.39676(10)	0.37200(4)	1/4	269(2)
C1	0.4713(6)	0.4775(2)	0.1294(3)	529(11)
C2	0.3360(5)	0.4409(2)	0.0874(3)	505(10)
C3	0.3783(6)	0.3602(3)	0.0627(3)	524(11)
C4	0.5404(5)	0.3493(3)	0.0874(3)	537(11)
C5	0.5987(5)	0.4217(3)	0.1295(3)	557(11)
CB1	0.1356(7)	0.3716(3)	1/4	499(16)
CB2	0.4191(7)	0.2320(4)	1/4	498(16)
COD1A	- 0.0754(9)	0.2385(5)	0.3273(7)	3.5(1)
COD1B	- 0.0986(8)	0.2366(5)	0.2805(5)	3.0(2)
COD2A	- 0.0806(12)	0.1664(5)	0.4001(8)	5.3(2)
COD2B	- 0.1410(10)	0.1600(5)	0.3420(7)	4.7(2)
COD3A	0.0112(10)	0.0912(5)	0.3571(7)	3.7(2)
COD3B	0.0018(11)	0.1169(5)	0.3885(7)	4.0(2)
COD4A	0.1573(10)	0.1125(5)	0.2881(6)	2.8(2)
COD4B	0.1522(10)	0.1214(5)	0.3184(7)	2.5(2)
CB1H	0.0747(41)	0.3825(21)	0.1918(26)	4.9(10)
CB2H1	0.4343(53)	0.1987(27)	0.1865(34)	9.2(14)
CB2H2	0.5129(69)	0.2633(31	1/4	5.7(15)

U_{eq} have been multiplied by 10^4

$$U_{eq} = 1/3 \sum_i \sum_j [U_{ij}\, a_i^* a_j^* \vec{a}_i \vec{a}_j]$$

$$\sigma(U_{eq}) = \frac{1}{\sqrt{6}} \left\langle \frac{\sigma U_{ii}}{U_{ii}} \right\rangle U_{eq}$$

Table II. (Cont.)

Atom	x	y	z	B
CPH1	479(4)	526(2)	152(3)	4.4(9)
CPH2	228(4)	462(2)	78(3)	4.1(8)
CPH3	303(4)	325(2)	45(3)	4.7(10)
CPH4	603(4)	299(2)	81(3)	5.0(9)
CPH5	698(4)	430(2)	156(3)	6.3(12)
COD:				
H1A	-54	290	358	5.0
H2AA	-192	152	410	5.0
H2AB	-34	182	466	5.0
H3AB	-62	59	316	5.0
H3AB	49	60	416	5.0
H4A	260	120	322	5.0
H2B	-87	286	319	5.0
H2BA	-196	124	295	5.0
H2BB	-213	175	398	5.0
H3BA	-26	61	398	5.0
H3BB	27	141	455	5.0
H4B	253	132	353	5.0

*positional parameters have been multiplied by 10^3

Table III. Anisotropic Thermal Displacement Parameters x 10^4.

Atom	U_{11}	U_{22}	U_{35}	U_{12}	U_{13}	U_{23}
Rh	156(2)	289(1)	369(1)	-18(2)	0	0
Ti	291(4)	248(4)	267(4)	-6(3)	0	0
C1	798(33)	413(23)	375(23)	-92(22)	86(21)	102(18)
C2	640(27)	547(23)	328(20)	127(23)	-18(21)	128(17)
C3	692(30)	566(24)	315(20)	-35(22)	-76(21)	-72(19)
C4	663(30)	597(25)	350(21)	147(22)	164(21)	16(19)
C5	510(25)	767(29)	393(23)	-131(24)	92(21)	107(21)
CB1	552(41)	295(27)	651(42)	-26(25	0	0
CB2	311(30)	500(36)	683(42)	-125(26	0	0

Appendix II.

Crystal Structure Data of $Cp_2Ti(\mu\text{-}CH_2)(\mu\text{-}p\text{-}(CH_3)_2NC_6H_4)Rh(COD)$

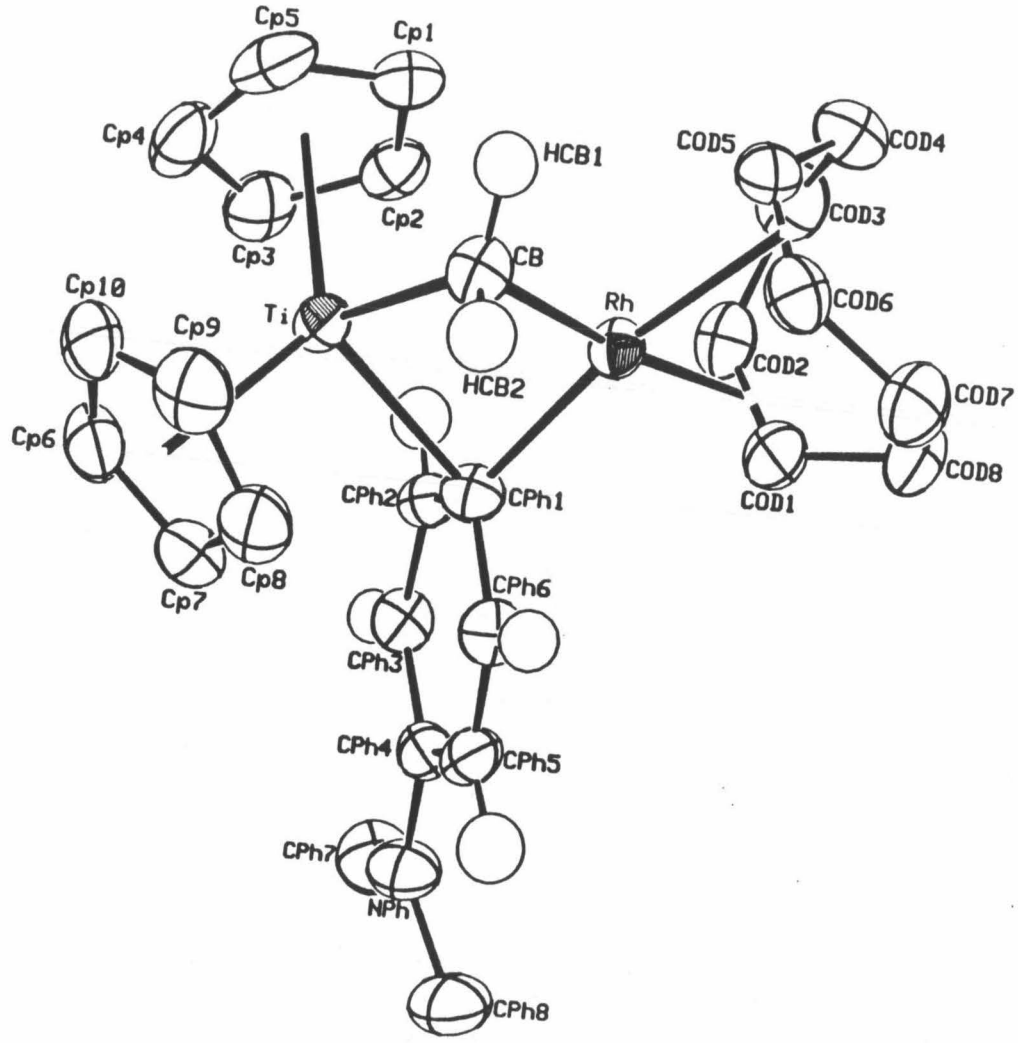

Figure 1. ORTEP diagram.

Table I. Complete Bond Distances and Angles.

	Distance(Å)		Distance(Å)
Rh -Ti	2.827(1)	CPh4 -NPh	1.377(5)
Rh -CPh1	2.122(4)	CPh5 -CPh6	1.368(5)
Rh -CPh6	2.880(4)	CPh5 -HPh5	0.96(3)
Rh -CB	2.131(4)	CPh6 -HPh6	0.97(3)
Rh -COD1	2.204(4)	NPh -CPh7	1.443(6)
Rh -COD2	2.173(4)	NPh -CPh8	1.451(6)
Rh -COD5	2.179(4)	CPh7 -HMe1	0.99(5)
Rh -COD6	2.153(4)	CPh7 -HMe2	0.93(5)
Ti -Cp1	2.473(4)	CPh7 -HMe3	0.85(5)
Ti -Cp2	2.440(4)	CPh8 -HMe4	0.97(5)
Ti -Cp3	2.386(4)	CPh8 -HMe5	0.87(5)
Ti -Cp4	2.399(4)	CPh8 -HMe6	1.01(4)
Ti -Cp5	2.427(4)	CB -HCB1	0.99(3)
Ti -Cp6	2.409(4)	CB -HCB2	0.98(3)
Ti -Cp7	2.436(4)	COD1-COD2	1.387(6)
Ti -Cp8	2.402(4)	COD1-COD8	1.524(6)
Ti -Cp9	2.396(4)	COD1-HCD1	0.99(4)
Ti -Cp10	2.398(4)	COD2-COD3	1.496(6)
Ti -CPh1	2.403(4)	COD2-HCD2	0.93(3)
Ti -CB	2.076(4)	COD3-COD4	1.516(6)
Cp1 -Cp2	1.390(5)	COD3-HCS1	0.89(4)
Cp1 -Cp5	1.403(6)	COD3-HCS2	0.90(5)
Cp1 -HCp1	0.89(3)	COD4-COD5	1.509(6)
Cp2 -Cp3	1.398(6)	COD4-HCS3	0.82(4)
Cp2 -HCp2	0.85(3)	COD4-HCS4	0.97(5)
Cp3 -Cp4	1.392(6)	COD5-COD6	1.371(6)
Cp3 -HCp3	0.90(4)	COD5-HCD3	0.79(3)
Cp4 -Cp5	1.394(6)	COD6-COD7	1.510(6)
Cp4 -HCp4	0.99(5)	COD6-HCD4	0.82(4)
Cp5 -HCp5	0.94(4)	COD7-COD8	1.518(6)
Cp6 -Cp7	1.393(6)	COD7-HCS5	0.96(5)
Cp6 -Cp10	1.418(6)	COD7-HCS6	0.98(5)
Cp6 -HCp6	0.89(4)	COD8-HCS7	0.95(4)
Cp7 -Cp8	1.400(6)	COD8-HCS8	0.97(4)
Cp7 -HCp7	0.89(4)		
Cp8 -Cp9	1.405(6)		
Cp8 -HCp8	0.90(4)		
Cp9 -Cp10	1.396(6)		
Cp9 -HCp9	0.89(4)		
Cp10-HCp0	0.94(4)		
CPh1-CPh2	1.403(5)		
CPh1-CPh6	1.425(5)		
CPh2-CPh3	1.383(5)		
CPh2-HPh2	0.91(3)		
CPh3-CPh4	1.397(5)		
CPh3-HPh3	0.89(3)		
CPh4-CPh5	1.405(5)		

Table I. (Cont.)

	Angle(°)		Angle(°)
Cp5 -Cp1 -Cp2	107.7(3)	CPh8 -NPh -CPh4	121.1(3)
HCp1-Cp1 -Cp2	126.8(20)	CPh8 -NPh -CPh7	116.5(3)
HCp1-Cp1 -Cp5	125.5(20)	HMe1-CPh7 -NPh	109.5(27)
Cp3 -Cp2 -Cp1	108.7(3)	HMe2-CPh7 -NPh	111.6(30)
HCp2-Cp2 -Cp1	125.6(23)	HMe3-CPh7 -NPh	110.5(32)
HCp2-Cp2 -Cp3	125.6(23)	HMe2-CPh7 -HMe1	105.0(40)
Cp4 -Cp3 -Cp2	107.2(4)	HMe3-CPh7 -HMe1	109.1(41)
HCp3-Cp3 -Cp2	130.9(22)	HMe3-CPh7 -HMe2	111.0(43)
HCp3-Cp3 -Cp4	121.9(22)	HMe4-CPh8 -NPh	112.0(28)
Cp5 -Cp4 -Cp3	108.7(4)	HMe5-CPh8 -NPh	114.8(31)
HCp4-Cp4 -Cp3	123.1(28)	HMe6-CPh8 -NPh	110.2(24)
HCp4-Cp4 -Cp5	128.1(28)	HMe5-CPh8 -HMe4	116.5(42)
Cp4 -Cp5 -Cp1	107.6(4)	HMe6-CPh8 -HMe4	104.4(37)
HCp5-Cp5 -Cp1	124.8(25)	HMe6-CPh8 -HMe5	97.0(39)
HCp5-Cp5 -Cp4	127.7(25)	HCB2-CB -HCB1	110.1(27)
Cp10-Cp6 -Cp7	108.1(4)	COD8-COD1-COD2	124.0(4)
HCp6-Cp6 -Cp7	124.6(23)	HCD1-COD1-COD2	115.2(22)
HCp6-Cp6 -Cp10	127.2(23)	HCD1-COD1-COD8	117.3(22)
Cp8 -Cp7 -Cp6	107.7(4)	COD3-COD2-COD1	126.2(4)
HCp7-Cp7 -Cp6	125.6(26)	HCD2-COD2-COD1	115.7(20)
HCp7-Cp7 -Cp8	126.7(26)	HCD2-COD2-COD3	114.9(20)
Cp9 -Cp8 -Cp7	108.7(4)	COD4-COD3-COD2	113.9(4)
HCp8-Cp8 -Cp7	127.2(24)	HCS1-COD3-COD2	105.7(27)
HCp8-Cp8 -Cp9	124.1(24)	HCS2-COD3-COD2	112.4(28)
Cp10-Cp9 -Cp8	107.6(4)	HCS1-COD3-COD4	109.2(27)
HCp9-Cp9 -Cp8	122.1(23)	HCS2-COD3-COD4	108.4(28)
HCp9-Cp9 -Cp10	130.1(23)	HCS2-COD3-HCS1	106.9(39)
Cp9 -Cp10-Cp6	107.8(4)	COD5-COD4-COD3	112.8(4)
HCp0-Cp10-Cp6	125.6(24)	HCS3-COD4-COD3	112.5(28)
HCp0-Cp10-Cp9	126.4(24)	HCS4-COD4-COD3	111.5(30)
CPh6-CPh1-CPh2	112.4(3)	HCS3-COD4-COD5	106.2(28)
CPh3-CPh2-CPh1	124.5(3)	HCS4-COD4-COD5	107.2(30)
HPh2-CPh2-CPh1	115.2(21)	HCS4-COD4-HCS3	106.1(41)
HPh2-CPh2-CPh3	120.3(21)	COD6-COD5-COD4	123.7(4)
CPh4-CPh3-CPh2	121.1(3)	HCD3-COD5-COD4	114.0(24)
HPh3-CPh3-CPh2	120.2(20)	HCD3-COD5-COD6	116.7(24)
HPh3-CPh3-CPh4	118.7(20)	COD7-COD6-COD5	124.8(4)
CPh5-CPh4-CPh3	116.3(3)	HCD4-COD6-COD5	122.1(25)
NPh -CPh4-CPh3	122.5(3)	HCD4-COD6-COD7	110.8(25)
NPh -CPh4-CPh5	121.2(3)	COD8-COD7-COD6	114.8(4)
CPh6-CPh5-CPh4	121.2(3)	HCS5-COD7-COD6	102.3(27)
HPh5-CPh5-CPh4	119.9(21)	HCS6-COD7-COD6	106.0(26)
HPh5-CPh5-CPh6	118.9(21)	HCS5-COD7-COD8	112.9(27)
CPh5-CPh6-CPh1	124.3(3)	HCS6-COD7-COD8	116.5(26)
HPh6-CPh6-CPh1	118.3(19)	HCS6-COD7-HCS5	102.7(38)
HPh6-CPh6-CPh5	117.3(19)	COD7-COD8-COD1	113.3(4)
CPh7-NPh -CPh4	119.9(3)	HCS7-COD8-COD1	106.3(24)

Table I. (Cont.)

	Angle(°)
HCS8-COD8-COD1	112.1(21)
HCS7-COD8-COD7	109.5(24)
HCS8-COD8-COD7	107.1(21)
HCS8-COD8-HCS7	108.6(32)
CB -Ti -CPh1	89.9(1)
Ti -CPh1 -Rh	77.0(1)
CPh1-Rh -CB	96.5(1)
Rh -CB -Ti	84.4(1)
Rh -CPh1 -CPh4	148.6(2)
Ti -CB -HCB1	121.7(18)
Ti -CB -HCB2	115.8(20)
Rh -CB -HCB1	109.2(18)
Rh -CB -HCB2	112.5(20)

Table II. Final Parameters.

	x, y, z and $U_{eq}{}^{a} \times 10^4$			
Atom	x	y	z	U_{eq} or B
Rh	1528(.3)	2701(.3)	2249(.2)	306(1)
Ti	3784(.7)	1174(.6)	2703(.4)	302(1)
CP1	4973(5)	3506(4)	3981(3)	428(10)
CP2	3982(4)	2712(4)	4397(3)	409(9)
CP3	4571(5)	1578(4)	4555(3)	462(10)
CP4	5955(5)	1697(5)	4251(3)	539(12)
CP5	6191(4)	2861(5)	3871(3)	524(12)
CP6	4372(5)	−1064(4)	2519(3)	495(10)
CP7	2904(5)	−1314(4)	1792(3)	477(10)
CP8	3128(5)	−581(4)	1063(3)	506(11)
CP9	4745(5)	100(4)	1322(3)	513(10)
CP10	5523(5)	−197(4)	2222(3)	508(10)
CPh1	974(4)	677(3)	2463(3)	333(8)
CPh2	725(4)	237(3)	3326(3)	342(8)
CPh3	−385(4)	−959(4)	3260(3)	367(8)
CPh4	−1417(4)	−1803(3)	2297(3)	338(8)
CPh5	−1226(4)	−1393(4)	1410(3)	364(8)
CPh6	−75(4)	−235(4)	1496(3)	371(8)
NPh	−2566(4)	−2977(3)	2208(3)	467(8)
CPh7	−2858(5)	−3283(4)	3136(4)	563(11)
CPh8	−3801(5)	−3685(4)	1232(4)	591(12)
CB	3599(4)	2534(4)	1781(3)	369(8)
COD1	−900(4)	2792(4)	2258(3)	444(10)
COD2	125(4)	3381(4)	3261(3)	427(9)
COD3	790(5)	4909(5)	3802(3)	564(11)
COD4	1433(5)	5750(4)	3136(3)	548(11)
COD5	2106(4)	4926(4)	2368(3)	420(9)
COD6	1244(5)	4184(4)	1362(3)	429(9)
COD7	−494(5)	4043(5)	891(3)	571(11)
COD8	−1553(5)	3635(4)	1550(3)	540(11)
HCP1	4848(36)	4271(30)	3792(23)	2.6(7) *
HCP2	3134(39)	2874(32)	4517(24)	3.3(7) *
HCP3	4206(40)	874(33)	4803(25)	3.7(8) *
HCP4	6593(55)	1013(45)	4278(35)	7.4(12) *
HCP5	7009(47)	3182(39)	3595(30)	5.5(10) *
HCP6	4534(40)	−1411(33)	3061(25)	3.6(8) *
HCP7	1993(45)	−1847(38)	1796(28)	5.0(9) *
HCP8	2381(43)	−529(35)	518(27)	4.3(8) *
HCP9	5116(41)	666(35)	969(26)	4.0(8) *
HCP0	6605(44)	167(37)	2598(28)	4.8(9) *
HCB1	4346(36)	3473(30)	1992(23)	2.7(7) *
HCB2	3360(38)	2113(32)	1030(24)	3.2(7) *
HPh2	1322(37)	827(31)	3963(24)	3.0(7) *
HPh3	−457(35)	−1200(30)	3835(23)	2.4(6) *
HPh5	−1909(39)	−1927(32)	731(25)	3.4(8) *

Table II. (Cont.)

Atom	x	y	z	U_{eq} or B
HPh6	−14(36)	1(30)	860(23)	2.6(7) *
HMe1	−3609(53)	−4220(45)	2941(33)	6.7(11)*
HMe2	−1942(57)	−3345(46)	3588(34)	7.1(12)*
HMe3	−3251(53)	−2675(45)	3442(33)	6.9(12)*
HMe4	−4498(55)	−4514(46)	1276(34)	7.1(12)*
HMe5	−4255(52)	−3138(45)	935(33)	6.5(11)*
HMe6	−3322(49)	−4043(41)	664(30)	5.7(10)*
HCS1	1575(50)	4972(40)	4357(30)	5.6(10)*
HCS2	83(51)	5299(42)	4044(32)	6.4(11)*
HCS3	2149(47)	6450(38)	3487(29)	5.2(9) *
HCS4	618(57)	6078(47)	2736(36)	7.7(12)*
HCS5	−733(51)	3356(44)	233(33)	6.7(11)*
HCS6	−549(50)	4902(44)	684(32)	6.5(11)*
HCS7	−2549(46)	3062(38)	1108(29)	5.2(10)*
HCS8	−1707(40)	4494(34)	1945(25)	3.7(8) *
HCD1	−1503(43)	1802(35)	2106(27)	4.3(8) *
HCD2	126(37)	2808(31)	3704(24)	2.9(7) *
HCD3	3033(37)	5215(31)	2474(24)	3.0(7) *
HCD4	1671(42)	3963(35)	902(26)	4.0(8) *

[a] $U_{eq} = \frac{1}{3}\sum_i \sum_j [U_{ij}(a_i^* a_j^*)(\vec{a}_i \cdot \vec{a}_j)]$
*Isotropic displacement parameter, B

Table III. Anisotropic Thermal Displacement Parameters x 10^4.

Atom	U_{11}	U_{22}	U_{33}	U_{12}	U_{13}	U_{23}
Rh	264(1)	337(2)	351(2)	78(1)	125(1)	127(1)
Ti	271(3)	341(3)	280(3)	84(3)	73(3)	61(3)
Cp1	408(22)	402(21)	361(21)	13(17)	48(17)	33(17)
Cp2	368(21)	485(22)	289(19)	78(17)	63(16)	4(17)
Cp3	483(24)	543(24)	310(20)	108(19)	31(18)	130(18)
Cp4	407(24)	667(29)	406(23)	206(21)	−46(19)	−3(21)
Cp5	276(20)	666(28)	453(24)	−26(19)	67(18)	−18(21)
Cp6	542(26)	418(22)	569(26)	241(20)	157(21)	128(19)
Cp7	496(25)	346(21)	522(24)	109(18)	118(20)	23(18)
Cp8	591(27)	503(24)	369(22)	214(21)	99(20)	−6(19)
Cp9	588(28)	542(25)	452(24)	206(21)	258(21)	59(20)
Cp10	445(24)	495(24)	580(26)	251(20)	166(20)	12(20)
CPh1	320(19)	334(19)	349(19)	39(15)	147(16)	94(15)
CPh2	304(18)	343(19)	323(19)	49(15)	70(15)	37(15)
CPh3	390(21)	414(20)	352(20)	90(17)	154(17)	180(17)
CPh4	286(18)	308(18)	433(21)	79(15)	125(16)	108(16)
CPh5	299(19)	397(20)	334(19)	66(16)	41(15)	57(16)
CPh6	410(21)	405(20)	316(19)	92(17)	131(16)	122(16)
NPh	407(19)	406(18)	534(20)	−16(15)	159(16)	112(16)
CPh7	496(26)	546(25)	710(29)	37(20)	287(23)	268(22)
CPh8	442(25)	506(25)	665(29)	−56(20)	115(22)	55(22)
CB	347(20)	436(21)	375(20)	103(16)	154(16)	165(17)
COD1	296(20)	464(22)	603(26)	104(17)	179(19)	156(19)
COD2	394(22)	561(24)	438(22)	202(19)	214(18)	198(19)
COD3	557(27)	647(28)	484(25)	243(22)	189(21)	39(21)
COD4	594(28)	377(22)	575(26)	94(20)	123(22)	19(19)
COD5	340(21)	333(20)	564(25)	34(16)	125(18)	136(18)
COD6	516(24)	413(21)	450(23)	157(18)	210(19)	200(18)
COD7	601(29)	617(28)	488(25)	205(23)	51(21)	212(21)
COD8	373(23)	605(27)	607(27)	196(20)	34(20)	155(22)

The form of the displacement factor is:

$$\exp -2\pi^2(U_{11}h^2a^{*2} + U_{22}k^2b^{*2} + U_{33}\ell^2c^{*2} + 2U_{12}hka^*b^* + 2U_{13}h\ell a^*c^* + 2U_{23}k\ell b^*c^*)$$

Appendix III.

Crystal Structure Data of $Cp_2Ti(\mu\text{-}CH_2)(\mu\text{-}Cl)Pt(Me)PMe_2Ph$

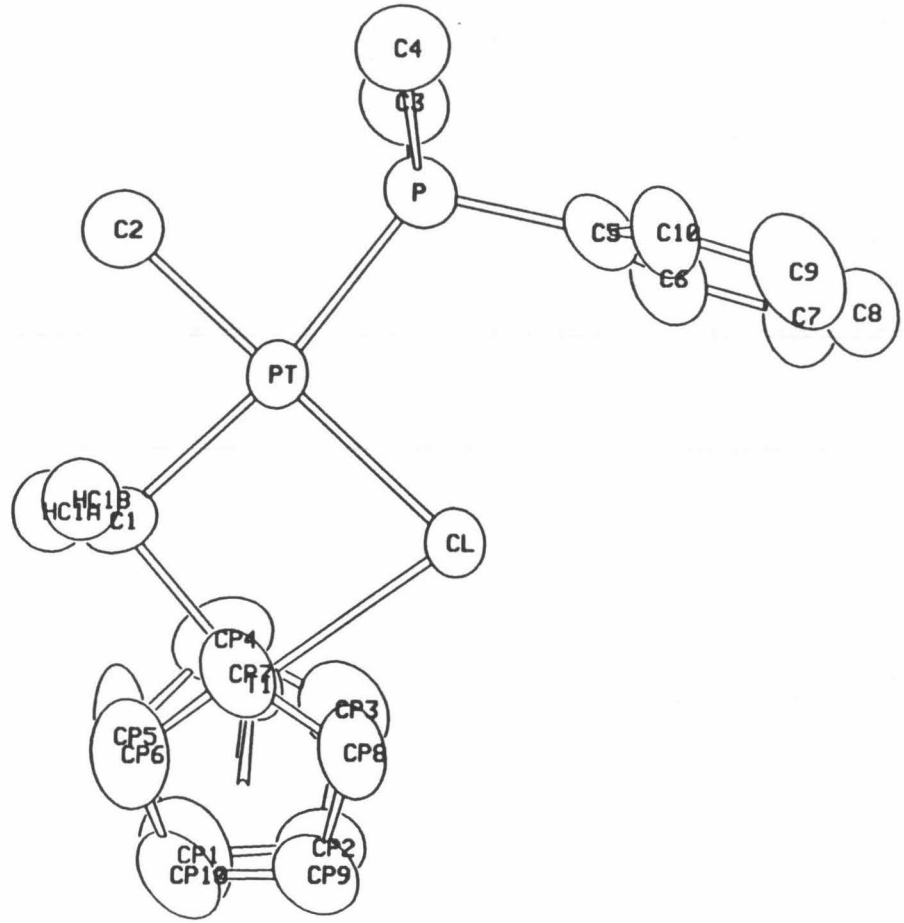

Figure 1. ORTEP diagram.

Table I. Complete Bond Distances and Angles.

	Angle(°)		Angle(°)		
C1	-Pt	-C2	83.1(6)	H10	-C10 -C5	119.9
C1	-Pt	-P	170.4(5)	H10	-C10 -C9	119.5
C1	-Pt	-Cl	96.6(5)	CP5	-CP1 -CP2	113.4(20)
Pt	-Cl	-Ti	75.7(1)	HP1	-CP1 -CP2	122.7
Cl	-Ti	-C1	97.0(5)	HP1	-CP1 -CP5	123.9
Cl	-Ti	-CPC1	106.2	CP3	-CP2 -CP1	104.3(17)
Cl	-Ti	-CPC2	105.2	HP2	-CP2 -CP1	127.7
C1	-Ti	-CPC1	105.0	HP2	-CP2 -CP3	127.9
C1	-Ti	-CPC2	105.8	CP4	-CP3 -CP2	108.8(16)
CPC1	-Ti	-CPC2	132.4	HP3	-CP3 -CP2	125.3
Ti	-C1	-Pt	90.3(7)	HP3	-CP3 -CP4	125.8
Pt	-C1	-HC1A	111.0(62)	CP5	-CP4 -CP3	107.0(17)
Pt	-C1	-HC1B	103.9(95)	HP4	-CP4 -CP3	126.3
Ti	-C1	-HC1A	118.7(62)	HP4	-CP4 -CP5	126.7
Ti	-C1	-HC1B	119.6(95)	CP4	-CP5 -CP1	106.3(19)
Pt	-P	-C3	113.0(5)	HP5	-CP5 -CP1	126.5
Pt	-P	-C4	116.3(5)	HP5	-CP5 -CP4	127.2
Pt	-P	-C5	117.2(5)	CP10	-CP6 -CP7	108.5(16)
C3	-P	-C4	102.3(7)	HP6	-CP6 -CP7	125.7
C3	-P	-C5	102.3(7)	HP6	-CP6 -CP10	125.7
C4	-P	-C5	103.7(7)	CP8	-CP7 -CP6	106.8(15)
P	-C5	-C6	121.4(12)	HP7	-CP7 -CP6	126.5
P	-C5	-C10	119.3(12)	HP7	-CP7 -CP8	126.7
HC1B	-C1	-HC1A	110.1(113)	CP9	-CP8 -CP7	108.6(15)
HC2B	-C2	-HC2A	110.4	HP8	-CP8 -CP7	125.5
HC2C	-C2	-HC2A	110.8	HP8	-CP8 -CP9	125.9
HC2C	-C2	-HC2B	111.2	CP10	-CP9 -CP8	107.4(15)
HC3B	-C3	-HC3A	110.7	HP9	-CP9 -CP8	125.5
HC3C	-C3	-HC3A	110.8	HP9	-CP9 -CP10	127.1
HC3C	-C3	-HC3B	111.6	CP9	-CP10 -CP6	108.4(16)
HC4B	-C4	-HC4A	111.8	HP10	-CP10 -CP6	126.1
HC4C	-C4	-HC4A	110.8	HP10	-CP10 -CP9	125.4
HC4C	-C4	-HC4B	110.8			
C10	-C5	-C6	118.8(14)			
C7	-C6	-C5	121.5(16)			
H6	-C6	-C5	119.3			
H6	-C6	-C7	119.3			
C8	-C7	-C6	117.3(17)			
H7	-C7	-C6	121.0			
H7	-C7	-C8	121.8			
C9	-C8	-C7	123.8(19)			
H8	-C8	-C7	118.3			
H8	-C8	-C9	118.0			
C10	-C9	-C8	118.0(18)			
H9	-C9	-C8	121.4			
H9	-C9	-C10	120.6			
C9	-C10	-C5	120.6(16)			

Table I. (Cont.)

	Distance(Å)		Distance(Å)
Pt	···Ti	2.962(2)	CP6 –HP6	0.940
Cl	···C1	3.374(18)	CP7 –CP8	1.39(2)
Pt	–Cl	2.399(4)	CP7 –HP7	0.960
Pt	–C1	2.112(17)	CP8 –CP9	1.39(2)
Pt	–C2	2.071(15)	CP8 –HP8	0.950
Pt	–P	2.261(4)	CP9 –CP10	1.38(3)
Ti	–Cl	2.427(5)	CP9 –HP9	0.950
Ti	–C1	2.066(18)	CP10–HP10	0.950
Ti	···CPC1	2.071	Pt ···HC1A	2.66(11)
Ti	···CPC2	2.082	Pt ···HC1B	2.44(13)
P	–C3	1.842(16)	Ti ···HC1A	2.71(11)
P	–C4	1.809(16)	Ti ···HC1B	2.57(13)
P	–C5	1.833(15)		
C1	–HC1A	1.026(11)		
C1	–HC1B	0.817(14)		
C2	–HC2A	0.950		
C2	–HC2B	0.950		
C2	–HC2C	0.940		
C3	–HC3A	0.950		
C3	–HC3B	0.940		
C3	–HC3C	0.940		
C4	–HC4A	0.940		
C4	–HC4B	0.940		
C4	–HC4C	0.950		
C5	–C6	1.38(2)		
C5	–C10	1.38(2)		
C6	–C7	1.37(3)		
C6	–H6	0.950		
C7	–C8	1.37(3)		
C7	–H7	0.950		
C8	–C9	1.36(3)		
C8	–H8	0.940		
C9	–C10	1.38(3)		
C9	–H9	0.950		
C10	–H10	0.950		
CP1	–CP2	1.36(3)		
CP1	–CP5	1.35(3)		
CP1	–HP1	0.950		
CP2	–CP3	1.43(3)		
CP2	–HP2	0.950		
CP3	–CP4	1.39(3)		
CP3	–HP3	0.940		
CP4	–CP5	1.42(3)		
CP4	–HP4	0.940		
CP5	–HP5	0.950		
CP6	–CP7	1.39(3)		
CP6	–CP10	1.38(3)		

Table II. Final Parameters.

x, y, z and $U_{eq}{}^{a} \times 10^4$

Atom	x	y	z	U_{eq} or B
Pt	2130(.5)	1353(.5)	60(.5)	446(1)
Ti	2268(2)	1594(2)	−1912(2)	451(7)
Cl	2061(4)	−150(3)	−1092(3)	598(12)
P	2203(3)	91(3)	1268(3)	510(12)
C1	2156(13)	2736(14)	−870(13)	557(50)
C2	2181(12)	2658(13)	1047(11)	663(50)
C3	3514(12)	165(12)	2408(10)	798(60)
C4	1178(13)	274(12)	1777(11)	817(51)
C5	2112(12)	−1440(12)	947(10)	521(40)
C6	3037(12)	−2058(14)	1028(12)	658(51)
C7	2959(15)	−3185(15)	732(13)	804(65)
C8	1923(20)	−3658(15)	311(12)	854(62)
C9	983(15)	−3084(18)	193(14)	957(70)
C10	1083(14)	−1955(14)	506(12)	663(53)
Cp1	3640(15)	2134(20)	−2440(16)	937(78)
Cp2	3729(13)	969(15)	−2371(13)	678(56)
Cp3	4102(13)	738(15)	−1312(15)	717(64)
Cp4	4179(13)	1766(19)	−809(12)	710(63)
Cp5	3920(15)	2657(14)	−1541(22)	960(95)
Cp6	748(14)	2729(13)	−2995(14)	732(65)
Cp7	311(13)	1811(16)	−2663(12)	636(51)
Cp8	494(14)	828(13)	−3115(13)	673(55)
Cp9	1128(14)	1125(15)	−3641(11)	706(58)

Table II. (Cont.)

Cp10	1272(14)	2301(16)	−3568(13)	748(59)	
HC1A	2811(86)	3273(85)	−495(78)	5.0	*
HC1B	1571(101)	3070(100)	−995(105)	5.0	*

[a] $U_{eq} = \frac{1}{3}\sum_i \sum_j [U_{ij}(a_i^* a_j^*)(\vec{a}_i \cdot \vec{a}_j)]$

*Isotropic displacement parameter, B

Table III. Hydrogen Parameters.

	x, y and $z \times 10^4$			
Atom	x	y	z	B
HC1A	2811(86)	3273(85)	−495(78)	5.0
HC1B	1571(101)	3070(100)	−995(105)	5.0
HC2A	2195	3370	731	5.5
HC2B	2834	2567	1647	5.5
HC2C	1542	2603	1178	5.5
HC3A	4093	−70	2223	6.7
HC3B	3460	−338	2894	6.7
HC3C	3620	930	2639	6.7
HC4A	1404	891	2236	7.0
HC4B	1138	−418	2096	7.0
HC4C	489	438	1226	7.0
HCP1	3391	2531	−3066	6.8
HCP2	3576	435	−2901	6.8
HCP3	4286	13	−1012	6.8
HCP4	4360	1855	−114	6.8
HCP5	3955	3460	−1423	6.8
HCP6	684	3512	−2860	5.9
HCP7	−47	1851	−2213	5.9
HCP8	220	87	−3081	5.9
HCP9	1402	606	−3985	5.9
HCP10	1678	2734	−3852	5.9
H6	3741	−1688	1281	5.6
H7	3603	−3617	825	6.8
H8	1855	−4425	91	7.5
H9	277	−3446	−93	8.2
H10	436	−1529	412	5.4

Table IV. Anisotropic Thermal Displacement Parameters x 10^4.

Atom	U_{11}	U_{22}	U_{33}	U_{12}	U_{13}	U_{23}
Pt	508(4)	388(3)	468(4)	−30(4)	228(3)	−27(5)
Ti	509(17)	356(16)	484(17)	18(13)	201(14)	93(13)
Cl	965(35)	372(22)	540(28)	−2(22)	396(26)	14(20)
P	484(30)	550(28)	561(31)	−34(22)	281(26)	30(24)
C1	606(138)	648(127)	502(119)	−95(95)	315(115)	−112(95)
C2	728(134)	691(114)	631(128)	−47(92)	342(108)	−32(92)
C3	882(134)	845(117)	389(103)	−252(97)	−16(96)	−17(88)
C4	797(132)	946(123)	788(130)	−121(102)	409(112)	−77(102)
C5	435(96)	576(97)	577(100)	−162(109)	233(83)	113(96)
C6	497(123)	609(113)	1026(139)	23(91)	473(107)	140(104)
C7	857(158)	569(138)	897(146)	244(105)	274(124)	158(101)
C8	1280(182)	571(112)	657(129)	−35(157)	347(133)	47(120)
C9	673(145)	925(164)	1127(167)	−57(122)	227(131)	288(133)
C10	729(140)	470(104)	710(124)	136(96)	217(104)	178(92)
Cp1	661(151)	885(182)	1140(203)	197(136)	249(146)	302(155)
Cp2	651(125)	827(142)	528(129)	277(100)	216(101)	136(99)
Cp3	450(120)	840(144)	754(162)	157(104)	142(110)	239(124)
Cp4	394(109)	1080(169)	611(133)	−77(102)	162(96)	−185(123)
Cp5	553(135)	340(117)	1830(252)	−115(94)	336(163)	50(153)
Cp6	455(118)	613(128)	823(149)	241(97)	−41(104)	171(111)
Cp7	585(118)	591(113)	655(126)	−16(89)	179(97)	149(98)
Cp8	703(131)	489(111)	716(136)	−113(98)	182(107)	37(101)
Cp9	767(130)	772(155)	463(109)	−112(106)	139(94)	91(97)
Cp10	788(148)	718(140)	739(143)	−106(113)	317(115)	211(108)

The form of the displacement factor is:

$$\exp -2\pi^2(U_{11}h^2a^{*2} + U_{22}k^2b^{*2} + U_{33}\ell^2c^{*2} + 2U_{12}hka^*b^* + 2U_{13}h\ell a^*c^* + 2U_{23}k\ell b^*c^*)$$

Appendix IV.

Crystal Structure Data of $Cp_2Ti(\mu\text{-}CH_2)(\mu\text{-}CH_3)Pt(Me)PMe_2Ph$

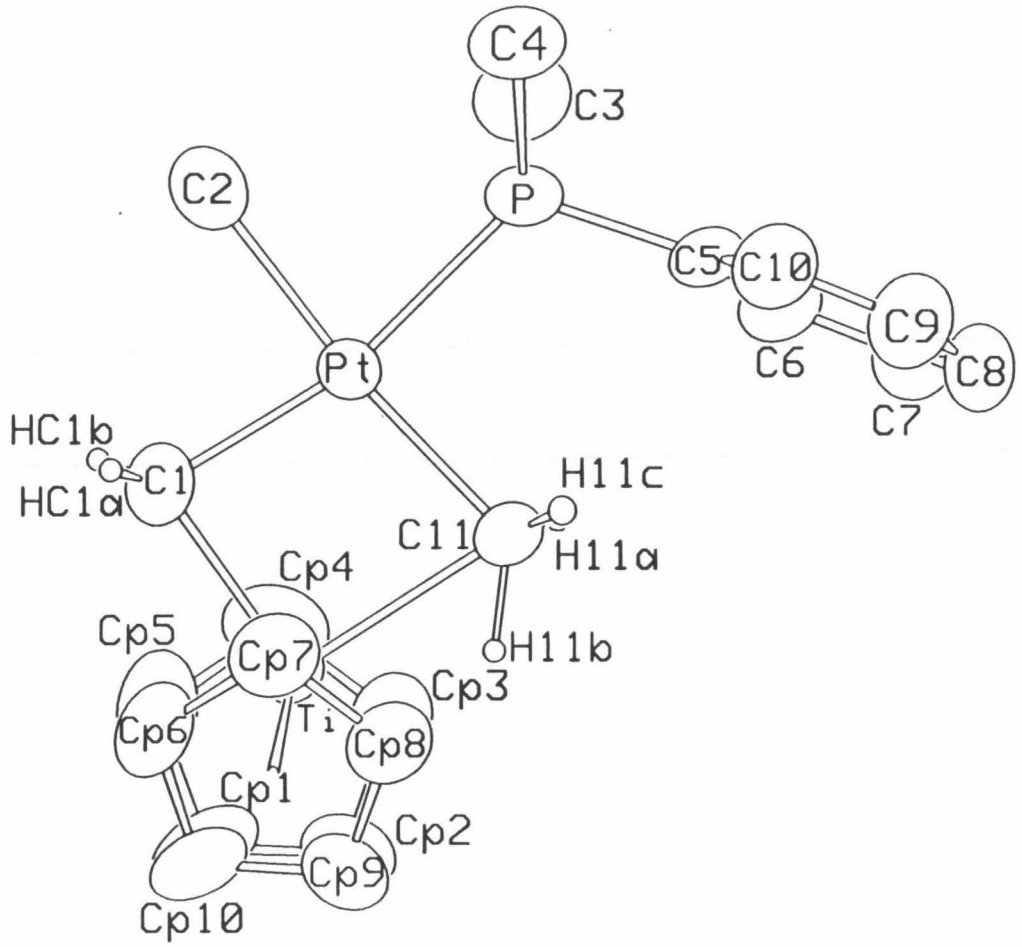

Figure 1. ORTEP diagram.

Table I. Complete Bond Distances and Angles.

	Distance(Å)		Distance(Å)
Pt –C1	2.078(7)	Ti ··HC1a	2.67(5)
Pt –C11	2.122(8)	Ti ··HC1b	2.74(5)
Pt –C2	2.108(6)	Ti ··HC11b	1.93(5)
Pt –P	2.279(2)	Ti ··HC11a	2.94(6)
Pt ··Ti	2.776(1)	Ti ··HC11c	3.07(7)
Pt ··HC1a	2.58(5)	C1 ··C11	3.348(11)
Pt ··HC1b	2.61(5)	P –C3	1.828(9)
Pt ··HC11a	2.48(6)	P –C4	1.829(9)
Pt ··HC11c	2.53(7)	P –C5	1.829(6)
Pt ··HC11b	2.89(5)	C1 –HC1a	0.94(5)
Ti –C1	2.115(7)	C1 –HC1b	0.96(5)
Ti –C11	2.395(8)	C3 –HC3a	0.96(8)
Ti –CpA	2.081	C3 –HC3b	0.89(7)
Ti –CpB	2.082	C3 –HC3c	1.08(8)
Ti –Cp1	2.377(9)	C4 –HC4a	0.92(6)
Ti –Cp2	2.395(7)	C4 –HC4b	0.89(9)
Ti –Cp3	2.430(7)	C4 –HC4c	1.08(8)
Ti –Cp4	2.382(8)	C5 –C6	1.394(9)
Ti –Cp5	2.365(9)	C5 –C10	1.396(9)
Ti –Cp6	2.367(7)	C6 –C7	1.367(11)
Ti –Cp7	2.409(7)	C6 –HC6	0.94(6)
Ti –Cp8	2.438(7)	C7 –C8	1.362(12)
Ti –Cp9	2.394(7)	C7 –HC7	0.91(6)
Ti –Cp10	2.368(7)	C8 –C9	1.367(13)

Table I. (Cont.)

	Distance(Å)		Distance(Å)
C8 –HC8	1.00(5)	Cp9 –Cp10	1.406(10)
C9 –C10	1.389(12)	Cp9 –HCp9	0.89(5)
C9 –HC9	0.76(6)	Cp10–HCp10	0.87(7)
C10 –HC10	0.94(6)		
C11 –HC11a	0.85(6)		
C11 –HC11b	1.06(5)		
C11 –HC11c	0.97(7)		
Cp1 –Cp2	1.372(11)		
Cp1 –Cp5	1.382(13)		
Cp1 –HCp1	0.80(6)		
Cp2 –Cp3	1.394(10)		
Cp2 –HCp2	0.94(6)		
Cp3 –Cp4	1.376(11)		
Cp3 –HCp3	1.02(6)		
Cp4 –Cp5	1.395(12)		
Cp4 –HCp4	0.97(7)		
Cp5 –HCp5	1.04(8)		
Cp6 –Cp7	1.407(10)		
Cp6 –Cp10	1.385(10)		
Cp6 –HCp6	1.00(7)		
Cp7 –Cp8	1.376(10)		
Cp7 –HCp7	0.92(6)		
Cp8 –Cp9	1.397(10)		
Cp8 –HCp8	0.99(6)		

Table I. (Cont.)

	Angle(°)				Angle(°)		
C1	-Pt	-C11	105.7(3)	HC11b	-C11	-HC11c	109.3(48)
C11	-Pt	-P	87.6(2)	HC11c	-C11	-HC11a	109.9(58)
P	-Pt	-C2	86.3(2)	Pt	-P	-C3	112.4(3)
C2	-Pt	-C1	80.3(3)	Pt	-P	-C4	115.9(3)
C1	-Ti	-C11	95.7(3)	Pt	-P	-C5	119.0(2)
CpA	-Ti	-CpB	133.3	C3	-P	-C4	102.7(4)
CpA	-Ti	-C1	105.3	C3	-P	-C5	102.3(3)
CpA	-Ti	-C11	106.1	C4	-P	-C5	102.4(3)
CpB	-Ti	-C1	104.5	P	-C5	-C6	121.3(4)
CpB	-Ti	-C11	105.9	P	-C5	-C10	121.6(4)
Pt	-C1	-Ti	82.9(3)	HC3b	-C3	-HC3a	104.7(64)
Pt	-C1	-HC1a	112.1(32)	HC3c	-C3	-HC3a	109.2(61)
Pt	-C1	-HC1b	113.1(31)	HC3c	-C3	-HC3b	113.9(61)
Ti	-C1	-HC1a	116.3(32)	HC4b	-C4	-HC4a	111.5(66)
Ti	-C1	-HC1b	121.1(31)	HC4c	-C4	-HC4a	109.3(54)
HC1a	-C1	-HC1b	109.0(45)	HC4c	-C4	-HC4b	109.8(70)
Pt	-C11	-Ti	75.6(2)	C10	-C5	-C6	117.0(6)
Pt	-C11	-HC11a	105.1(42)	C7	-C6	-C5	121.9(7)
Pt	-C11	-HC11c	103.7(40)	HC6	-C6	-C5	118.2(37)
Pt	-C11	-HC11b	127.1(28)	HC6	-C6	-C7	119.7(37)
Ti	-C11	-HC11b	51.7(27)	C8	-C7	-C6	120.8(8)
Ti	-C11	-HC11a	122.3(42)	HC7	-C7	-C6	119.4(38)
Ti	-C11	-HC11c	126.3(40)	HC7	-C7	-C8	119.7(38)
HC11a	-C11	-HC11b	101.2(50)	C9	-C8	-C7	118.7(8)

Table I. (Cont.)

	Angle(°)		Angle(°)
HC8 –C8 –C7	124.2(32)	HCp6 –Cp6 –Cp7	126.2(40)
HC8 –C8 –C9	117.0(32)	HCp6 –Cp6 –Cp10	125.9(40)
C10 –C9 –C8	121.8(8)	Cp8 –Cp7 –Cp6	108.5(6)
HC9 –C9 –C8	123.6(47)	HCp7 –Cp7 –Cp6	122.6(38)
HC9 –C9 –C10	114.6(47)	HCp7 –Cp7 –Cp8	128.4(38)
C9 –C10 –C5	119.8(7)	Cp9 –Cp8 –Cp7	107.9(6)
HC10–C10 –C5	115.0(38)	HCp8 –Cp8 –Cp7	123.1(38)
HC10–C10 –C9	125.2(39)	HCp8 –Cp8 –Cp9	128.4(38)
Cp5 –Cp1 –Cp2	108.9(8)	Cp10 –Cp9 –Cp8	108.0(6)
HCp1–Cp1 –Cp2	126.8(46)	HCp9 –Cp9 –Cp8	123.1(33)
HCp1–Cp1 –Cp5	124.3(46)	HCp9 –Cp9 –Cp10	128.4(33)
Cp3 –Cp2 –Cp1	107.8(7)	Cp9 –Cp10–Cp6	107.7(6)
HCp2–Cp2 –Cp1	129.3(37)	HCp10–Cp10–Cp6	124.8(44)
HCp2–Cp2 –Cp3	122.9(37)	HCp10–Cp10–Cp9	127.2(44)
Cp4 –Cp3 –Cp2	107.7(7)		
HCp3–Cp3 –Cp2	122.7(36)		
HCp3–Cp3 –Cp4	129.3(37)		
Cp5 –Cp4 –Cp3	108.4(7)		
HCp4–Cp4 –Cp3	120.2(40)		
HCp4–Cp4 –Cp5	131.1(40)		
Cp4 –Cp5 –Cp1	107.1(8)		
HCp5–Cp5 –Cp1	120.8(44)		
HCp5–Cp5 –Cp4	132.1(44)		
Cp10 –Cp6 –Cp7	107.8(6)		

Table II. Final Parameters.

	x, y, z and $U_{eq}{}^{a} \times 10^4$			
Atom	x	y	z	U_{eq} or B
Pt	2178(.2)	1307(.2)	−4(.1)	396
Ti	2287(.7)	1541(.7)	−1883(.6)	385(2)
P	2246(1)	16(1)	1213(1)	454(3)
C1	2195(6)	2759(5)	−832(5)	562(16)
C2	2216(5)	2580(5)	1051(4)	702(16)
C3	3552(6)	81(8)	2367(5)	726(21)
C4	1214(7)	203(8)	1726(6)	704(19)
C5	2128(4)	−1509(5)	898(4)	460(13)
C6	3055(6)	−2161(6)	1033(5)	600(16)
C7	2973(7)	−3289(7)	758(6)	760(20)
C8	1969(8)	−3814(7)	314(5)	810(23)
C9	1044(8)	−3201(7)	177(6)	818(24)
C10	1102(6)	−2056(6)	455(5)	634(17)
C11	2156(7)	−103(6)	−944(5)	541(16)
Cp1	3630(6)	2105(8)	−2476(7)	782(22)
Cp2	3707(5)	937(7)	−2380(5)	663(18)
Cp3	4103(5)	673(6)	−1338(5)	609(17)
Cp4	4219(5)	1683(7)	−810(6)	716(20)
Cp5	3933(6)	2583(7)	−1514(8)	840(24)
Cp6	751(6)	2652(6)	−2967(5)	669(19)
Cp7	304(5)	1746(6)	−2618(5)	646(17)
Cp8	494(5)	738(6)	−3012(5)	609(17)
Cp9	1072(5)	997(6)	−3601(5)	605(17)

Table II. (Cont.)

Atom	x	y	z	U_{eq} or B
Cp10	1217(6)	2190(6)	−3581(5)	654(19)
HC1a	1535(42)	3175(41)	−1048(37)	3.6(12)*
HC1b	2804(40)	3259(41)	−460(36)	3.5(12)*
HC11a	2719(47)	−503(50)	−575(44)	4.7(17)*
HC11b	2233(38)	−76(39)	−1649(38)	3.6(11)*
HC11c	1482(54)	−510(52)	−1043(47)	5.8(18)*
HCp1	3433(48)	2468(52)	−3001(46)	5.4(16)*
HCp2	3549(45)	375(48)	−2893(44)	5.0(15)*
HCp3	4204(49)	−148(52)	−1072(45)	5.5(16)*
HCp4	4394(50)	1672(53)	−80(49)	7.3(18)*
HCp5	3938(59)	3462(65)	−1421(56)	9.1(22)*
HCp6	747(53)	3482(57)	−2793(50)	7.9(19)*
HCp7	25(47)	1847(49)	−2136(43)	5.3(15)*
HCp8	331(49)	−22(52)	−2807(46)	5.8(16)*
HCp9	1360(39)	464(41)	−3858(36)	3.1(11)*
HCp10	1477(51)	2586(55)	−3941(46)	6.7(18)*
HC6	3759(47)	−1821(49)	1371(42)	5.2(16)*
HC7	3600(46)	−3695(50)	882(41)	5.3(14)*
HC8	1853(39)	−4618(46)	40(38)	3.7(12)*
HC9	464(45)	−3454(51)	−43(44)	4.4(16)*
HC10	493(48)	−1596(50)	372(44)	5.9(17)*

Table II. (Cont.)

Atom	x	y	z	U_{eq} or B
HC3a	3532(58)	−442(61)	2875(55)	7.8(21)*
HC3b	3544(52)	771(55)	2624(49)	6.4(19)*
HC3c	4279(63)	−88(60)	2240(53)	8.5(20)*
HC4a	1394(41)	−289(44)	2276(41)	3.7(12)*
HC4b	534(68)	72(72)	1247(60)	10.2(27)*
HC4c	1276(59)	1073(65)	1993(55)	9.4(22)*
HC2a	2221	3334	769	6.3 *
HC2b	2855	2514	1679	6.3 *
HC2c	1571	2538	1183	6.3 *
HC2d	2211	2256	1652	6.3 *
HC2e	2861	3053	1238	6.3 *
HC2f	1577	3077	742	6.3 *

[a] $U_{eq} = \frac{1}{3}\sum_i \sum_j [U_{ij}(a_i^* a_j^*)(\vec{a}_i \cdot \vec{a}_j)]$

*Isotropic displacement parameter, B

Table III. Anisotropic Thermal Displacement Parameters x 10^4.

Atom	U_{11}	U_{22}	U_{33}	U_{12}	U_{13}	U_{23}
Pt	484(1)	393(1)	370(1)	1(1)	238(1)	−7(1)
Ti	458(5)	350(5)	383(5)	26(4)	212(4)	59(4)
P	476(8)	571(9)	377(7)	−11(7)	240(7)	31(7)
C1	659(44)	434(36)	623(39)	22(36)	301(35)	27(32)
C2	943(46)	594(37)	673(37)	−9(34)	444(35)	−83(31)
C3	635(46)	880(60)	523(40)	−60(44)	109(34)	50(43)
C4	769(53)	872(57)	706(47)	58(46)	539(45)	106(45)
C5	513(32)	540(37)	375(26)	25(28)	234(24)	111(25)
C6	659(44)	655(45)	584(37)	93(37)	357(34)	152(33)
C7	964(59)	676(50)	715(45)	288(47)	428(44)	158(38)
C8	1309(74)	470(42)	690(44)	46(50)	461(47)	8(38)
C9	1001(69)	676(51)	731(49)	−255(52)	323(49)	−41(40)
C10	587(42)	686(46)	624(39)	−15(37)	251(33)	65(34)
C11	823(51)	439(36)	452(36)	5(38)	358(37)	58(30)
Cp1	635(46)	1000(66)	881(58)	191(43)	485(45)	452(54)
Cp2	602(40)	897(54)	552(38)	164(37)	305(33)	−7(38)
Cp3	562(40)	628(44)	661(45)	195(34)	281(35)	140(37)
Cp4	440(35)	1110(66)	595(42)	−105(37)	217(32)	−96(43)
Cp5	700(49)	592(47)	1462(84)	−198(40)	684(55)	−57(54)
Cp6	678(44)	547(41)	663(42)	165(35)	167(35)	200(35)
Cp7	540(37)	789(48)	626(41)	88(34)	264(33)	108(37)
Cp8	573(39)	679(44)	509(36)	−139(35)	165(30)	21(33)

Table III. (Cont.)

Cp9	600(38)	747(50)	434(32)	−14(35)	185(29)	−105(32)
Cp10	644(43)	825(52)	424(35)	46(38)	159(32)	271(35)

The form of the displacement factor is:

$$\exp -2\pi^2(U_{11}h^2a^{*2} + U_{22}k^2b^{*2} + U_{33}\ell^2c^{*2} + 2U_{12}hka^*b^* + 2U_{13}h\ell a^*c^* + 2U_{23}k\ell b^*c^*)$$

Appendix V.

Crystal Structure Data of $Cp_2Ti(\eta^2\text{-}CH_2S)PMe_3$

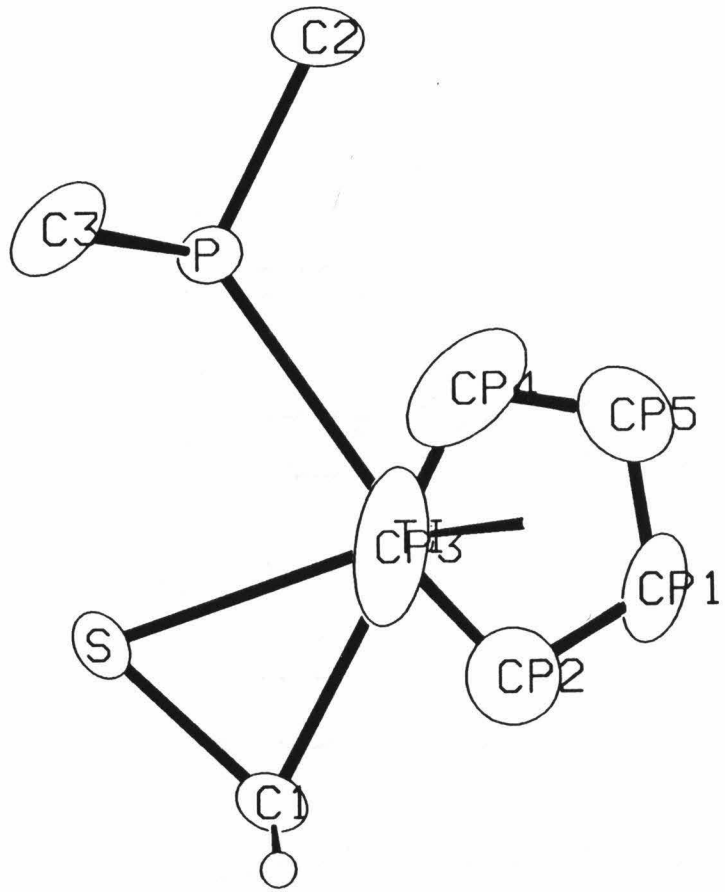

Figure 1. ORTEP diagram.

Table I. Complete Bond Distances and Angles.

Distance(Å)			Angle(°)			
Ti	–S	2.452(1)	CPa	–Ti	–S	115.6(0)
Ti	–P	2.601(1)	CPa	–Ti	–P	102.3(0)
Ti	–C1	2.245(3)	CPa	–Ti	–C1	104.2(1)
Ti	–CP1	2.406(3)	CPb	–Ti	–CPa	127.4(0)
Ti	–CP2	2.390(3)	S	–Ti	–P	74.1(0)
Ti	–CP3	2.380(4)	C1	–Ti	–S	43.3(1)
Ti	–CP4	2.384(5)	C1	–S	–Ti	62.0(1)
Ti	–CP5	2.406(4)	Ti	–P	–C2	118.4(2)
Ti	–CPa	2.097(0)	Ti	–P	–C3	116.9(1)
Ti	–CPb	2.097(0)	C3	–P	–C2	100.5(2)
S	–C1	1.744(3)	C3	–P	–C3	100.4(2)
P	–C2	1.824(5)	S	–C1	–Ti	74.7(1)
P	–C3	1.813(4)	H1a	–C1	–Ti	118.2(19)
C1	–H1a	0.90(3)	H1a	–C1	–S	115.2(19)
C2	–H2a	0.87(5)	H1a	–C1	–H1a	111.1(27)
C2	–H2b	0.85(4)	H2a	–C2	–P	110.8(33)
C3	–H3a	0.80(4)	H2b	–C2	–P	113.4(24)
C3	–H3b	0.87(4)	H2b	–C2	–H2a	117.9(40)
C3	–H3c	0.96(4)	H2b	–C2	–H2b	80.6(34)
CP1	–CP2	1.356(4)	H3a	–C3	–P	122.1(29)
CP1	–CP5	1.329(4)	H3b	–C3	–P	110.5(24)
CP1	–H1	0.84(3)	H3c	–C3	–P	105.2(24)
CP2	–CP3	1.399(5)	H3b	–C3	–H3a	117.1(38)
CP2	–H2	0.78(3)	H3c	–C3	–H3a	90.5(37)
CP3	–CP4	1.362(7)	H3c	–C3	–H3b	107.4(34)
CP3	–H3	0.70(4)	CP5	–CP1	–CP2	109.9(3)
CP4	–CP5	1.340(6)	CP3	–CP2	–CP1	106.6(3)
CP4	–H4	0.70(4)	CP4	–CP3	–CP2	105.8(4)
CP5	–H5	1.00(4)	CP5	–CP4	–CP3	109.9(4)
			CP1	–CP5	–CP4	107.8(3)
			H1	–CP1	–CP2	128.8(20)
			H1	–CP1	–CP5	121.3(20)
			H2	–CP2	–CP1	130.0(25)
			H2	–CP2	–CP3	123.4(25)
			H3	–CP3	–CP2	124.7(34)
			H3	–CP3	–CP4	129.5(34)
			H4	–CP4	–CP3	127.9(34)
			H4	–CP4	–CP5	122.1(34)
			H5	–CP5	–CP1	122.6(22)
			H5	–CP5	–CP4	129.5(22)

Table II. Final Parameters.

x, y, z and $U_{eq}{}^{a} \times 10^4$

Atom	x	y	z	U_{eq} or B
Ti	1532(.3)	2500	716(.4)	277(1)
S	−247(.5)	2500	438(.9)	689(3)
P	1195(.5)	2500	−2237(.8)	499(2)
C1	237(2)	2500	2298(4)	741(11)
C2	2234(4)	2500	−3550(6)	1350(23)
C3	500(3)	1376(4)	−3000(4)	956(11)
Cp1	2641(2)	1311(2)	2033(4)	664(7)
Cp2	1734(2)	891(2)	2203(4)	833(8)
Cp3	1423(3)	582(2)	732(7)	1134(14)
Cp4	2167(5)	838(3)	−240(5)	1170(14)
Cp5	2899(3)	1288(3)	556(4)	883(9)
H1a	117(21)	1902(25)	2852(33)	8.1(8) *
H1	3010(20)	1571(24)	2708(33)	7.3(7) *
H2	1417(24)	820(29)	2946(40)	8.9(10)*
H3	962(30)	359(36)	565(42)	10.8(12)*
H4	2205(29)	724(34)	−1025(45)	11.2(14)*
H5	3525(26)	1602(31)	175(46)	11.4(11)*
H2a	2039(34)	2500	−4506(60)	9.5(14)*
H2b	2680(24)	2053(31)	−3294(40)	11.7(14)*
H3a	593(28)	768(33)	−2726(47)	11.3(16)*
H3b	371(27)	1477(31)	−3974(39)	10.1(10)*
H3c	−109(28)	1390(31)	−2453(48)	10.7(12)*

$^{a}\ U_{eq} = \frac{1}{3}\sum_i \sum_j [U_{ij}(a_i^* a_j^*)(\vec{a}_i \cdot \vec{a}_j)]$

*Isotropic displacement parameter, B

Table III. Anisotropic Thermal Displacement Parameters x 10^4.

Atom	U_{11}	U_{22}	U_{33}	U_{12}	U_{13}	U_{23}
Ti	251(2)	290(3)	290(2)	0	0(2)	0
S	261(4)	1299(8)	506(5)	0	27(3)	0
P	421(4)	769(6)	308(4)	0	7(3)	0
C1	412(17)	1380(40)	432(18)	0	116(14)	0
C2	731(29)	2866(100)	454(24)	0	213(22)	0
C3	1197(29)	1120(32)	551(16)	−236(22)	−268(19)	−228(19)
CP1	706(15)	393(12)	892(19)	95(11)	−415(15)	36(13)
CP2	900(20)	670(18)	928(23)	51(15)	−15(18)	477(17)
CP3	1095(27)	326(13)	1980(51)	−179(15)	−917(33)	154(20)
CP4	1949(50)	706(24)	856(25)	817(32)	−438(30)	−374(21)
CP5	770(19)	826(20)	1053(26)	474(16)	126(18)	107(19)

The form of the displacement factor is:

$$\exp -2\pi^2(U_{11}h^2a^{*2} + U_{22}k^2b^{*2} + U_{33}\ell^2c^{*2} + 2U_{12}hka^*b^* + 2U_{13}h\ell a^*c^* + 2U_{23}k\ell b^*c^*)$$

Appendix VI.

Crystal Structure Data of $[Cp_2Ti(\eta^2\text{-}CH_2SCH_3)PMe_3]^+ I^- \cdot CH_3CN$

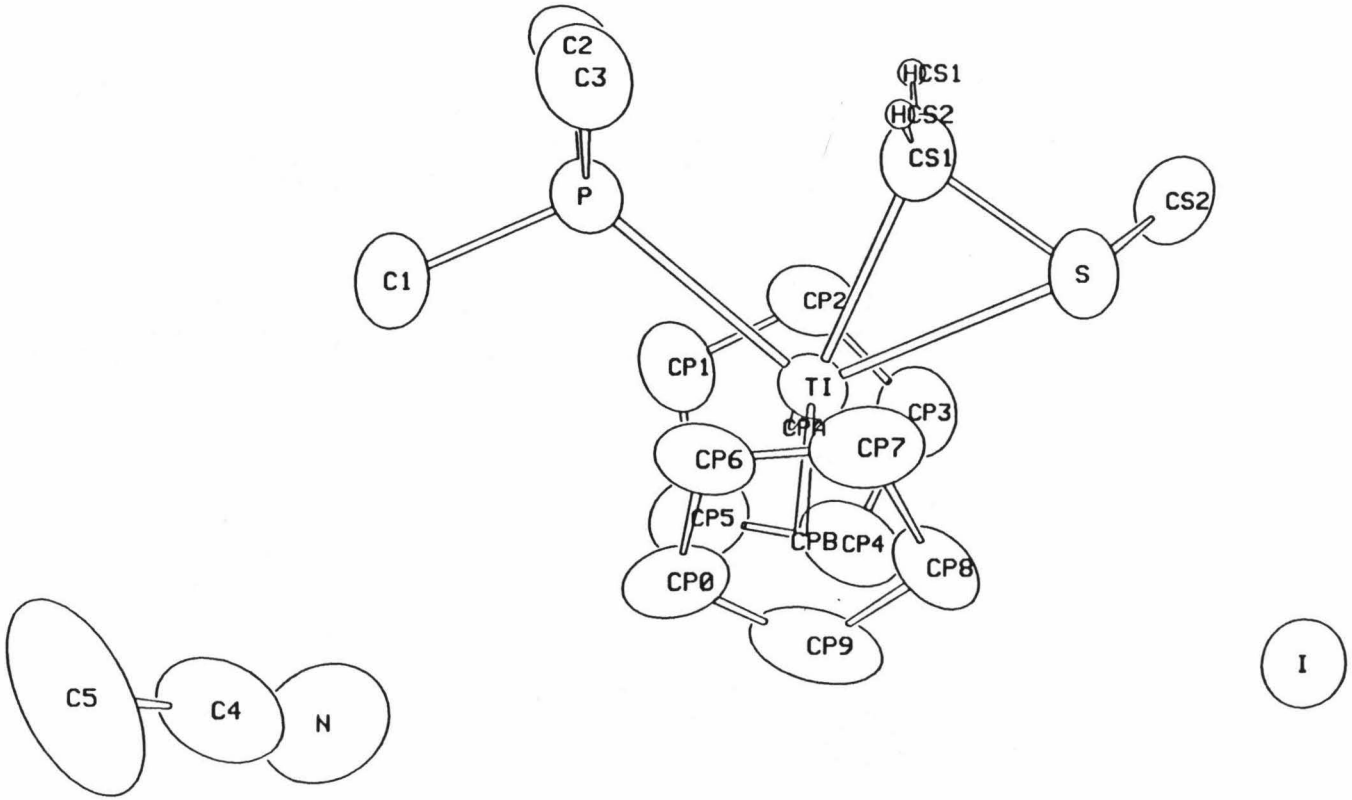

Figure 1. ORTEP diagram.

Table I. Complete Distances and Angles.

		Distance(Å)			Distance(Å)
Ti	-S	2.555(1)	CS2	-HCS4	1.17(6)
Ti	-CS1	2.215(5)	CS2	-HCS5	1.03(4)
Ti	-P	2.581(1)	C1	-HC1	0.93(5)
Ti	-CpA	2.065(1)	C1	-HC2	0.94(5)
Ti	-CpB	2.078(1)	C1	-HC3	0.87(5)
S	-CS1	1.751(5)	C2	-HC4	0.96(5)
S	-CS2	1.803(7)	C2	-HC5	0.91(4)
I	-Ti	5.027(1)	C2	-HC6	0.94(4)
I	-S	4.075(1)	C3	-HC7	1.06(6)
N	-Ti	5.132(7)	C3	-HC8	0.94(5)
N	-S	5.372(7)	C3	-HC9	0.73(4)
P	-C1	1.818(7)	N	-C4	1.099(10)
P	-C2	1.817(6)	C4	-C5	1.414(11)
P	-C3	1.827(6)	HCS1	-HCS2	1.47(6)
Ti	-Cp1	2.388(5)	HCS3	-HCS5	1.43(6)
Ti	-Cp2	2.380(5)	HC1	-HC2	1.48(7)
Ti	-Cp3	2.381(5)	HC1	-HC3	1.43(7)
Ti	-Cp4	2.379(5)	HC2	-HC3	1.39(7)
Ti	-Cp5	2.383(5)	HC4	-HC5	1.52(6)
Ti	-Cp6	2.410(6)	HC4	-HC6	1.58(6)
Ti	-Cp7	2.372(6)	HC5	-HC6	1.44(6)
Ti	-Cp8	2.366(6)	HC7	-HC9	1.36(7)
Ti	-Cp9	2.372(7)	HC8	-HC9	1.35(6)
Ti	-Cp0	2.380(8)			
Cp1	-Cp2	1.393(7)			
Cp1	-Cp5	1.404(7)			
Cp1	-HCp1	0.90(4)			
Cp2	-Cp3	1.406(7)			
Cp2	-HCp2	0.94(4)			
Cp3	-Cp4	1.368(7)			
Cp3	-HCp3	0.91(4)			
Cp4	-Cp5	1.400(8)			
Cp4	-HCp4	1.00(4)			
Cp5	-HCp5	0.93(4)			
Cp6	-Cp7	1.346(9)			
Cp6	-Cp0	1.369(10)			
Cp6	-HCp6	1.02(5)			
Cp7	-Cp8	1.405(8)			
Cp7	-HCp7	0.73(4)			
Cp8	-Cp9	1.343(9)			
Cp8	-HCp8	0.93(5)			
Cp9	-Cp0	1.357(10)			
Cp9	-HCp9	0.89(5)			
Cp0	-HCp0	0.72(4)			
CS1	-HCS1	0.94(4)			
CS1	-HCS2	0.91(4)			
CS2	-HCS3	0.86(5)			

Table I. (Cont.)

	Angle(°)		Angle(°)
CpA -Ti -CpB	130.7	Cp9 -Cp8 -Cp7	106.8(5)
CpA -Ti -P	102.3	HCp8-Cp8 -Cp7	123.2(30)
CpB -Ti -P	102.4	HCp8-Cp8 -Cp9	129.4(30)
CpA -Ti -S	107.3	Cp0 -Cp9 -Cp8	108.7(6)
CpB -Ti -S	99.6	HCp9-Cp9 -Cp8	126.2(32)
CpA -Ti -CS1	115.8(1)	HCp9-Cp9 -Cp0	125.1(32)
CpB -Ti -CS1	112.1(1)	Cp9 -Cp0 -Cp6	108.9(6)
P -Ti -CS1	73.0(1)	HCp0-Cp0 -Cp6	118.9(34)
S -Ti -CS1	42.3(1)	HCp0-Cp0 -Cp9	132.2(34)
S -Ti -P	115.2(.4)	HCS4-CS2 -HCS3	115.3(42)
Ti -CS1 -S	79.3(2)	HCS5-CS2 -HCS3	97.7(39)
Ti -S -CS1	58.4(2)	HCS5-CS2 -HCS4	109.1(38)
CS1 -S -CS2	105.4(3)	HC2 -C1 -HC1	105.3(44)
Ti -S -CS2	119.0(2)	HC3 -C1 -HC1	105.2(45)
HCS1-CS1 -HCS2	104.9(35)	HC3 -C1 -HC2	100.8(43)
S -CS1 -HCS1	115.7(23)	HC5 -C2 -HC4	109.0(38)
S -CS1 -HCS2	116.0(26)	HC6 -C2 -HC4	112.9(38)
Ti -CS1 -HCS1	122.9(23)	HC6 -C2 -HC5	102.7(34)
Ti -CS1 -HCS2	117.0(26)	HC8 -C3 -HC7	122.7(43)
C5 -C4 -N	177.0(8)	HC9 -C3 -HC7	97.4(47)
Ti -P -C1	116.4(2)	HC9 -C3 -HC8	106.8(44)
Ti -P -C2	116.3(2)	HCS2-HCS1-CS1	36.7(21)
Ti -P -C3	116.3(2)	HCS1-HCS2-CS1	38.4(22)
C1 -P -C2	102.7(3)	HCS5-HCS3-CS2	45.7(28)
C1 -P -C3	101.9(3)	HCS3-HCS5-CS2	36.7(24)
C2 -P -C3	100.9(3)	HC2 -HC1 -C1	37.5(28)
Cp5 -Cp1 -Cp2	108.3(4)	HC3 -HC1 -C1	35.9(27)
HCp1-Cp1 -Cp2	131.1(25)	HC3 -HC1 -HC2	57.0(33)
HCp1-Cp1 -Cp5	120.5(25)	HC1 -HC2 -C1	37.2(28)
Cp3 -Cp2 -Cp1	106.6(4)	HC3 -HC2 -C1	37.8(27)
HCp2-Cp2 -Cp1	125.2(25)	HC3 -HC2 -HC1	59.4(34)
HCp2-Cp2 -Cp3	128.1(25)	HC1 -HC3 -C1	38.9(29)
Cp4 -Cp3 -Cp2	109.7(5)	HC2 -HC3 -C1	41.4(29)
HCp3-Cp3 -Cp2	124.6(26)	HC2 -HC3 -HC1	63.5(35)
HCp3-Cp3 -Cp4	125.7(26)	HC5 -HC4 -C2	34.4(23)
Cp5 -Cp4 -Cp3	107.7(5)	HC6 -HC4 -C2	33.1(22)
HCp4-Cp4 -Cp3	128.1(25)	HC6 -HC4 -HC5	55.3(26)
HCp4-Cp4 -Cp5	124.2(25)	HC4 -HC5 -C2	36.6(24)
Cp4 -Cp5 -Cp1	107.8(5)	HC6 -HC5 -C2	39.3(22)
HCp5-Cp5 -Cp1	121.8(27)	HC6 -HC5 -HC4	64.3(29)
HCp5-Cp5 -Cp4	130.3(27)	HC4 -HC6 -C2	34.0(23)
Cp0 -Cp6 -Cp7	107.1(6)	HC5 -HC6 -C2	38.0(22)
HCp6-Cp6 -Cp7	126.7(31)	HC5 -HC6 -HC4	60.3(28)
HCp6-Cp6 -Cp0	126.1(31)	HC9 -HC7 -C3	32.3(25)
Cp8 -Cp7 -Cp6	108.4(5)	HC9 -HC8 -C3	31.3(24)
HCp7-Cp7 -Cp6	136.6(33)	HC7 -HC9 -C3	50.3(36)
HCp7-Cp7 -Cp8	114.9(33)	HC8 -HC9 -C3	41.9(30)
		HC8 -HC9 -HC7	80.6(39)

Table II. Final Parameters.

x, y, z and $U_{eq}{}^{a} \times 10^4$

Atom	x	y	z	U_{eq} or B
Ti	2489(.5)	1409(.4)	4067(.4)	337(1)
P	3358(.7)	1788(.7)	5238(.6)	413(3)
S	3123(.8)	2092(.8)	2909(.6)	553(3)
Cp1	2982(4)	49(3)	4582(3)	523(15)
Cp2	3464(4)	174(3)	3942(3)	519(14)
Cp3	2835(4)	130(3)	3374(3)	597(15)
Cp4	1989(4)	9(3)	3651(3)	614(17)
Cp5	2068(4)	−49(3)	4405(3)	590(18)
Cp6	1620(3)	2526(4)	4678(4)	641(16)
Cp7	1711(4)	2770(4)	3981(4)	615(18)
Cp8	1251(4)	2158(4)	3545(3)	642(15)
Cp9	901(3)	1552(4)	3993(5)	747(20)
Cp0	1128(4)	1763(5)	4684(4)	864(22)
CS1	3660(3)	2225(4)	3747(3)	495(12)
CS2	3893(4)	1457(5)	2363(3)	750(18)
C1	2819(4)	1483(5)	6086(3)	646(17)
C2	4474(3)	1308(4)	5329(3)	562(14)
C3	3607(5)	2952(4)	5388(4)	637(16)
I	1244(.2)	1039(.2)	1553(.2)	633(1)
N	464(5)	4635(4)	1151(3)	1281(23)
C4	382(5)	4252(4)	1652(4)	963(23)
C5	255(6)	3799(5)	2314(5)	1673(33)
HCS1	4261(25)	2020(26)	3771(20)	4.6(11)*
HCS2	3682(26)	2784(27)	3922(23)	4.8(12)*
HCS3	4323(30)	1810(30)	2241(26)	5.9(15)*
HCS4	3615(37)	1009(36)	1896(34)	10.9(18)*
HCS5	4254(29)	1074(28)	2723(25)	6.5(13)*
HC1	2281(33)	1771(37)	6181(28)	8.6(17)*
HC2	2689(33)	882(32)	6129(26)	7.0(18)*
HC3	3147(30)	1565(30)	6468(25)	5.8(13)*
HC4	4450(32)	678(31)	5362(27)	8.0(16)*
HC5	4817(25)	1462(25)	4941(22)	4.1(11)*
HC6	4784(26)	1567(26)	5716(21)	4.7(11)*
HC7	4076(38)	3148(40)	4988(34)	11.7(21)*
HC8	3067(30)	3261(31)	5476(24)	6.1(14)*
HC9	3899(27)	3022(30)	5704(23)	4.2(13)*
HCp1	3168(25)	−7(26)	5044(22)	3.9(11)*
HCp2	4085(27)	294(27)	3914(21)	4.9(11)*
HCp3	2975(27)	178(27)	2898(22)	4.9(12)*
HCp4	1412(28)	−63(29)	3381(23)	6.0(12)*
HCp5	1628(27)	−104(29)	4757(23)	5.6(13)*
HCp6	1849(34)	2857(36)	5121(31)	9.9(18)*
HCp7	1928(27)	3131(28)	3782(23)	3.4(12)*
HCp8	1284(30)	2157(31)	3044(27)	7.3(15)*
HCp9	567(32)	1088(33)	3864(27)	7.5(15)*

Table II. (Cont.)

Atom	x	y	z	U_{eq} or B
HCp0	1044(27)	1549(28)	5023(22)	2.8(12)*
HA1	793	3622	2563	15.2 *
HA2	497	3196	2322	15.2 *
HA3	−102	3239	2254	15.2 *
HA4	−405	3707	2428	15.2 *
HA5	−109	4133	2669	15.2 *
HA6	490	4090	2737	15.2 *

[a] $U_{eq} = \frac{1}{3}\sum_i \sum_j [U_{ij}(a_i^* a_j^*)(\vec{a}_i \cdot \vec{a}_j)]$
*Isotropic displacement parameter, B

Table III. Anisotropic Thermal Displacement Parameters x 10^4.

Atom	U_{11}	U_{22}	U_{33}	U_{12}	U_{13}	U_{23}
Ti	340(3)	277(3)	394(4)	10(3)	−37(4)	9(4)
P	418(6)	411(6)	411(7)	0(5)	−49(5)	4(6)
S	622(7)	619(8)	418(7)	11(6)	2(6)	120(6)
Cp1	770(39)	276(26)	523(35)	76(24)	−99(31)	24(24)
Cp2	501(32)	363(27)	694(38)	107(24)	−63(28)	−81(26)
Cp3	853(40)	396(28)	541(35)	150(26)	−34(35)	−79(28)
Cp4	618(37)	304(28)	920(49)	12(25)	−226(33)	−103(28)
Cp5	675(37)	222(26)	873(45)	−43(24)	154(37)	79(27)
Cp6	467(31)	796(43)	661(41)	265(30)	−110(31)	−235(37)
Cp7	550(34)	311(32)	984(54)	91(26)	135(35)	81(37)
Cp8	657(33)	740(40)	530(36)	376(33)	−177(32)	−91(34)
Cp9	403(30)	477(37)	1360(67)	16(26)	−200(37)	−143(44)
Cp0	581(39)	1067(61)	945(57)	384(40)	327(43)	492(53)
CS1	508(32)	545(34)	432(26)	−105(27)	6(24)	20(24)
CS2	662(40)	1068(50)	520(37)	70(40)	124(32)	55(35)
C1	693(40)	829(48)	415(33)	11(37)	−11(27)	26(32)
C2	421(28)	650(40)	616(36)	−12(26)	−127(28)	35(31)
C3	739(43)	518(34)	653(40)	−77(32)	−171(38)	−134(31)
I	640(2)	766(2)	493(2)	25(2)	−13(2)	−117(2)
N	1438(52)	1119(55)	1286(60)	586(43)	241(47)	39(43)
C4	913(45)	693(50)	1282(73)	258(36)	−224(50)	8(45)
C5	2366(98)	1055(58)	1599(76)	−543(59)	−1052(73)	518(57)

The form of the displacement factor is:

$$\exp -2\pi^2(U_{11}h^2a^{*^2} + U_{22}k^2b^{*^2} + U_{33}\ell^2c^{*^2} + 2U_{12}hka^*b^* + 2U_{13}h\ell a^*c^* + 2U_{23}k\ell b^*c^*)$$